U. S. ARMY
TRANSPORTATION RESEARCH COMMAND
FORT EUSTIS, VIRGINIA

TREC TECHNICAL REPORT 60-56

THE TWO-DIMENSIONAL EFFECTS OF SLIPSTREAM SHEAR ON AIRFOIL CHARACTERISTICS

Project 9-38-01-000, ST 902

Contract DA 44-177-TC-439

September 1960

prepared by :

Cornell Aeronautical Laboratory, Inc.
Buffalo, New York

2494—60

CORNELL AERONAUTICAL LABORATORY, INC.
OF CORNELL UNIVERSITY

BUFFALO, N. Y.

Report No. AI-1190-A-5

THE TWO-DIMENSIONAL EFFECTS OF SLIPSTREAM SHEAR ON AIRFOIL CHARACTERISTICS

R. J. Vidal
J. H. Hilton
J. T. Curtis

SEPTEMBER 1960

Project No. 9-38-01-000 Task 902
Contract No. DA 44-177-TC-439

U.S. Army Transportation Research and Development Command
Transportation Corps
Fort Eustis, Virginia

By R. J. Vidal
R. J. Vidal

J. H. Hilton

J. T. Curtis

Approved: A. Hertzberg
A. Hertzberg, Head
Aerodynamic Research Department

FOREWORD

The research on which this report is based was performed by the authors, Mr. R. J. Vidal, Mr. J. H. Hilton, and Dr. J. T. Curtis of the Aerodynamic Research Department of Cornell Aeronautical Laboratory, Inc., Buffalo, New York, under Army Contract DA 44-177-TC-439, Project Number 9-38-01-000, ST902. The Transportation Corps., U. S. Army Transportation Research Command, Fort Eustis, Virginia, is the monitoring agency. This work represents a part of a research program, still in progress, which is devoted to investigations of several specific problems associated with STOL/VTOL flight, as well as more general research on the aerodynamics of low speed flight. This report is one of a series to be published covering the entire program of research.

TABLE OF CONTENTS

ABSTRACT

The available theories for two-dimensional airfoils in uniform and non-uniform shear flows of infinite extent are reviewed, and an image analysis is presented to make these results applicable to shear flows of finite extent. Experiments with a two-dimensional symmetrical Joukowsky airfoil in uniform shear flow and in simulated two-dimensional propeller slipstreams are described, and the results are compared with the applicable theory. It is found that the airfoil section characteristics can be predicted with good accuracy at all positions tested in the slipstream.

FOREWORD

The research on which this report is based was performed by the authors, Mr. R. J. Vidal, Mr. J. H. Hilton, and Dr. J. T. Curtis of the Aerodynamic Research Department of Cornell Aeronautical Laboratory, Inc., Buffalo, New York, under Army Contract DA 44-177-TC-439, Project Number 9-38-01-000, ST902. The Transportation Corps., U. S. Army Transportation Research Command, Fort Eustis, Virginia, is the monitoring agency. This work represents a part of a research program, still in progress, which is devoted to investigations of several specific problems associated with STOL/VTOL flight, as well as more general research on the aerodynamics of low speed flight. This report is one of a series to be published covering the entire program of research.

TABLE OF CONTENTS

LIST OF ILLUSTRATIONS

LIST OF ILLUSTRATIONS (Cont'd)

LIST OF SYMBOLS

U	velocity at any point in the undisturbed stream
U_0	undisturbed stream velocity at the airfoil midchord position
x, y	stream coordinates (Fig. 2)
c	airfoil reference chord length
k	shear parameter
t	airfoil maximum thickness
τ	t/c
a_0, θ_0	airfoil shape parameters (Ref. 6)
h	maximum height of the airfoil mean line
ρ	stream density
p	stream static pressure
L	lift
M	pitching moment about the airfoil midchord, positive nose up
C_L	section lift coefficient based on local velocity, $\frac{L}{\rho/2\, U_0^2\, c}$
C_M	section moment coefficient about the airfoil midchord based on local velocity, $\frac{M}{\rho/2\, U_0^2\, c^2}$
α	geometric angle of attack
U_1	undisturbed stream velocity at plane of flow symmetry
q	shear derivative
ψ_0	stream function of the undisturbed stream
ψ_1	disturbance stream function
ψ_i	stream function of the image system
r, θ	polar coordinates (Fig. 2)
γ_L	strength parameter of the lifting image system

ν_t	strength parameter of the thickness image system
ν'_L	strength parameter of the equivalent lifting system
ν'_t	strength parameter of the equivalent thickness system
w_x	longitudinal disturbance velocity
w_y	lateral disturbance velocity
U_e	undisturbed velocity at the slipstream boundary
U'	free stream velocity
ξ	$x - c/4$
Λ	source and sink strength
K_1	Eq. 26
K_2	Eq. II-4
K_3	Eq. 27
H	slipstream half-height (Fig. 3)
η	$\frac{H}{c}$
δ	distance of wing above slipstream center plane
ϵ	δ/H
$\Delta\alpha$	change in angle of attack due to slipstream interference
$C_{M_{a.c.}}$	pitching moment coefficient about the aerodynamic center
$x_{a.c.}$	location of aerodynamic center, measured from airfoil midchord
K	screen loss coefficient $\frac{\Delta p}{\rho/2\ U^2}$
σ	screen solidity
u_o, u_1, u_2, u_3	longitudinal stream velocities (Fig. I-1)
β	refraction coefficient (Eq. I-2)
A_n, B_n, C_n	Fourier coefficients (Eq. I-5, I-8, I-9)
γ	$1 + \frac{w_x}{u_o}$
ζ	$\frac{y}{H}$

INTRODUCTION

The effect of a propeller slipstream interacting with a wing is a classical problem which has been present since the introduction of the airplane. The propeller-driven aircraft has, with few exceptions, evolved into a tractor configuration with the propeller situated ahead of the lifting surfaces, and portions of these surfaces are then subjected to a high velocity slipstream. Hence in calculating the wing characteristics, one should allow for the fact that the wing is acted upon by a non-uniform stream; that is, the uniform free stream with the superimposed non-uniform propeller slipstream.

This problem has been the subject of theoretical research for a number of years. One of the earliest efforts was that of Koning[1] in 1934, in which the slipstream was taken to be uniform and with a velocity slightly larger than that of the free stream. These results were subsequently extended by Graham, Lagerstrom, Licher, and Beane[2] to allow for larger slipstream velocities, and by Rethorst[3] to include a more realistic model of the slipstream boundary. In all these cases the slipstream is assumed to have no gradients of velocity. It is tacitly assumed that the influence of slipstream velocity gradients on wing lift is small in comparison with the gross effects of the high velocity jet interacting with the wing.

Tsien[4] in 1943 investigated the influence of vertical gradients of velocity on a thick symmetric profile. In that research a two-dimensional model in a stream with a linear velocity gradient was considered, and it was found that because of the interaction of the gradients with the wing thickness, the wing characteristics were substantially different from those obtained in uniform flow. This early result was subsequently augmented in an investigation by von Karman and Tsien[5] in which Prandtl lifting line theory was reformulated for a flow with

spanwise gradients of velocity. As noted in that paper, the complete solution of a wing in non-uniform flow with both spanwise and vertical gradients of velocity requires a complete knowledge of the section characteristics including the effects of vertical gradients of velocity. The use of these characteristics in the Kármán-Tsien lifting line theory would enable one to treat the complete problem.

The Cornell Aeronautical Laboratory has been conducting a program of research on the aerodynamics of STOL/VTOL configurations. Included in this program is research on the influence of vertical gradients of stream velocity on the section characteristics of thick airfoils. The first part of this investigation was devoted to an extension of Tsien's theory[4] for symmetric Joukowsky sections to include camber[6], and was undertaken to provide a basis for calculating the aerodynamics of the highly flapped wings, or alternatively highly cambered wings, characteristic of vectored slipstream configurations. This research was continued in experimental investigations of two-dimensional airfoil characteristics in two-dimensional propeller-like slipstreams. The purpose of this report is to present the results of the experimental research and to present methods for applying Sowyrda's[6] theory in determining section characteristics. In this connection, the first section is devoted to a review of the applicable theories for airfoils in flows with linear and non-linear vertical gradients of velocity. The second section presents the experimental results and compares them with the appropriate theory.

THEORY

Considering the slipstream of an unyawed propeller, the important features, as regards its interactions with a wing, are that the longitudinal velocity distribution is axially symmetric, and it is roughly V-shaped as indicated in Figure 1.

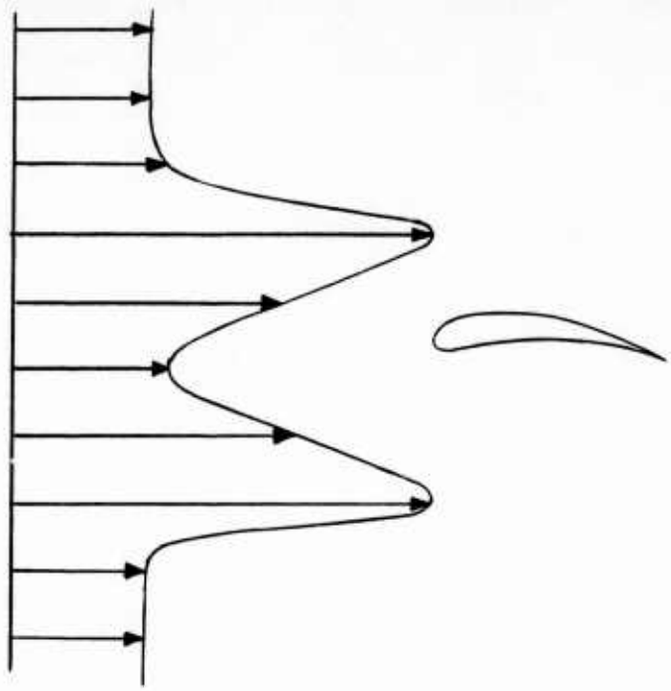

Figure 1 TYPICAL SLIPSTREAM VELOCITY DISTRIBUTION

In addition there is a rotational velocity component which is axially asymmetric and a function only of radial position. In anticipation of a final lifting line development, the rotational velocity component can be neglected in determining airfoil section characteristics since this component will only alter the section angle of attack. This component must of course be included in the final lifting line development.

Referring to Fig. 1, it can be seen that there are three important slipstream features to be considered. In the immediate vicinity of the slipstream axis, the velocity distribution is markedly nonlinear, a region of non-uniform shear. Farther out in the slipstream the velocity distribution is approximately linear, a region of uniform shear. Now if the influence of the slipstream boundary could be neglected, one might expect that non-uniform shear theory would apply in the vicinity of the slipstream axis, and uniform shear theory might be valid further out in the slipstream. The third important effect, slipstream boundary interference, can be included using an appropriate image analysis. The theory for each of these items will be reviewed in the rest of this section.

Uniform Shear

As noted in the Introduction, the two-dimensional theory for thick Joukowsky profiles in uniform shear was reported by Tsien[4], and was subsequently extended by Sowyrda[6] to profiles with camber. The important aspects and the results of these theories will be reviewed here; the details of the development can be obtained in the original references.

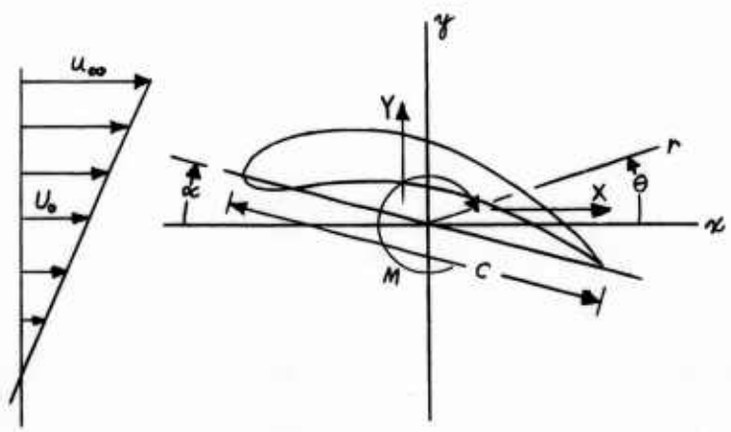

Figure 2 AIRFOIL AND SHEAR STREAM SYSTEM

Consider the model shown in Fig. 2 with the remote stream velocity given by $U = U_o(1+k\frac{y}{c})$, where U is the undisturbed velocity at the position, y, above the airfoil midchord position, U_o is the undisturbed velocity at the airfoil midchord position, k is the shear parameter defining the linear velocity gradient, and c is the airfoil reference chord length. The important feature of this flow is that at locations far upstream of the airfoil, the vorticity is constant throughout the stream. Now since it is assumed that the flow is inviscid and incompressible, it follows that the vorticity must be everywhere the same throughout the entire flow field.

In writing down the stream function for the undisturbed flow and superimposing a disturbance stream function to describe the entire flow field, it is found that because the vorticity is everywhere the same, the disturbance stream function satisfies Laplace's equation. Therefore, any solution to Laplace's equation, combined with the stream function for the undisturbed flow and subject to the appropriate boundary conditions, will yield a solution to the airfoil problem. The boundary conditions are that there be no flow through the airfoil, that the Kutta condition be satisfied at the airfoil trailing edge, and that the airfoil disturbances vanish at infinity.

Since Laplace's equation holds for the problem, the powerful Joukowsky transformation can be applied, subject to certain restrictions. This allows one to obtain an exact potential solution to the problem, including the effects of thickness and camber. The exact results for the lift and pitching moment about the airfoil midchord are given in Refs. 4 and 6 as a function of the stream shear, k, and the airfoil shape parameters. The drag on the airfoil is identically zero, since it is a two-dimensional closed body in uniform shear[4,6] subject to no spanwise velocity variations. Considerable insight into the

effects of stream shear on the airfoil characteristics can be obtained by specializing the results of Ref. 6 to the case of small airfoil thickness and camber. The airfoil maximum thickness and camber, to the second order in the airfoil shape parameters, are given by

$$\tau \equiv t/c = a_0 (1 + a_0) \tag{1}$$

$$h/c = -\frac{a_0 \theta_0}{2} \tag{2}$$

where t is the maximum thickness, h is the maximum height of the airfoil camber line, and a_0 and θ_0 are airfoil shape parameters defined in Ref. 6. The lift coefficient and moment coefficient about the airfoil midchord are, to the first order in thickness and camber

$$C_L = \frac{L}{\rho/2\, U_0^2 c} \approx \left[1 + \tau + \frac{\tau k^2}{32}\right] 2\pi\alpha + 2\pi \left[\frac{\tau k}{4} + 2\frac{h}{c}\left(1 + \frac{k^2}{32}\right)\right] \tag{3}$$

$$C_M = \frac{M}{\rho/2\, U_0^2 c^2} \approx \left[1 + \tau + \frac{\tau k^2}{16}\right] \frac{\pi}{2}\, \alpha + \frac{\tau \pi k}{64} \tag{4}$$

where a positive pitching moment is a stalling moment.

Equations (3) and (4) show that the effect of shear is to cause a small increase in the slope of the lift and moment curves determined by the stream shear and the airfoil thickness. More important, there is an overall increase in the lift and moment. This overall increase in lift is proportional to the shear and the airfoil thickness and camber, while the overall increase in moment is a function only of the shear and thickness. In addition it will be noted in Eq. (3) that the thickness and camber interactions with the shear are super-

imposed. This is true for thin airfoils with small camber. However, the exact theory shows that in addition there is a coupling between thickness and camber which also increases the lift. For certain values of the shear, it is found that this coupling effect is as large as the thickness effect and the camber effect[6].

In order to have a physical feel for the magnitude of each of these shear interactions, consider a 17% thick airfoil with 11% camber in a shear flow defined by $k = 5$. This corresponds to about the steepest velocity gradient found in a propeller slipstream. In Ref. 6 it is shown that at zero angle of attack, the lift obtained with no shear is $C_L \approx 1.6$, while with $k = 5$, the lift is $C_L \approx 4.9$. This increment in lift of $\Delta C_L \approx 3.3$ is due to a pure thickness effect, a pure camber effect, and a coupling of thickness and camber effects. Calculations indicate that for this particular combination of shear and airfoil parameters, each of these three effects is roughly the same.

Non-Uniform Shear

Some insight into the influence of non-uniform shear flows on airfoil section characteristics can be obtained from the two-dimensional investigations made by Jones[7,8]. In Ref. 7, Jones considers a thin cambered airfoil in a flow with a parabolic velocity distribution given by $U = U_1 \left[1 + 8q\left(\frac{y}{c}\right)^2\right]$, where U is the undisturbed stream velocity at a height, y, above the plane of flow symmetry, U_1 is the undisturbed stream velocity in the plane of flow symmetry, and q is a constant defining the non-uniform shear. In contrast to the uniform shear flow just described, this undisturbed flow is characterized by a stream vorticity which is not constant, but varies between streamlines. From

Helmholtz's law for the rate of change of vorticity in a fluid, it is known that the vorticity must be conserved along a streamline, implying that the disturbance stream function for a profile in this flow satisfies the flow equation, $\nabla^2 \psi_1 = f(\psi)$. This then leads to the requirement that the disturbance stream function satisfy the flow equation

$$\nabla^2 \psi_1 = f(\psi_0 + \psi_1) - f(\psi_0) \tag{5}$$

where ψ_0 is the stream function of the undisturbed stream.

The fundamental difficulty in treating non-uniform shear flows is apparent by comparing Eq. (5) with its counterpart in uniform shear flow. In uniform shear flow it is necessary that the disturbance stream function satisfy Laplace's equation, which then allows one to employ conformal transformation techniques. Such is not the case in non-uniform shear flows, and one must employ other methods.

Jones obtains approximate solutions for the lift, drag, and pitching moment of a slightly cambered thin airfoil in non-uniform shear flow by assuming the airfoil thickness is small and by assuming that $8q\left(\frac{y}{c}\right)^2 \ll 1$. Through a separation of variables, Jones reduces the problem to a pair of Mathieu differential equations which are solved subject to the same boundary conditions employed in the uniform shear development. His results for the lift and moment about the midchord position are, to the first order in α and $q\left(\frac{y}{c}\right)$,

$$C_L = \frac{L}{\rho/2\ U_0^2 c} \approx 2\pi\left[(1 + 1.116\,q)\alpha + 2\frac{h}{c}\right] \tag{6}$$

$$C_M = \frac{M}{\rho/2\ U_0^2 c^2} \approx \frac{\pi}{2}\alpha\left[1 + .866\,q\right] \tag{7}$$

where U_o is the undisturbed stream velocity at the airfoil midchord position. To the same approximation, the corresponding results in uniform shear flow are the usual thin airfoil results.

$$C_L = 2\pi\left(\alpha + \frac{2h}{c}\right) \tag{8}$$

$$C_M = \frac{\pi}{2}\alpha \tag{9}$$

It is first noted in Eqs. 3 and 4 that for uniform shear, if the product of the airfoil thickness and shear parameter is neglected and if the shear is assumed small, the theory reduces to uniform flow theory, and there is no effect of shear. Comparing these with Eqs. 6 and 7, it then appears that Jones, in stipulating small airfoil thickness and, in essence, small shear, loses the shear effect on lift and moment which Ref. 6 shows to be associated with thickness and camber. However, Jones demonstrates that one effect of shear is to increase the slope of the lift and moment curves. Moreover, these increases do not depend on the local shear, $q\frac{y}{c}$, but rather on the derivative of shear, q. This result then indicates that for a wing in a propeller slipstream near the axis of symmetry, the lift and moment curves would exhibit higher slopes in proportion to q, the first derivative of shear or the second derivative of the velocity.

Jones, in his subsequent investigation,[8] treated profiles of elliptic cross section in a stream with a velocity distribution given by $U = U_1 \cosh(y/l)$, where l is an arbitrary reference length. This problem is analogous to the one just described in that the stream vorticity is not constant but varies from streamline to streamline. The development of the flow equation follows that for the cambered thin airfoil to the point where the three boundary conditions are applied. For the elliptic profile, the Kutta condition is not applicable because there is

no sharp trailing edge. Consequently, there is no boundary condition fixing the circulation about the profile.

In order to fix the circulation, Jones makes the assumption that the circulation around the profile is identically that around the same contour in the undisturbed stream. This is the same assumption used by Tsien[4] in treating a circular cylinder in uniform shear flow, and by Murray and Mitchell[9] in treating a circular cylinder in non-uniform shear flow. This condition is correct for uniform shear flows since it follows from the fact that the vorticity is everywhere the same in a disturbed uniform shear flow. However, for non-uniform shear flows, the applicability of this boundary condition is open to question since the vorticity varies between streamlines.

Jones determines the lift and moment for an ellipse of any thickness in a stream of small non-uniform shear. To the first order in thickness and the second order in angle of attack, his results for the lift are

$$C_L = \frac{L}{\rho/2\, U_0^2 c} = \frac{\pi}{2} k_\ell (\tau + \alpha^2) \qquad (10)$$

where k_ℓ is the undisturbed stream shear at the airfoil position, the local shear. The comparable approximation for the lift in uniform shear is

$$C_L = \frac{L}{\rho/2\, U_0^2 c} = 2\pi (1+\tau)\alpha + \frac{\pi}{2} k\tau \qquad (11)$$

Now Jones' result for non-uniform shear, Eq. (10), shows that in the limit of $k = 0$, a uniform stream, there is no lift on the elliptic profile regardless of angle of attack. This might be anticipated since the profile lacks a sharp trailing edge. Considering the zero angle of attack condition with shear, Eqs.

(10) and (11) are seen to yield equivalent predictions for the lift increment due to shear if for the non-uniform shear flow the local shear is used. This suggests that in non-uniform shear flows, the lift increment due to shear could be predicted on the basis of uniform shear theory.

The fact that Jones' result for the elliptic profile does not yield a lift curve slope that agrees with either uniform shear theory, or more important, his result for a thin airfoil in non-uniform shear, is interesting. It seems plausible that this is associated with the lack of a sharp trailing edge on the elliptic profile, and that his result for the thin cambered plate is the better description of airfoil lift curve slope in non-uniform shear flow. Since this result does not allow for thickness effects, the question remains as to how to account for it in non-uniform shear, though one might intuitively expect that it would be the uniform shear result, superimposed on the thin airfoil result.

Slipstream Boundary Interference

It can be expected from the theory for a uniform two-dimensional slipstream[10] that, in general, the characteristics of an airfoil immersed in any slipstream will be different from those in a flow without the discontinuity. These changes stem from the fact that there can be no flow through the boundary and, for practical purposes, the pressure on both sides of the boundary must be equal to the ambient stream pressure. In the case of a uniform slipstream, the two-dimensional slipstream boundary effects can be calculated by considering the combined effects of two equivalent systems of airfoils. One system consists of the actual airfoil and an array of images in a uniform stream with a velocity equal to that of the slipstream. By suitably arranging the image spacing and strength, this system duplicates the disturbance velocities inside the slipstream. The other system consists of an equivalent or effective airfoil in a uniform stream with a velocity

equal to that of the external stream. The strength of this equivalent airfoil is adjusted so that it duplicates the disturbance velocities external to the slipstream. In these systems the airfoil parameters and the image spacing are adjusted so that the pressure and flow continuity requirements are satisfied at the slipstream boundary, and the disturbance velocities at the original airfoil are calculated using the system of image airfoils. In this calculation it is usually assumed that the volume effect stemming from airfoil thickness is negligibly small, and only the effects associated with lift are considered.

An analogous image analysis for airfoils in two-dimensional non-uniform slipstreams can be derived by employing certain assumptions. In this analysis the first order effects of both lift and airfoil thickness will be considered, and it will be assumed that the theory for Joukowsky airfoils in uniform shear flows is adequate for establishing the flow model.

Considering symmetrical airfoils, the disturbance stream function for a Joukowsky section in uniform shear flow is, to the first order in thickness and angle of attack[4]:

$$\psi_1 = 2U_0\left\{\alpha \ln r + \frac{1}{r}(\alpha\cos\theta - a_0\sin\theta) - \frac{1}{r^2}\left(\alpha\cos 2\theta - \frac{a_0}{2}\sin 2\theta\right)\right\} \quad (12)$$

where r and θ are defined in Fig. 2. Equation (12) shows that in this approximation, the lift and thickness effects are independent, and the disturbance stream function can be taken to be

$$\psi_1 = \psi_1(\alpha) + \psi_1(a_0) \quad (13)$$

Moreover, it is seen that to this order of approximation, the stream function is independent of the shear parameter, k, so that in calculating the boundary interference, the image system need not simulate the stream shear so long as the correct wing lift is used and the actual stream velocities are used in satisfying conditions at the slipstream boundary. Accordingly, the disturbance velocities inside the slipstream can be calculated using an image system, shown in Fig. 3, consisting of a pair of images described by the stream function,

$$\psi_i = \nu_L \psi_1(\alpha) - \nu_T \psi_1(a_0) \tag{14}$$

and the array of their repeated reflections in a uniform stream of velocity, U_0. Similarly, the disturbance velocities outside the slipstream can be calculated using the equivalent system of a wing, described by the stream function,

$$\psi = \nu_L' \psi_1(\alpha) + \nu_T' \psi_1(a_0) \tag{15}$$

in a uniform stream of velocity, U'.

The conditions to be satisfied at the slipstream boundary are that the pressure be continuous across the boundary and that there be no flow through the boundary. The latter condition requires that

$$\frac{w_{ye}}{U_e + w_{xe}} = \frac{w_y'}{U' + w_x'} \tag{16}$$

where w_x and w_y are the disturbance velocities in the x and y direction, respectively, the prime denotes conditions just outside the boundary, and the subscript, e, denotes conditions just inside the boundary. Assuming

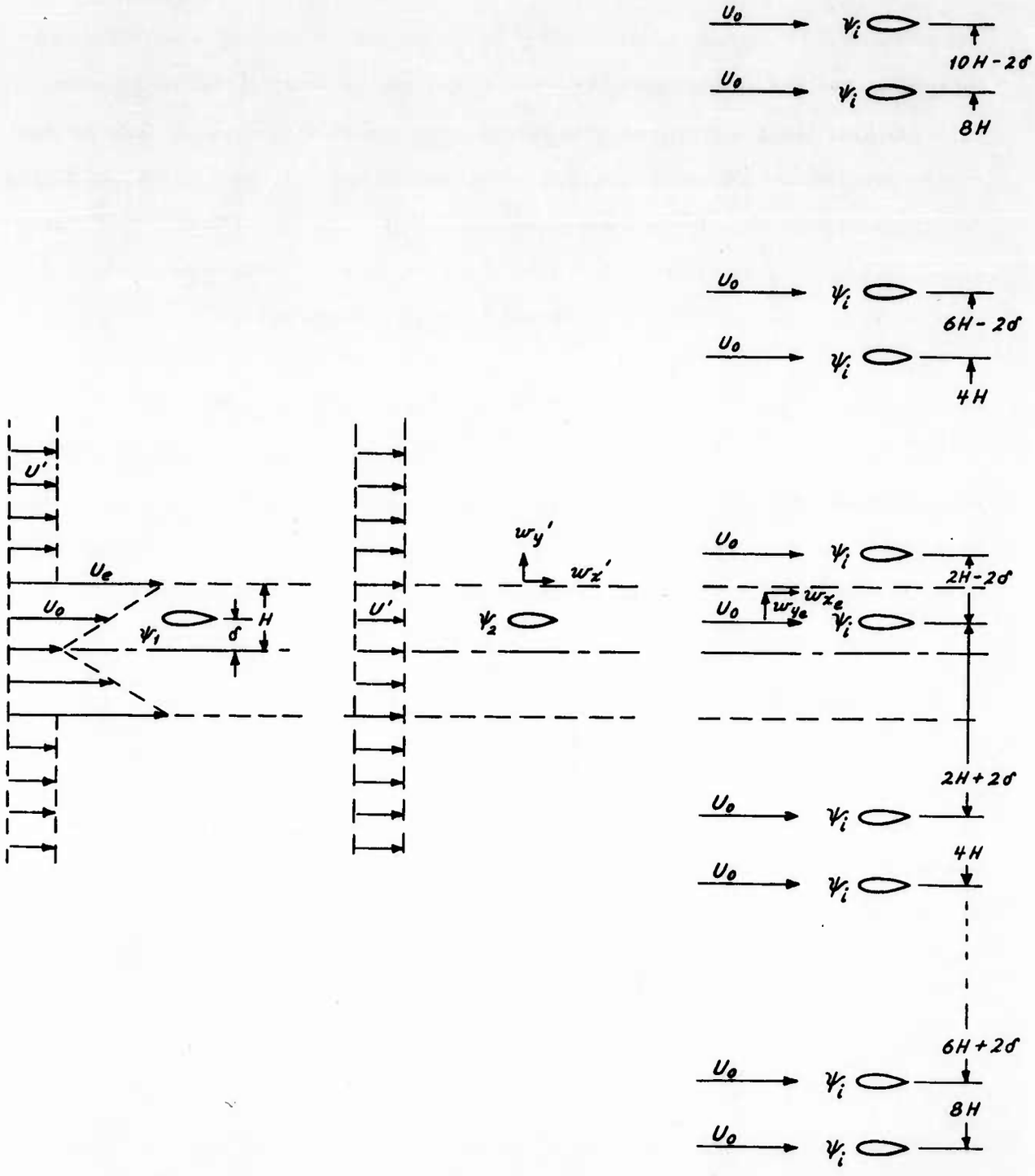

(a) SLIPSTREAM MODEL (b) EQUIVALENT WING (c) IMAGE SYSTEM

Figure 3 SLIPSTREAM AND EQUIVALENT WING AND IMAGE SYSTEM

the disturbance velocities are small in comparison with the freestream and slipstream velocities, Eq. (16) can be expanded in terms of the disturbance velocities to yield the first order boundary condition.

$$\frac{w_{y_e}}{U_e} = \frac{w_y'}{U'} \tag{17}$$

The condition that the pressure be constant across the boundary is obtained by applying Bernoulli's equation on both sides of the boundary and by expanding these relations in terms of the disturbance velocities to obtain the first order boundary condition,

$$U_e w_{x_e} = U' w_x' \tag{18}$$

The boundary conditions, Eq. (17) and (18), are to be satisfied by calculating the disturbance velocities at the boundaries from the original wing and its image system, Fig. 3C, and by calculating the disturbance velocities at the boundaries from the equivalent system, Fig. 3b, and using these in the boundary conditions to determine the constants, γ_L, γ_T, γ_L', and γ_T'. These constants fix the lift and the thickness of the images and the equivalent wing, and if these are such as to satisfy the boundary conditions, the image system duplicates the effects of the slipstream boundary. It can then be used to calculate the disturbance velocities at the original airfoil position due to the presence of the slipstream boundary.

Using a suitable model for the lifting wing with thickness, the slipstream boundary effects can be calculated. Tsien's model (Eq. 12) could be employed in this calculation; however, because this model consists of only a vortex, a pair

of dipoles, and a pair of quadripoles, it breaks down in regions close to the airfoil. Instead, the model used here will be a source and sink model with a length equal to the airfoil chord to simulate the effects of airfoil thickness, and a single vortex located at the airfoil quarter chord to simulate the effects of airfoil lift. The disturbance stream functions for each of these models are

$$\psi_1(\alpha) = \frac{L}{4\pi\rho U_0} \ln(x^2+y^2) \tag{19}$$

$$\psi_1(a_0) = \frac{\Lambda}{2\pi} \tan^{-1}\left(\frac{2ys}{\xi^2+y^2-s^2}\right) \tag{20}$$

where Λ is the strength of the source and sink, s is their spacing, and $\xi = x - \frac{c}{4}$. In order to be consistent with the preceding development, it is assumed that the airfoil thickness ratio is small so that only the first order thickness terms are retained. With this approximation the disturbance velocities from the images follow

$$\frac{\partial}{\partial y}\psi_1(\alpha) = \frac{L}{2\pi\rho U_0} \frac{y}{x^2+y^2} \tag{21}$$

$$\frac{\partial}{\partial x}\psi_1(\alpha) = -\frac{L}{2\pi\rho U_0} \frac{x}{x^2+y^2} \tag{22}$$

$$\frac{\partial}{\partial y}\psi_1(a_0) = \frac{U_0 c^2 \gamma}{2\pi}\left\{\frac{\xi^2-y^2-(c/2)^2}{\left[\xi^2+y^2-(c/2)^2\right]^2+y^2c^2}\right\} \tag{23}$$

$$\frac{\partial}{\partial x}\psi_1(a_0) = \frac{U_0 c^2 \gamma}{\pi} \frac{\xi y}{\left[\xi^2+y^2-(c/2)^2\right]^2+y^2c^2} \tag{24}$$

The question arises as to where on the airfoil the corrections to be obtained with Eqs. (21-24) are to be applied. The form of the relations demonstrates

that the effect of the boundary is to subject the airfoil to a disturbance field which varies along the chord. Hence, the airfoil is in a curved flow field, or equivalently, the airfoil characteristics will be those of a cambered section. There are a number of techniques normally employed to account for this variation. In particular, the lift is taken to be known and the angle of attack is to be obtained. One could average the appropriate relations to obtain the average longitudinal disturbance velocity, an average angle of attack correction, and an average camber or flow curvature correction. The method used here to account for the lateral component of the disturbance velocity is that originated by Pistolesi[11] and used in the Weissinger lifting line theory[12]. It is shown that for two-dimensional thin wings with circular arc camber, the wing characteristics are predicted exactly if the wing boundary conditions are satisfied at the 75% chord station. The use of this criterion in the present problem is equivalent to assuming that the flow curvature at the wing has a constant radius of curvature.

With regard to the longitudinal component of the disturbance velocity, it is noted that a weighted average value should be used. It is assumed here that this average value can be approximated with the disturbance velocity at the airfoil quarter chord.

Returning to the application of the boundary conditions at the slipstream edge, these are applied by calculating the disturbance velocities at the slipstream boundary using Eqs. (21-24), the image system (Fig. 3c), and the equivalent wing (Fig. 3b). These disturbance velocities must then satisfy Eqs. (17) and (18). After some algebraic manipulations it follows that the boundary conditions are satisfied for:

$$\nu_L = \frac{1 - \left(\frac{U'}{U_e}\right)^2}{1 + K_1\left(\frac{U_1}{U_e}\right)^2} \qquad \nu_L' = (1 - \nu_L)\frac{U_e}{U_o} \tag{25}$$

$$\nu_T = \frac{1-\left(\frac{U'}{U_e}\right)^2}{1+K_s+\left(\frac{U'}{U_e}\right)^2} \qquad \nu_T' = (1+\nu_T)\frac{U_o}{U_e} \tag{26}$$

where

$$K_1 = 1+2(1-\epsilon)^2\left\{\sum_{n=1}^{\infty}\frac{1}{(4n-1+\epsilon)^2}+\sum_{n=1}^{\infty}\frac{1}{(4n+1-\epsilon)^2}\right\} \tag{27}$$

$$K_s = \left[\frac{1}{2}+2\eta^2(1-\epsilon)\right]^2\left\{\sum_{n=1}^{\infty}\frac{1}{\frac{1}{4}+\eta^2(4n-1+\epsilon)^2}+\sum_{n=1}^{\infty}\frac{1}{\frac{1}{4}+\eta^2(4n+1-\epsilon)^2}\right\} \tag{28}$$

and $\epsilon = \delta/H$, $\eta = H/c$.

The slipstream boundary interference on the wing is expressed as a change in angle of attack and stream velocity. These are calculated from the geometry of Fig. 3 using Eqs. (21-24), and employing the substitution from thin airfoil theory, $\tau = a_o$, $\alpha = \frac{C_L}{2\pi}$.

$$\frac{\Delta\alpha}{\nu_L C_L} = -\frac{1}{8\pi}\left\{\sum_{n=1}^{\infty}\frac{1}{\frac{1}{4}+4\eta^2(2n-1-\epsilon)^2}+\sum_{n=1}^{\infty}\frac{1}{\frac{1}{4}+4\eta^2(2n-1+\epsilon)^2}+2\sum_{n=1}^{\infty}\frac{1}{\frac{1}{4}+4\eta^2(2n)^2}\right\} \tag{29}$$

$$\frac{\Delta\alpha}{\nu_T\tau} = -\frac{1}{4\pi}\left\{\sum_{n=1}^{\infty}\frac{2\eta(2n-1-\epsilon)}{\left[4\eta^2(2n-1-\epsilon)^2-3/16\right]^2+4\eta^2(2n-1-\epsilon)^2}-\sum_{n=1}^{\infty}\frac{2\eta(2n-1+\epsilon)}{\left[4\eta^2(2n-1+\epsilon)^2-3/16\right]^2+4\eta^2(2n-1+\epsilon)^2}\right\} \tag{30}$$

$$\frac{w_x/U_o}{\nu_L C_L} = -\frac{1}{8\pi\eta}\sum_{n=1}^{\infty}\left\{\frac{1}{2n-1-\epsilon} - \frac{1}{2n-1+\epsilon}\right\} \tag{31}$$

$$\frac{w_x/U_o}{\nu_T \tau} = -\frac{1}{2\pi}\left\{\sum_{n=1}^{\infty}\frac{4\eta^2(2n-1-\epsilon)^2 + 3/16}{[4\eta^2(2n-1-\epsilon)^2 - 3/16]^2 + 4\eta^2(2n-1-\epsilon)^2}\right.$$

$$+\sum_{n=1}^{\infty}\frac{4\eta^2(2n-1+\epsilon)^2 + 3/16}{[4\eta^2(2n-1+\epsilon)^2 - 3/16]^2 + 4\eta^2(2n-1+\epsilon)^2} \tag{32}$$

$$\left.+2\sum_{n=1}^{\infty}\frac{4\eta^2(2n)^2 + 3/16}{[4\eta^2(2n)^2 - 3/16]^2 + 4\eta^2(2n)^2}\right\}$$

The results given by Eqs. (25-32) can be used in conjunction with an appropriate theory for a wing in a shear flow of infinite extent to predict the two-dimensional slipstream boundary interference. This is done by noting that the lift can be expressed as

$$L = \rho/2\ U^2 c\left[\left(\frac{\partial C_L}{\partial \alpha}\right)(\alpha + \Delta\alpha) + C_{L_s}\right] \tag{33}$$

where C_{L_s} is the theoretical lift increment due to shear, camber, and thickness, $\frac{\partial C_L}{\partial \alpha}$ is the theoretical lift curve slope, α is the geometric angle of attack, $\Delta\alpha$ is the angle of attack correction given by Eqs. (29) and (30), and

$$U^2 \approx U_o^2\left[1 + 2\frac{w_x}{U_o}\right]$$

It follows that the corrected lift coefficient, C_{L_o}, based on the velocity, U_o, is given by the following quadratic equation

$$\left\{2\,\frac{\partial C_L}{\partial \alpha}\left(\frac{\Delta\alpha}{C_L}\right)\left(\frac{w_x/U_o}{C_L}\right)\right\}C_{L_o}^2+\left\{\left[1+2\left(\frac{w_x}{U_o}\right)_\tau\right]\frac{\partial C_L}{\partial \alpha}\left(\frac{\Delta\alpha}{C_L}\right)+2\left(\frac{w_x/U_o}{C_L}\right)\left[\left(\frac{\partial C_L}{\partial \alpha}\right)\alpha\right.\right.$$

$$\left.\left.+C_{L_s}+\left(\frac{\partial C_L}{\partial \alpha}\right)\Delta\alpha_\tau\right]-1\right\}C_{L_o}+\left[1+2\left(\frac{w_x}{U_o}\right)_\tau\right]\left[\left(\frac{\partial C_L}{\partial \alpha}\right)\alpha+C_{L_s}+\left(\frac{\partial C_L}{\partial \alpha}\right)\Delta\alpha_\tau\right]=0 \tag{34}$$

In Eq. (34) the subscript, τ , denotes the corrections obtained from Eq. (30) or (32), and the terms, $\frac{w_x/U_o}{C_L}$ and $\frac{\Delta\alpha}{C_L}$, are obtained respectively from Eq. (31) and (29).*

Similarly the pitching moment can be resolved into a component independent of lift and a component due to C_L acting at the aerodynamic center.

$$M=\rho/2\;U^2c^2\,C_{M_{a.c.}}+x_{a.c.}\;\rho/2\;U_o^2\,c\,C_{L_o} \tag{35}$$

yielding the following for the pitching moment coefficient, C_{M_o} , based upon the velocity, U_o .

$$C_{M_o}=\left[1+2\left(\frac{w_x}{U_o}\right)_\tau\right]\;C_{M_{a.c.}}+\left[\frac{x_{a.c.}}{c}+2\left(\frac{w_x/U_o}{C_L}\right)C_{M_{a.c.}}\right]C_{L_o} \tag{36}$$

where $C_{M_{a.c.}}$ and $x_{a.c.}$ are the theoretical moment coefficient about the

---

* It should be noted that Eq. (34) can be simplified considerably if the boundary corrections are small. In this case the products of the corrections can be neglected to yield

$$C_{L_o}=\left(\frac{\partial C_L}{\partial \alpha}\right)\Delta\alpha_\tau+\left[\left(\frac{\partial C_L}{\partial \alpha}\right)\alpha+C_{L_s}\right]\left[1+2\left(\frac{w_x}{U_o}\right)_\tau+2\left(\frac{w_x/U_o}{C_L}\right)\left(\frac{\partial C_L}{\partial \alpha}\alpha+C_{L_s}\right)+\left(\frac{\partial C_L}{\partial \alpha}\right)\left(\frac{\Delta\alpha}{C_L}\right)\right]$$

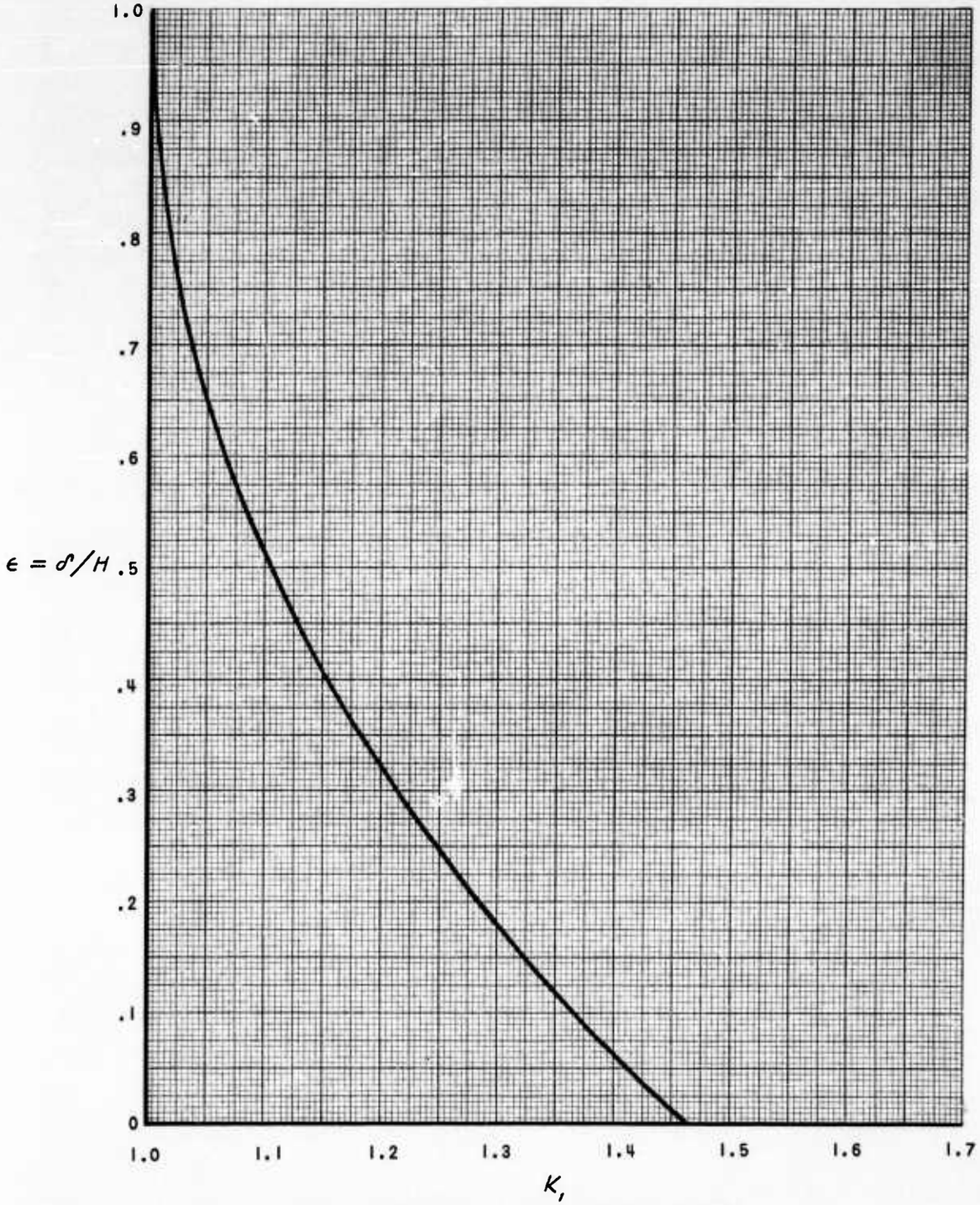

Figure 4 STRENGTH OF LIFTING IMAGE SYSTEM

aerodynamic center and the theoretical center of pressure position.

The slipstream boundary corrections given by Eqs. (27-32) have been calculated for typical slipstream heights on a high speed computing machine using the first 100 terms, and are plotted in Fig. (4) through (9) as a function of the airfoil location in the slipstream. It should be noted that the method of images does not apply in the limit of the airfoil located at the boundary. Moreover, the models used in the image system are inapplicable in the vicinity of the boundary.

Considering Figs.(6) and (7), it is seen that one effect of the boundary is to cause a change in the slipstream velocity as the airfoil is moved off the centerline. The effects of this change in velocity would appear as non-linear airfoil characteristics. Considering a typical slipstream, the boundary interference causes a decrease in stream velocity and hence a loss in lift. This effect is minimized at the slipstream centerline where the lift effect is zero (Fig. 6) and only the thickness effect (Fig. 7) enters. Since the lift effect is asymmetric about the slipstream axis while the thickness effect is symmetric, one could reduce this adverse effect to zero, or perhaps obtain a beneficial interference effect by locating the airfoil below the slipstream axis. The effect of decreasing the ratio of slipstream height to wing chord is to cause a further loss in lift.

Figures 8 and 9 show that another effect of the slipstream boundary is to adversely influence the lift by decreasing the wing angle of attack. This effect is also more pronounced for small H/c . At the slipstream axis, the effect of wing thickness vanishes and the effect of wing lift is a minimum. The thickness effect is asymmetric about the slipstream axis (Fig. 9) and the lift effect is symmetric (Fig. 8), suggesting that the two might cancel at

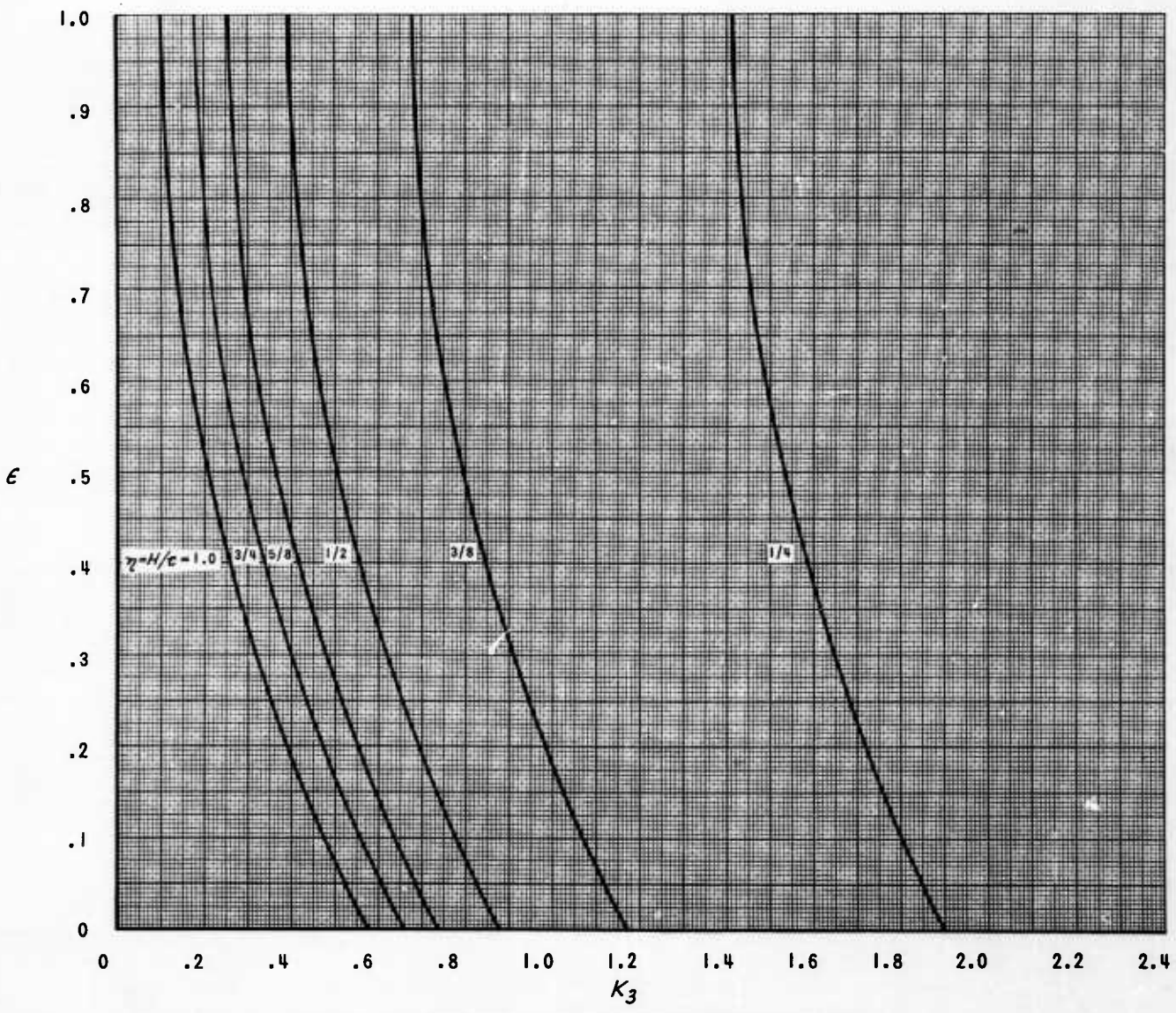

Figure 5 STRENGTH OF THICKNESS IMAGE SYSTEM

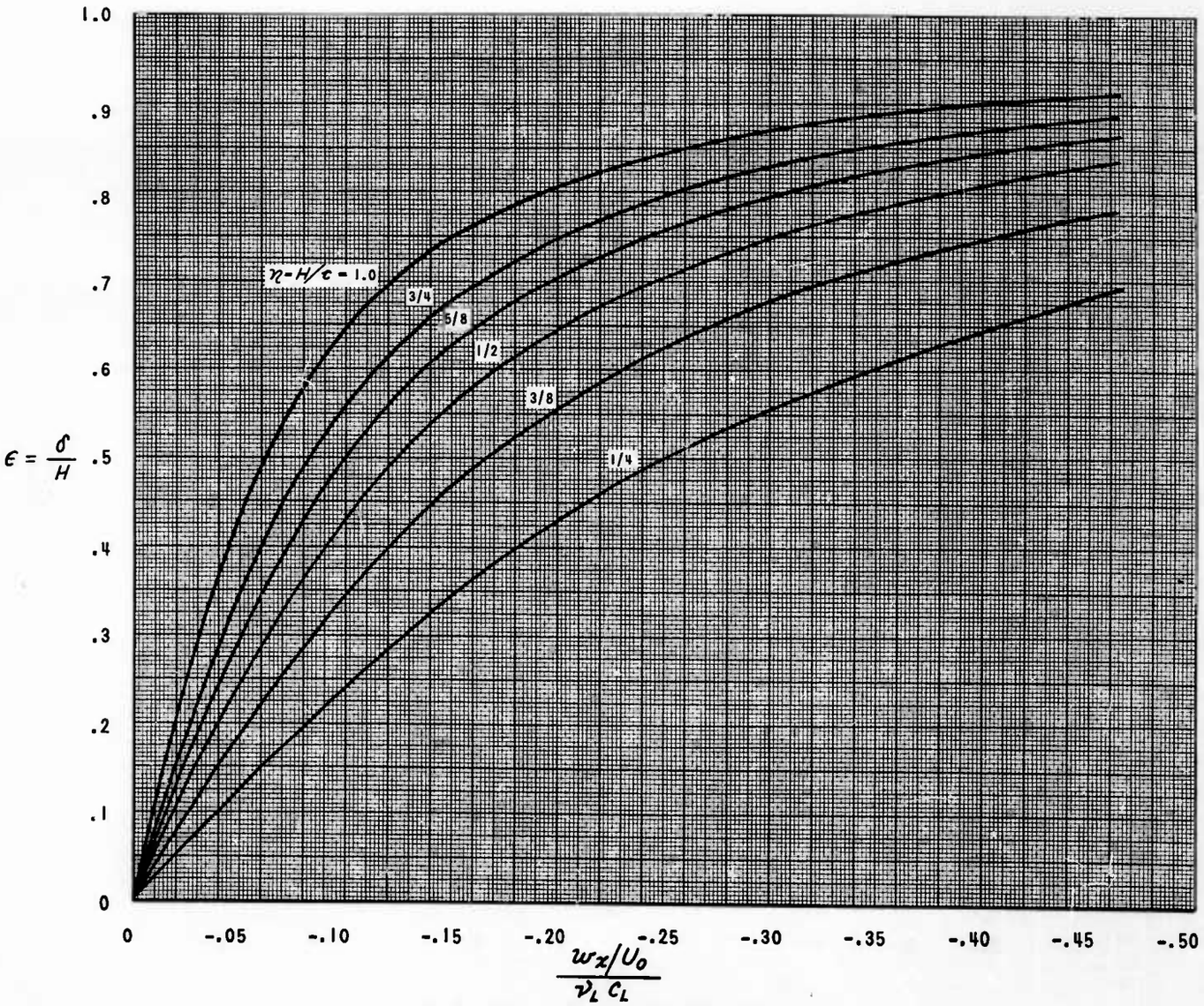

Figure 6 LONGITUDINAL DISTURBANCE VELOCITY DUE TO LIFT

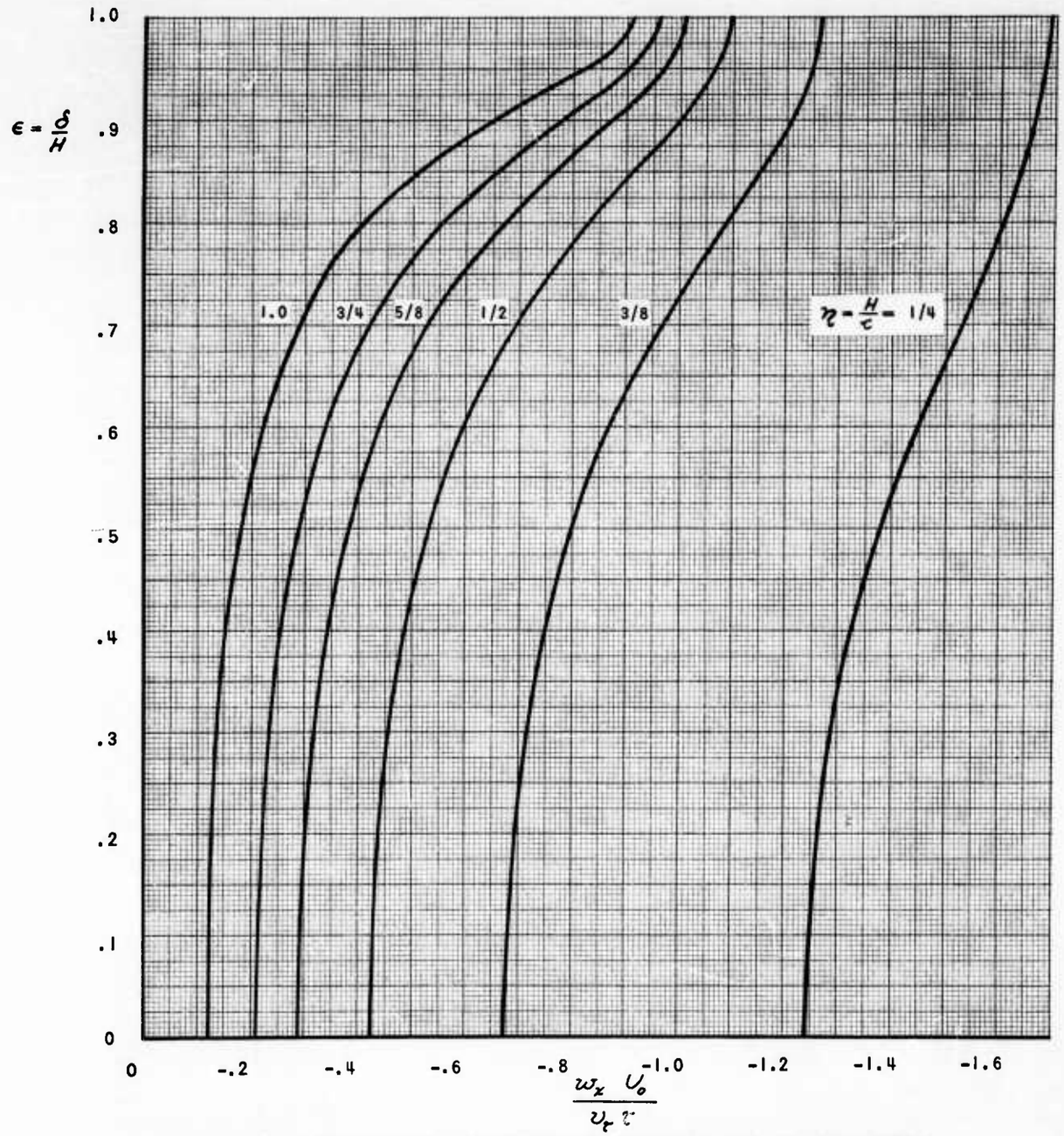

Figure 7 LONGITUDINAL DISTURBANCE VELOCITY DUE TO THICKNESS

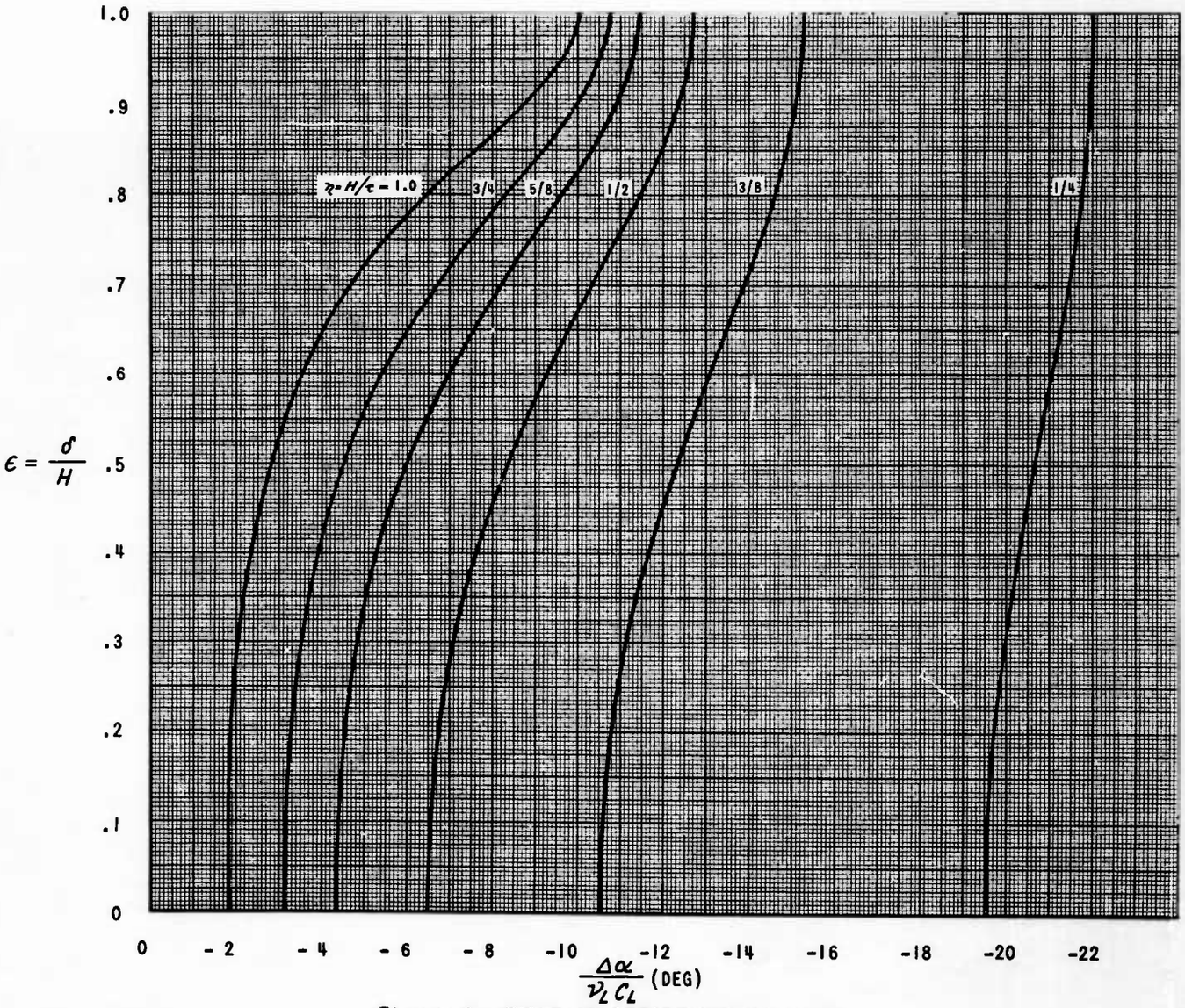

Figure 8 ANGLE OF ATTACK DUE TO LIFT

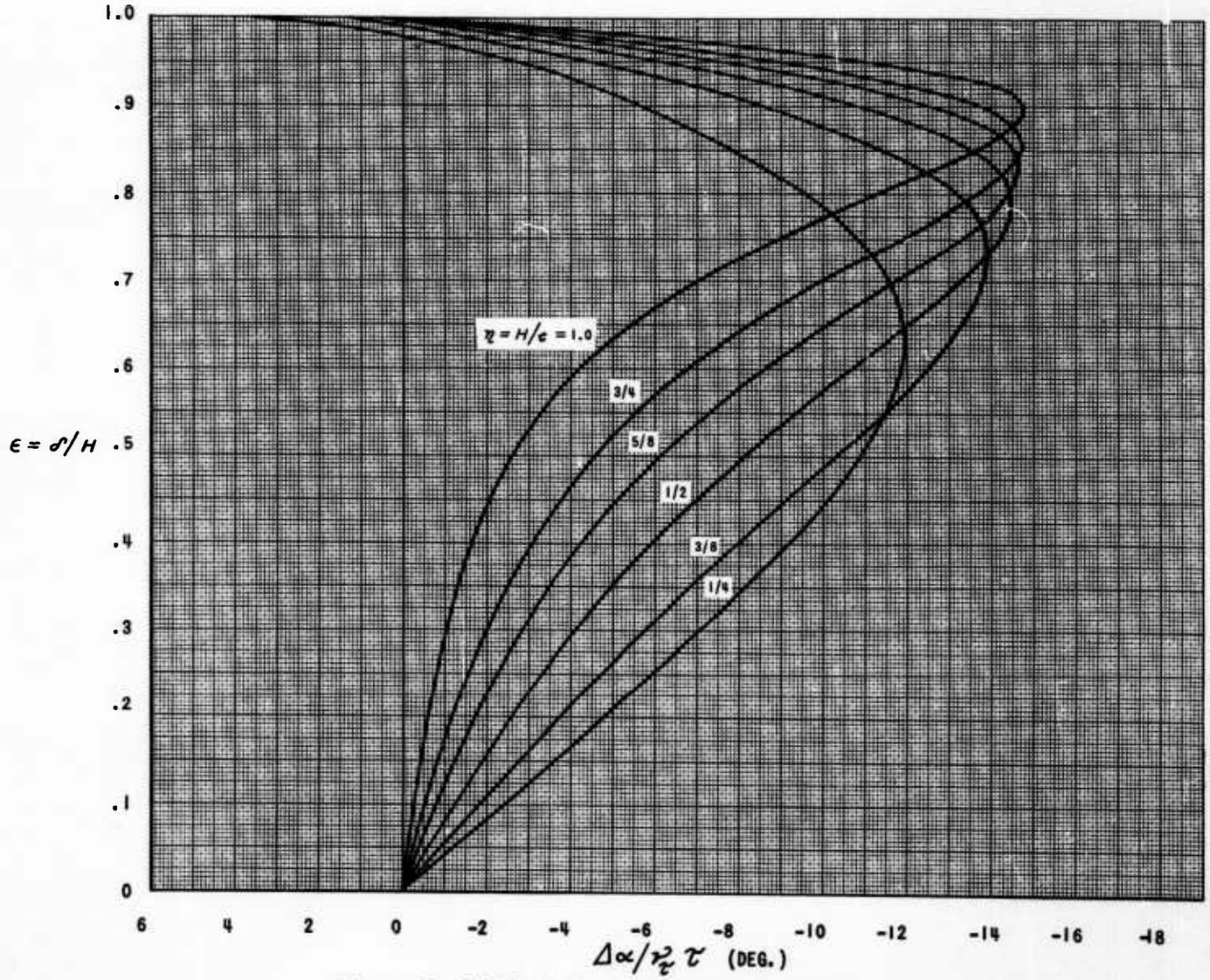

Figure 9 ANGLE OF ATTACK DUE TO THICKNESS

certain positions below the slipstream axis and for certain angles of attack. It should be noted, however, that the thickness effect is usually smaller than the lift effect so that beneficial interference from the boundary is unlikely.

EXPERIMENT

An experimental program of research is in progress at the Cornell Aeronautical Laboratory and is devoted to investigating the aerodynamics of airfoils in non-uniform flows. The specific aim of this research is first to check the theory for wings in uniform shear, and then to extend these results to the case of two-dimensional and axially-symmetric slipstreams. The research on two-dimensional airfoils in a flow with uniform shear and in simulated two-dimensional slipstreams is largely completed, and the results are presented here.

The test flows used in this program were (1) a uniform flow, (2) a flow with small uniform shear, (3) a two-dimensional propeller-type slipstream with small shear and (4) its equivalent uniform slipstream, (5) a two-dimensional propeller-type slipstream with large shear and (6) its equivalent uniform slipstream. The equivalent uniform slipstream was defined as a two-dimensional slipstream of equal dimensions with a velocity equal to the average velocity in the non-uniform slipstream. The momentum in the uniform and non-uniform slipstreams were then roughly equivalent. These equivalent uniform slipstreams were included in the present research in order to obtain a check on the image analysis and to experimentally demonstrate the importance of shear in estimating section characteristics.

The experiments were conducted out in the subsonic leg[13] of the C.A.L. One Foot High Speed Wind Tunnel[14]. This leg of the wind tunnel, shown in Fig. 10, has a test section with a cross section of 17" x 24" and is operated as a closed throat non-return type tunnel. The wind tunnel operates at atmospheric stagnation pressure over a speed range of 0-180 f.p.s. The tunnel was modified for the present program to provide a longer test section.

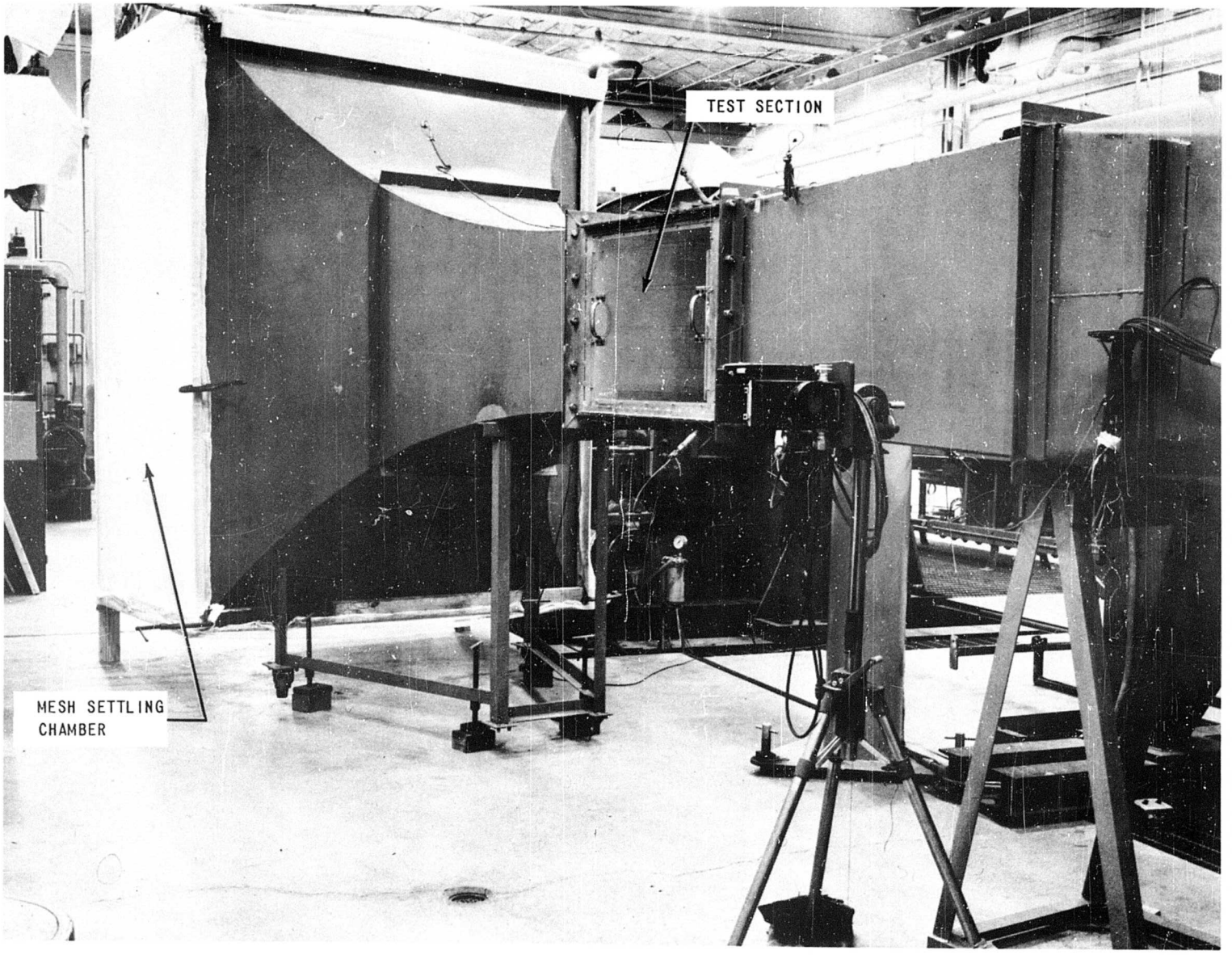

Figure 10 SUBSONIC WIND TUNNEL LEG

The test flows were generated by non-uniform screens or grids placed across the wind tunnel test section upstream of the model. In effect these screens produce the inverse of a propeller flow in that they remove energy from the free stream, and distribute the energy within the slipstream by selectively introducing losses. The advantages of this technique are that it affords a relatively simple method for generating two-dimensional propeller-like slipstreams and the test flows are easily repeated. Moreover, this technique can be used to generate axially-symmetric slipstreams and allows the systematic study of slipstream flow non-uniformities without the complication of the rotational flow component found in a propeller slipstream.

In designing the screens for producing a uniform or non-uniform shear flow, it must be noted that the static pressure immediately behind the screen is not constant over the screen because non-uniform losses are being introduced. Consequently, the flow expands from that at the screen to its final configuration, and it is not possible to simply extrapolate the desired velocity distribution back to the screen to determine the required screen losses.

Owen and Zienkiewicz[15] have considered the flow produced by a non-uniform screen and present a method for designing screens to produce a uniform shear. Their method is restricted to two-dimensional flows with a linear velocity gradient and to screens which only slightly perturb the flow. The present research is concerned with large non-uniform and discontinuous shear, and it was necessary to extend the theory of Ref. 15 to include these cases. This extension is presented in Appendix I.

This design method consists of postulating disturbance stream functions associated with the non-uniform screen which vanish at large distances from the screen. Further these disturbance functions are different on either side of

the screen and equal at the screen. It is required that the longitudinal velocity be continuous through the screen and that the vertical velocity change through the screen by a factor related to the local resistance of the screen. These two conditions then fix the screen disturbance stream function as a function of the desired velocity distribution. The requirement that the static pressure be uniform across the flow at large distances from the screen and that on any streamline the difference in total pressure be the local screen loss then relates the desired velocity distribution to the distribution of screen resistance.

Having fixed the distribution of resistance, the screen design then reduces to selecting the screen solidity necessary to produce the losses. It is assumed that the local losses in a non-uniform screen are identical to those of a uniform screen with the same solidity, and existing experimental data and empirical relations[16] were used. In designing the screens it was decided to consider solidities only in the range of 15%-85%. The lower limit was fixed by structural and fabrication considerations, while the upper limit was selected to insure that the screens would not choke. These limits then fixed the maximum shear that could be generated. Experience gained with the first screen tested indicated that the available screen resistance data and empirical formulas were not applicable to the non-uniform screens, apparently because of the high Reynolds numbers on the screen elements. It was found that for large solidities the screen resistance was greater than the published data. A series of experiments was made with high solidity screens made of large diameter wire to determine the loss coefficient at high Reynolds numbers. These results are compared in Fig. 11 with other data and the empirical relations for low and high solidities. The C.A.L. data is seen to agree well with the high solidity relation, $\frac{\Delta p}{\rho/2\ U^2} = \left(\frac{\sigma}{1-\sigma}\right)^2$. However, it was found that good agreement was obtained with the C.A.L. data and

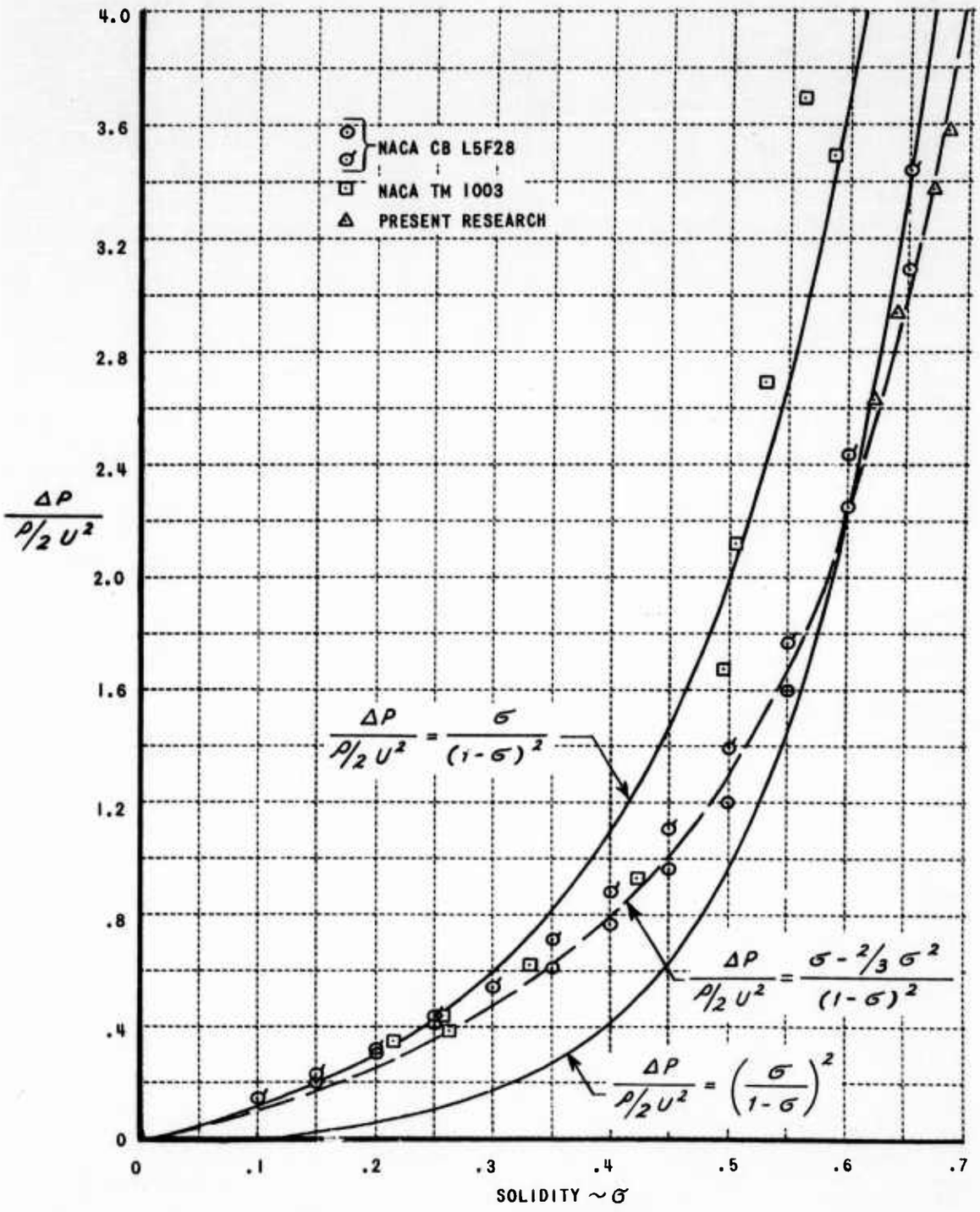

Figure II SCREEN RESISTANCE

that from Ref. 17 using the relation,

$$\frac{\Delta p}{\rho/2\ U^2} = \frac{\sigma - \frac{2}{3}\sigma^2}{(1-\sigma)^2} \qquad (37)$$

Equation (37) was then used in all subsequent screen designs.

The three screens used in the present research, shown in Figs. 12, 13 and 14, were constructed of 1/8" - 1/2" diameter bars spaced to provide the desired solidity, and supported in a steel frame. Early in the research it was found that in the regions of high solidity the observed velocity distribution differed markedly from the design value. This was attributed to the screen phenomenon investigated by von Bohl[18]. Immediately behind a screen the flow consists of alternate wakes from each screen element and high velocity jets from between the elements. At a sufficient distance from the screen, viscous mixing between the jets and wakes has taken place so that a uniform flow is obtained. von Bohl observed that at sufficiently high solidities, 37% - 46% for polygonal screen elements, the jets tend to close around the wakes without mixing, resulting in lower losses than anticipated.

It was concluded that this non-mixing phenomenon was occurring in the high solidity portions of the screens used in this research, and the metal honeycomb seen in Figs. 12 through 14 was added to the downstream side of the screens. This honeycomb, about two inches thick, locally constrains the flow behind the bars and allows mixing to begin. The honeycomb is bonded to the downstream side of the screen and also serves to stiffen the structure.

The uniform two-dimensional slipstreams were produced by using a uniform screen with an opening in it, and constraining the slipstream flow with metal plates. The gap size, screen resistance, and plate spacing were fixed by

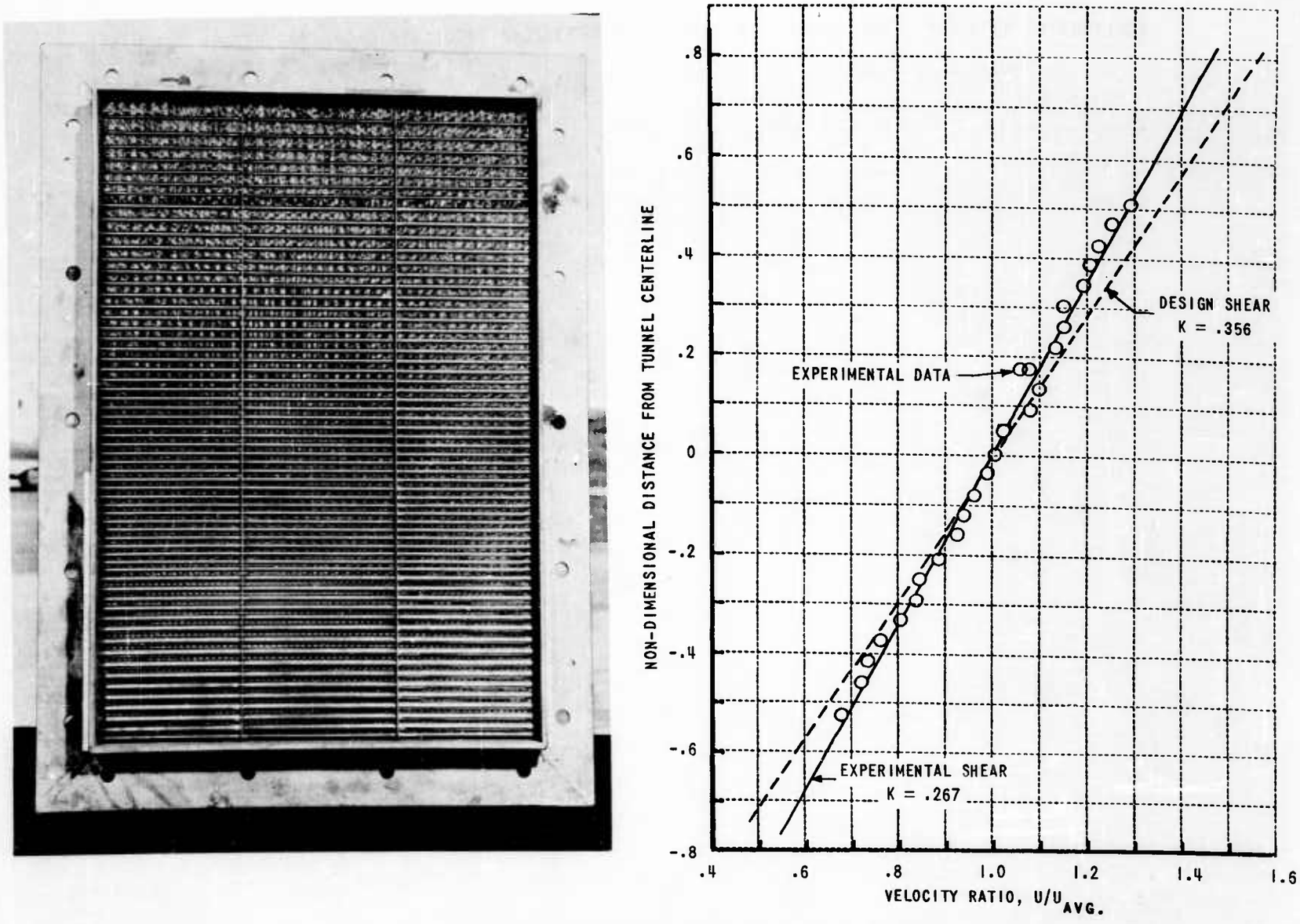

Figure 12 SCREEN FOR UNIFORM SHEAR AND FLOW CALIBRATION

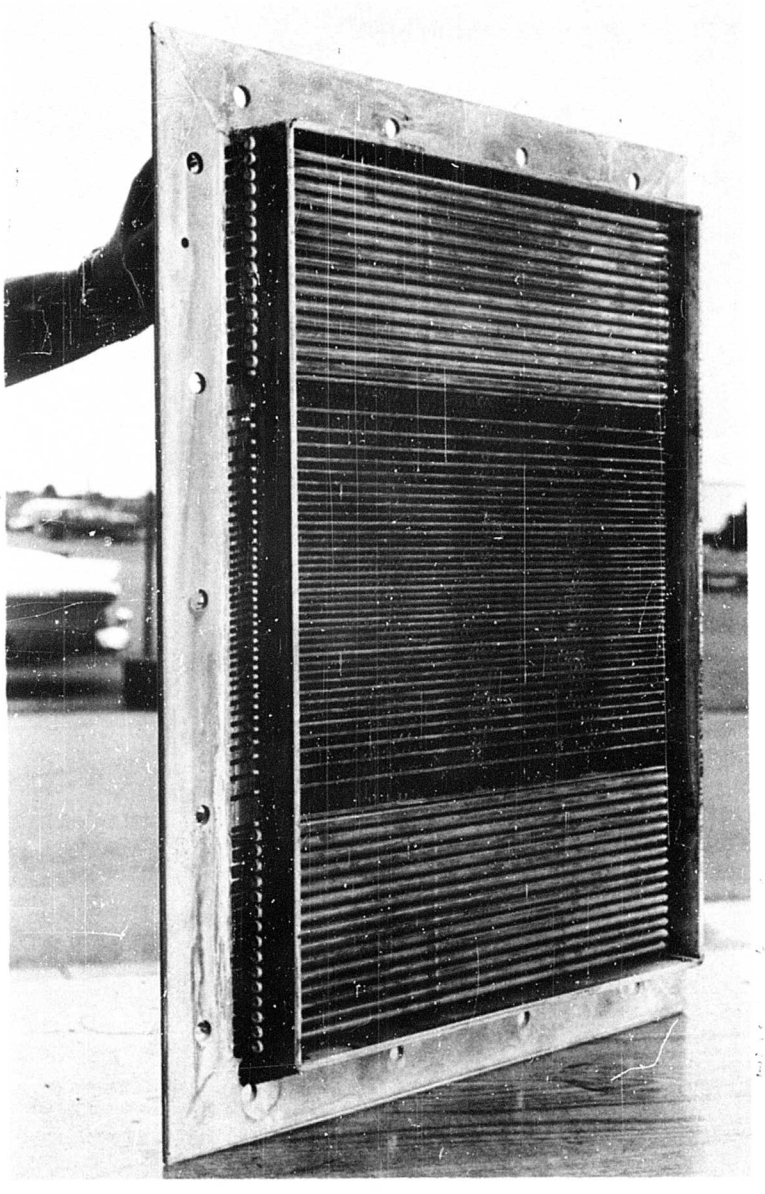

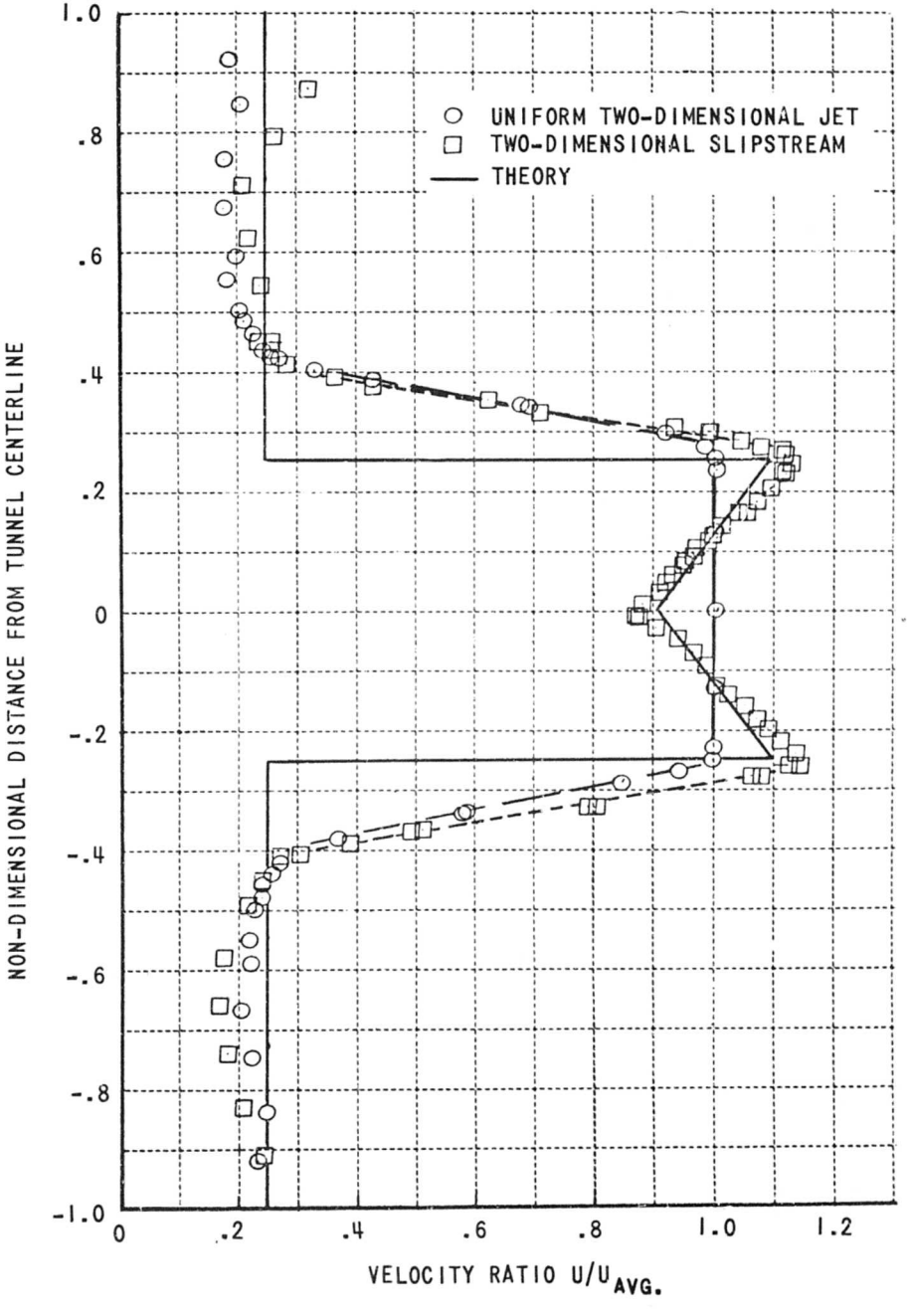

Figure 13 SCREEN FOR TWO-DIMENSIONAL PROPELLER SLIPSTREAM WITH SMALL SHEAR AND FLOW CALIBRATION

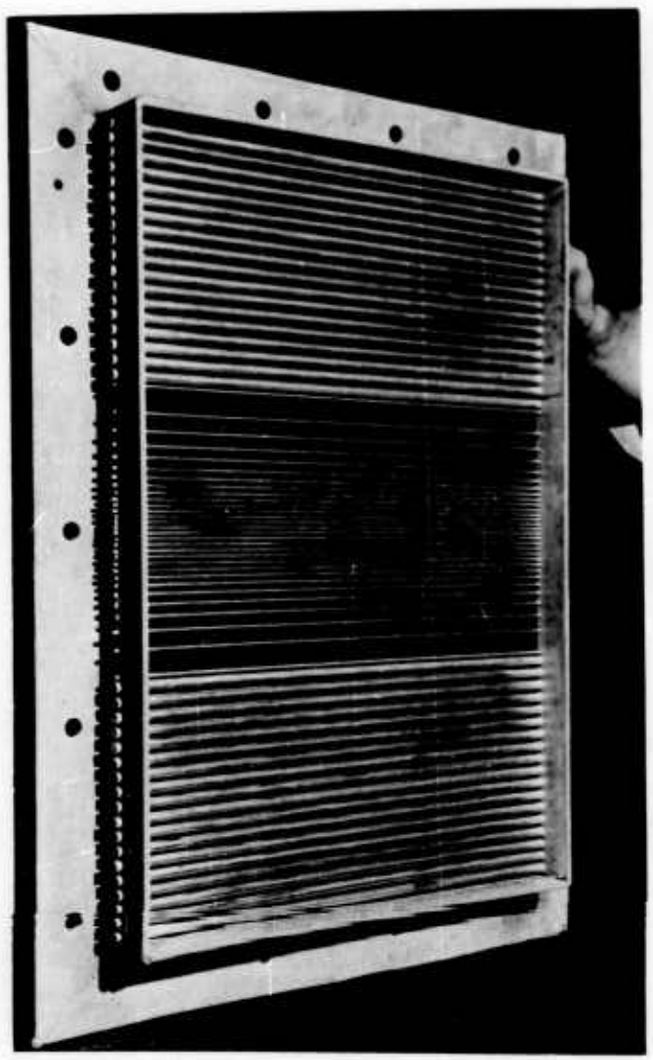

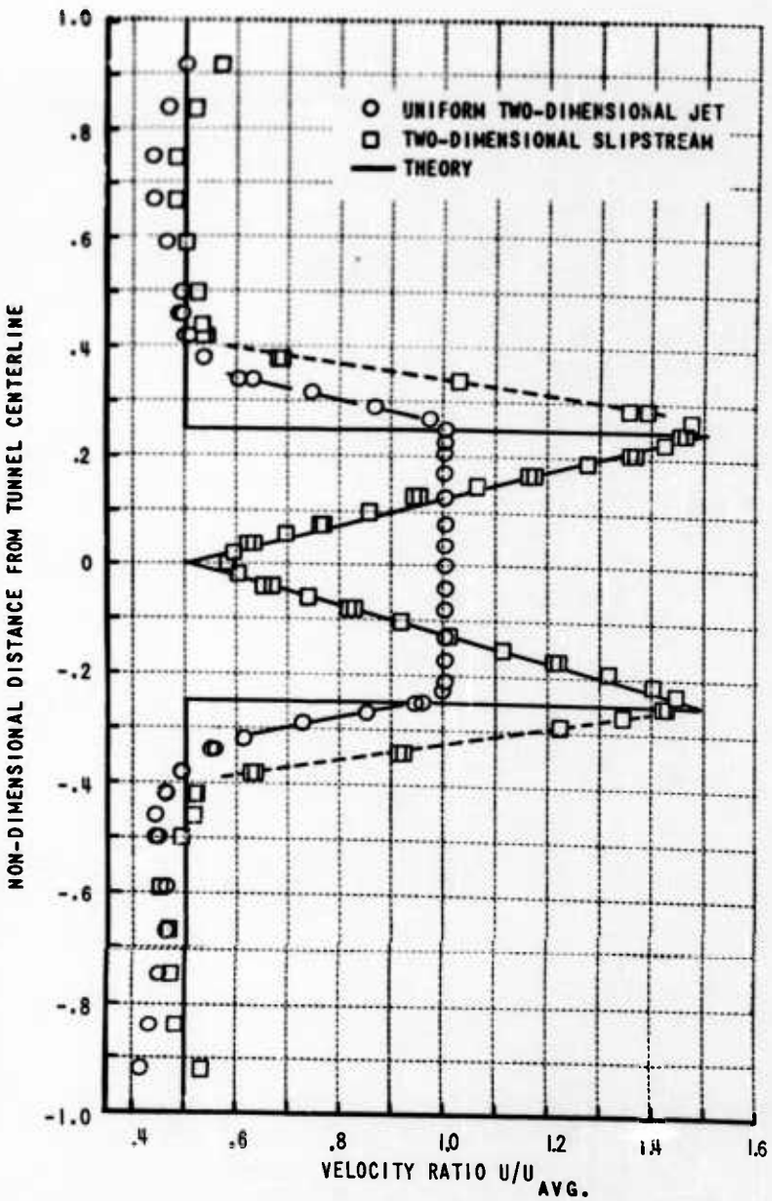

Figure 14 SCREEN FOR TWO-DIMENSIONAL PROPELLER SLIPSTREAM WITH LARGE SHEAR AND FLOW CALIBRATION

elementary mass flow considerations.

The initial calibrations of the flows simulating two-dimensional slipstreams showed that viscous mixing and the sharp change in static pressure along the initial portions of the slipstream edges resulted in a flow which did not meet with the design requirements. This difficulty was rectified by constraining the slipstreams with plates to a point about two airfoil chord lengths ahead of the test position. These plates allowed the slipstreams and external "free stream" to independently expand to the final design values.

All test flows were calibrated using a 3/16" diameter pitch-yaw pitot-static probe. The calibrations for the five test flows are shown in Figs. 12, 13, and 14. These data are not corrected for the shear flow displacement effect. The theory of Hall[19] shows that for the 3/16" diameter probe used in this research, the displacement of the stagnation point is less than 1/2% of the slipstream half-height and is negligible. The same theory shows, however, that the effect of shear on the probe is to distort the pressure distribution on the probe so that the usual pitch-yaw pressure probe will indicate flow angularity at zero angle of attack. This effect was negligibly small for the experiments in small shear, but amounted to a flow angularity error of about 1° for a shear rate of $k \approx 3$. The flow angularity data were corrected for this effect using Hall's theory.

The model used in this research was a two-dimensional Joukowsky airfoil of 17% thickness spanning the wind tunnel (Fig. 15 and 16). Anticipating future tests in an axially symmetric slipstream, the wing was constructed and instrumented to measure forces on a narrow section (a span of about 10% of the chord) of the wing at the midspan. A conventional three-component strain gage balance was used to measure the section lift, drag, and pitching moment. After assembly,

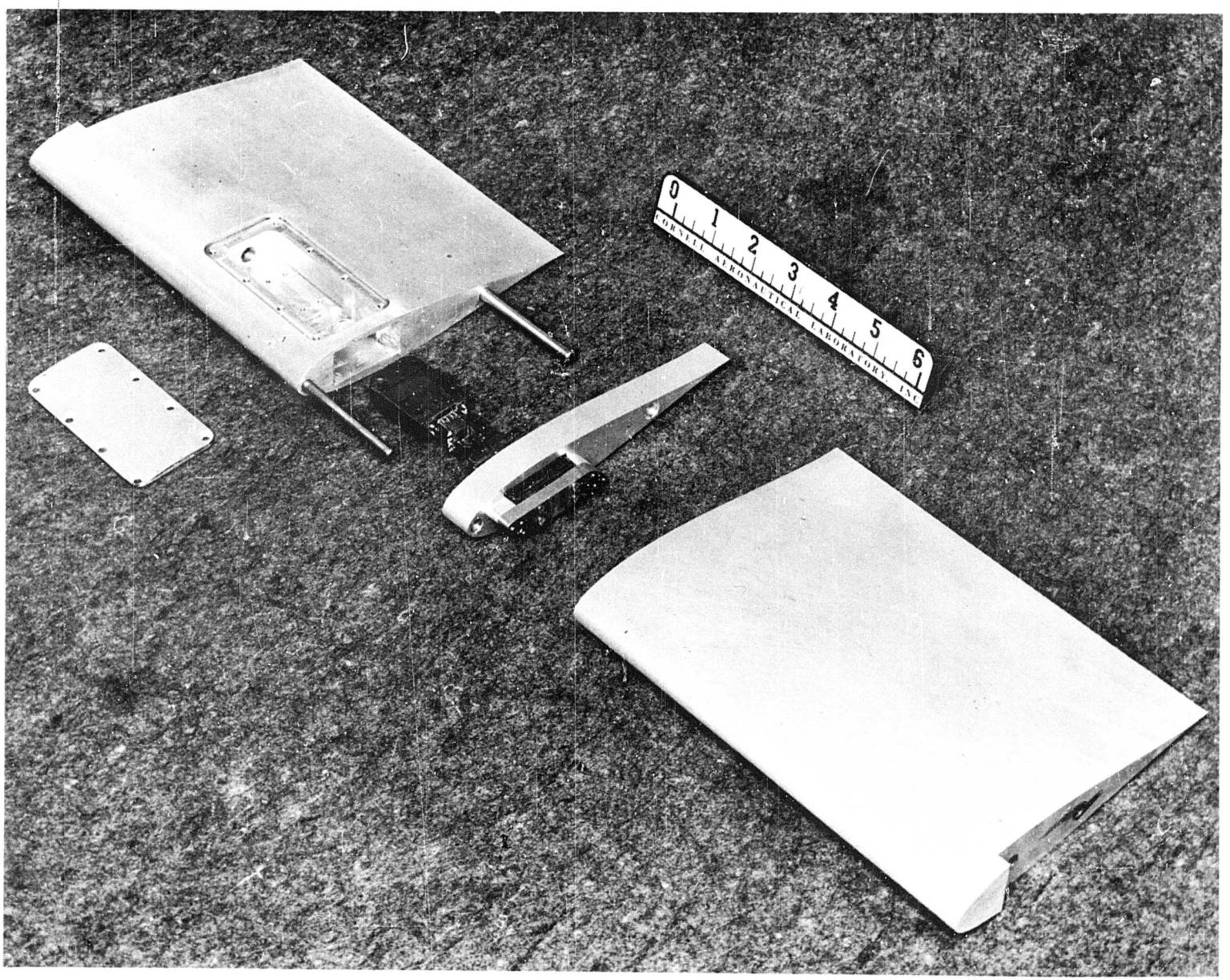

Figure 15 TWO-DIMENSIONAL AIRFOIL MODEL AND FORCE BALANCE

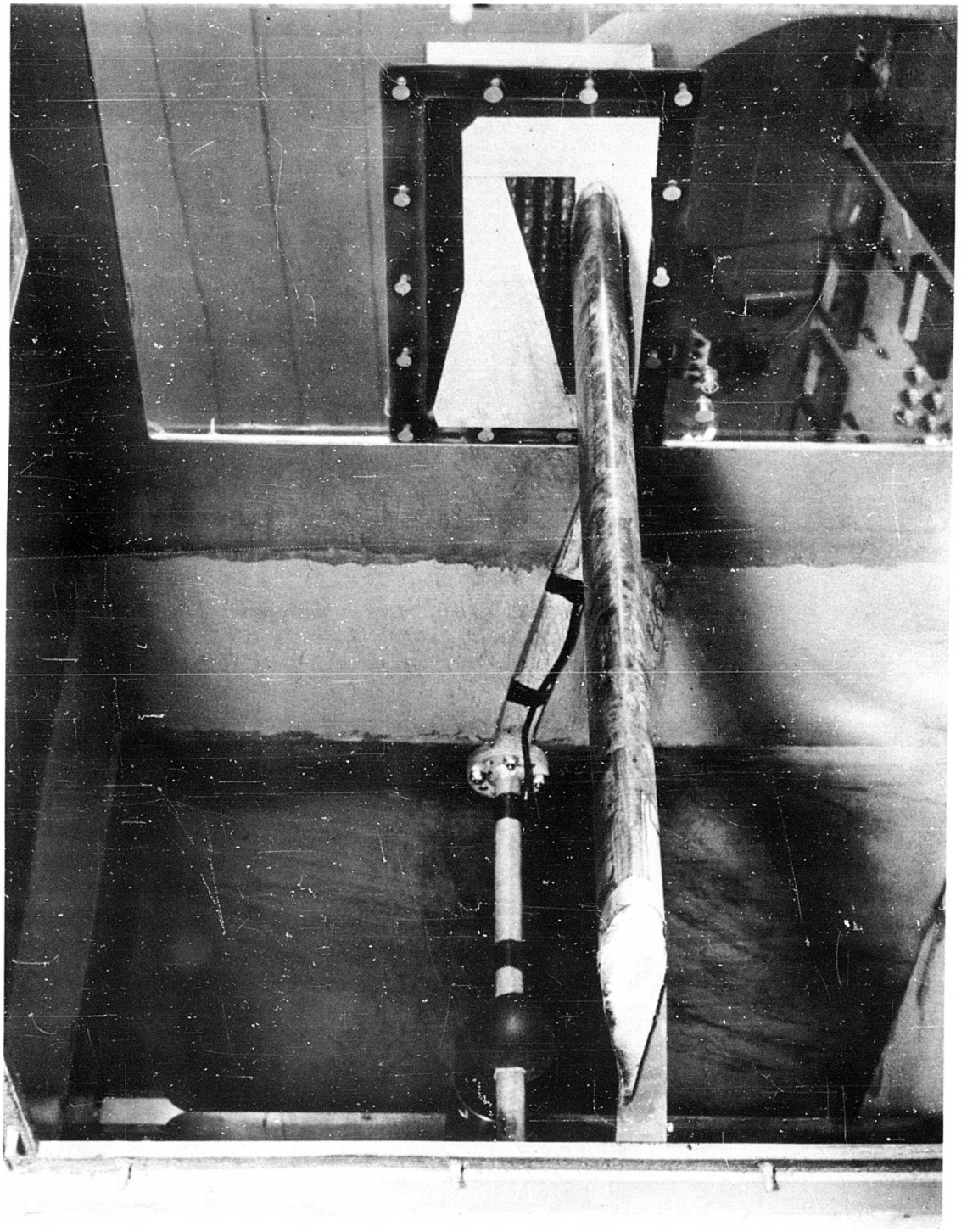

Figure 16 TWO-DIMENSIONAL AIRFOIL MODEL IN TUNNEL

the entire wing was wrapped with .005" thick sheet rubber to prevent flow between the sections of the wing. The balance system was then calibrated with the sheet rubber in place.

The model was mounted in the wind tunnel on a yoke support (Fig. 16) on a conventional pitching system and was pitched about the airfoil midchord. The gaps between the wing edges and the wind tunnel walls were sealed with Insulite plastic foam. As shown in Fig. 16, provisions were made to bleed the tunnel side wall boundary layer in order to alleviate early wall boundary layer separation and its subsequent effects on the wing. The exact distribution of the wall porosity and suction settings were experimentally determined to maintain two-dimensional flow on the wing.

The experiments consisted of measuring the lift, drag, and pitching moment on the airfoil in uniform shear and at various vertical positions in the uniform and non-uniform two-dimensional slipstreams. In addition oil-film studies were made for certain conditions to investigate the boundary layer separation pattern.

RESULTS

Uniform Shear

The first of the experiments was to test the symmetric airfoil in uniform flow and in uniform shear flow (Fig. 9) in order to obtain a check on the theory for airfoils in uniform shear flow. These tests were run at an airspeed of 100 m.p.h. at the airfoil position, and the Reynolds number based on the airfoil chord was 4.5×10^5. The data were corrected using the conventional solid boundary corrections. It can be shown that for uniform shear flow in a wind tunnel, the solid boundary corrections apply. The lift and pitching moment data from these experiments are shown by the symbols in Fig. 17 and are compared with the appropriate theory. These data are referred to the undisturbed stream velocity at the airfoil position. The theory is seen to overestimate the slope of both the lift curve and the moment curve. This might be anticipated since Tsien's theory for airfoils in uniform shear flow reduces, in the limit of zero shear, to the classical thick airfoil theory including the thickness correction to the lift and moment curve slope. In other uniform flow experiments, a thickness effect on the slopes of the lift and moment curve has been observed, but of a magnitude less than that predicted by theory. This reduction in lift curve slope, presumably due to viscous effects, also occurs in shear flow.

The increments in lift and moment due to shear have been determined by fairing the experimental data and subtracting the lift and moment measured in uniform flow. This shear increment is plotted and compared with Tsien's theory at the bottom of Fig. 17. It can be seen that the theory and experiment are in good agreement at small angles of attack where the separation effects are small, thereby confirming the theory.

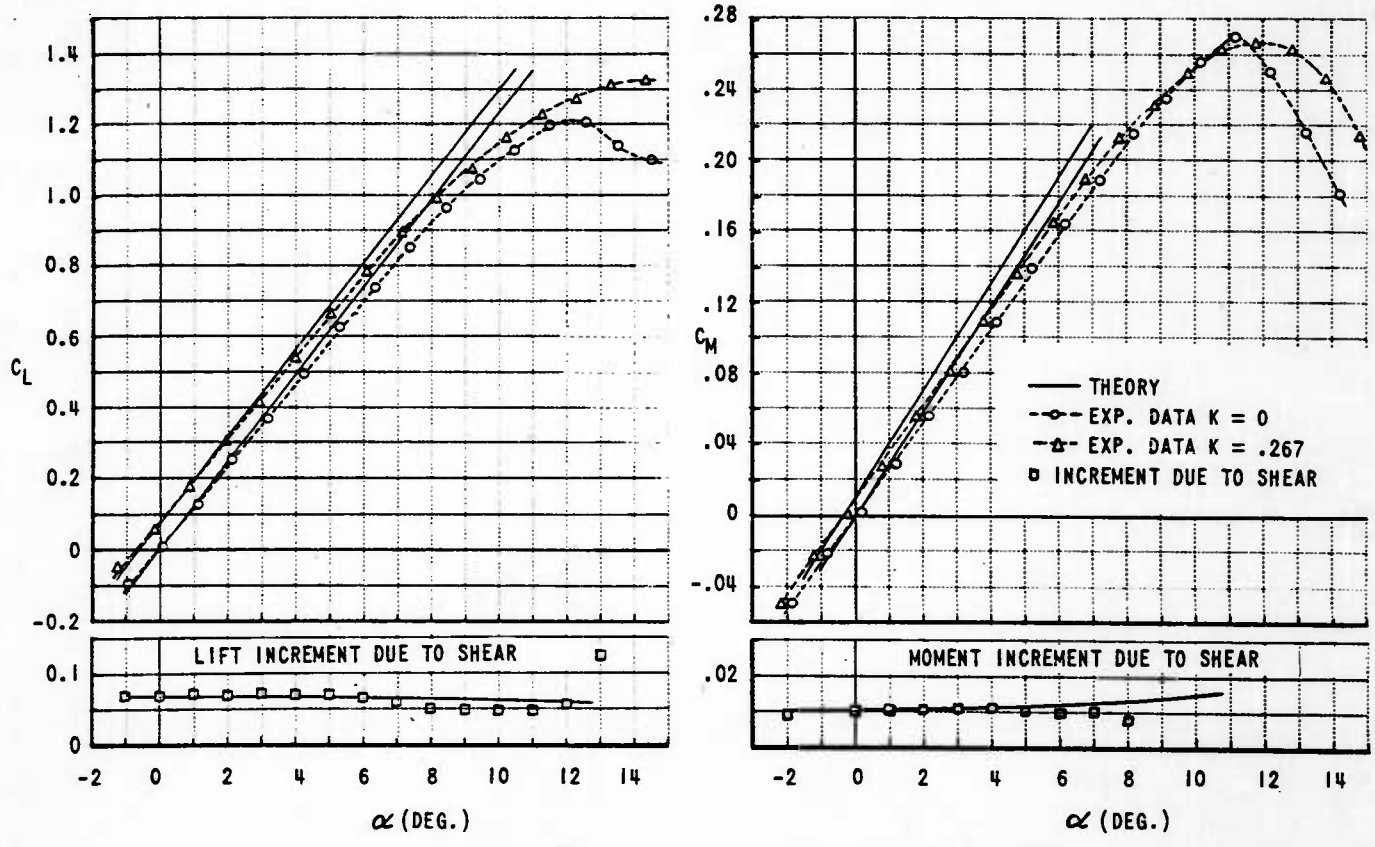

Figure 17 EFFECT OF UNIFORM SHEAR ON LIFT AND MOMENT

The drag measured on the airfoil in uniform flow and uniform shear flow is presented in Fig. 18. Considering the uniform flow data, it is seen that the drag coefficient at zero lift is $C_D \approx .0075$ which is in good agreement with flat plate laminar skin friction theory when adjusted for thickness effects. The data obtained in uniform shear flow indicate a drag coefficient of about $C_D \approx .002$; much less than predicted by laminar theory. Tsien's theory shows that there is no drag due to lift for two-dimensional sections in uniform shear flow, so that the observed drag reduction in shear flow must stem from an effect on skin friction.

The effects of shear on flat plate laminar skin friction have been recently investigated by Li[20,21], by Glauert[22], and by Ting[23], and it is demonstrated that the effect of positive shear is to cause an increase in laminar skin friction. Applying these results to the present research, one would expect the drag on the airfoil upper surface to be increased by about 3%, but the drag on the lower surface would be decreased a comparable amount since it is in negative shear. Hence, the theory shows no net change in drag on the airfoil.

It is believed that the observed drag behavior is associated with the method used in generating the shear flow. In particular, the flow is generated by a screen composed of thick bars which introduce turbulence into the stream. It appears that this turbulence is such as to cause a marked decrease in viscous drag. As a check on this hypothesis, the airfoil was tested in a stream with a uniform high solidity screen at the normal position of the shear screen. This uniform screen was constructed of 1/16" diameter wire, crudely corresponding to the elements of a shear screen, and only introduced turbulence in the stream. The drag data obtained under these conditions was about half that obtained in a uniform flow without artificial turbulence, and showed that screen-induced

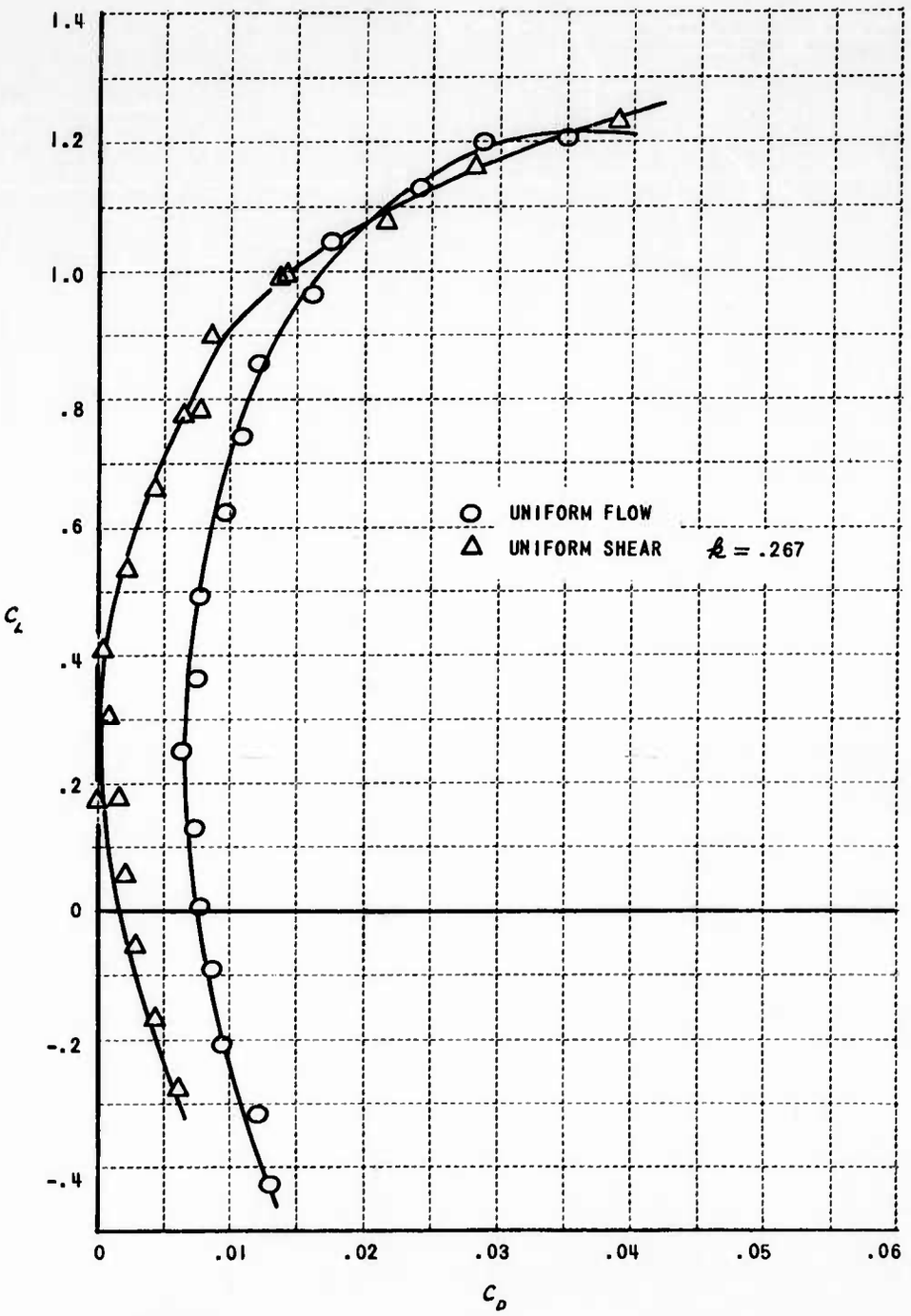

Figure 18 EFFECT OF UNIFORM SHEAR ON DRAG

turbulence is primarily responsible for the low drags observed in shear flow.

Slipstream with Large Shear

Following this confirmation of uniform shear theory, a series of experiments was made with the symmetric Joukowsky airfoil in the $k = 2$ two-dimensional slipstream (Fig. 14). These experiments consisted of measuring the forces on the model at four positions in the slipstream, and the results are shown in Fig. 19. The force and moment coefficients are based upon the undisturbed stream velocity at the airfoil position and have been corrected for tunnel wall interference using the results of Appendix II. The drag data are not presented because they reflect the unusual influence of screen-induced turbulence.

The experimental data are compared in Fig. 19 with Jones' theoretical results for airfoils in non-uniform shear flow and with Tsien's results for airfoils in uniform shear flow. Considering the data obtained on the slipstream plane of symmetry (Fig. 19a), it can be seen that the slipstream boundary corrections bring the theory and experiment into rather good agreement. Indeed, the agreement is quite surprising since Jones' theory is valid only for small values of the stream shear derivative, q, while the experimental slipstream corresponded to a value of $q \approx 1.7$. The non-zero lift observed at zero angle of attack reflects the fact that the airfoil was not located precisely on the plane of symmetry. This lift increment at zero angle of attack is analogous to that observed with airfoils in uniform shear flow and should be proportional to the airfoil thickness. This thickness effect is not predicted by Jones, apparently because his analysis is restricted to thin airfoils and small values of the shear parameter, q, and products of the thickness and q were neglected.

The most notable feature of the data in Fig. 19a is that a lift coefficient in excess of 3.0 was measured without any apparent signs of airfoil stalling.

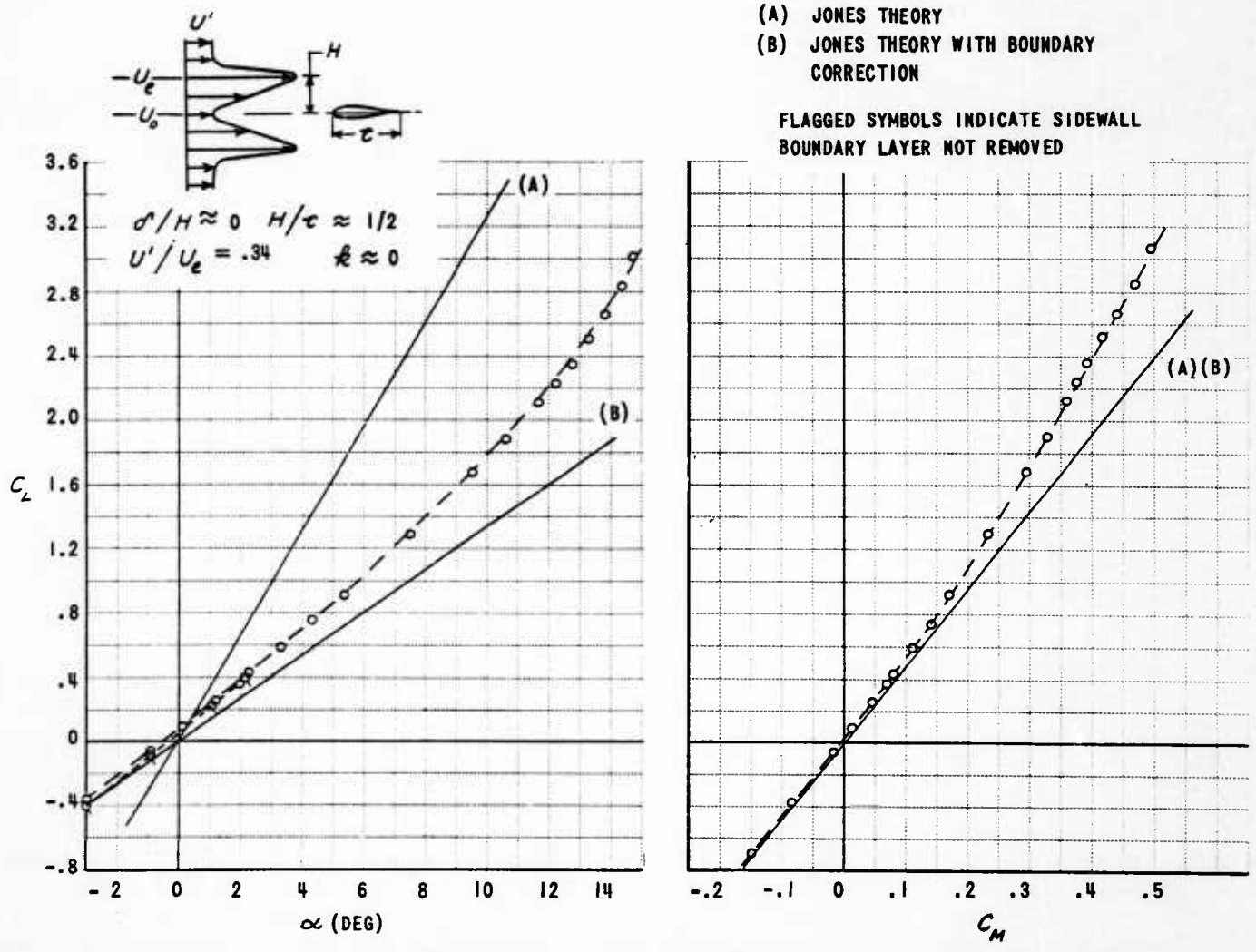

Figure 19a LIFT AND MOMENT IN A TWO-DIMENSIONAL SLIPSTREAM WITH LARGE SHEAR

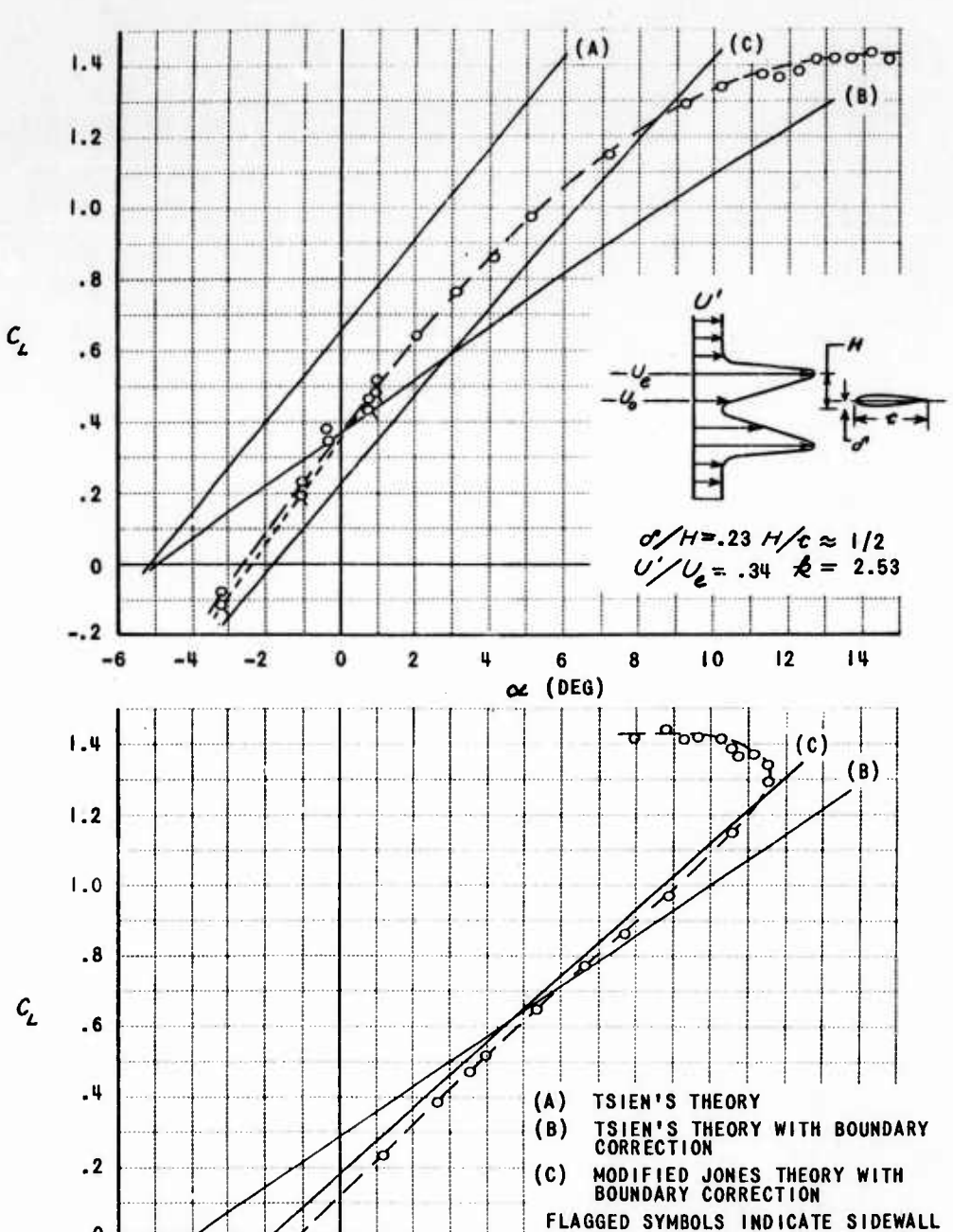

Figure 19b LIFT AND MOMENT IN A TWO-DIMENSIONAL SLIPSTREAM WITH LARGE SHEAR

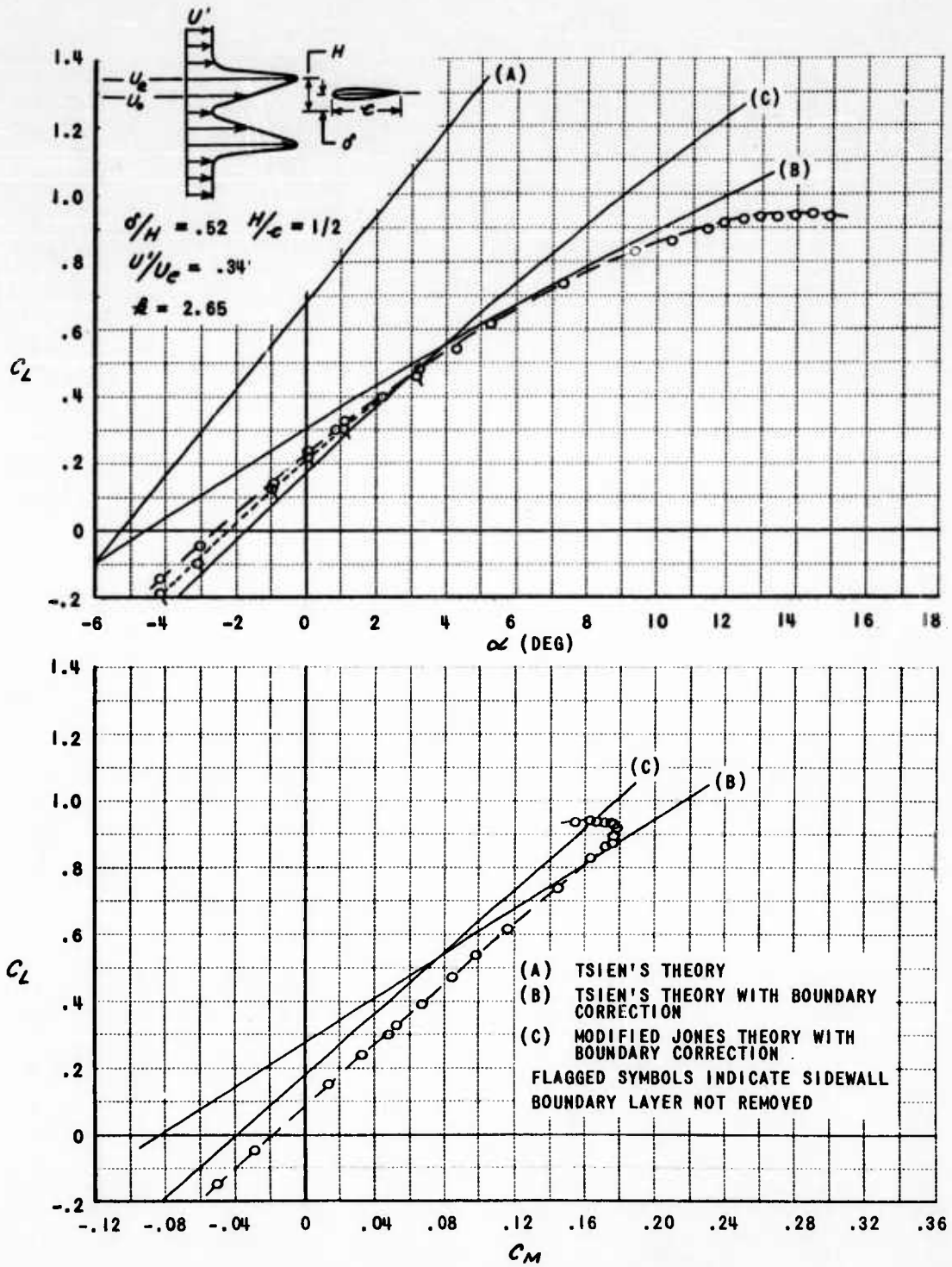

Figure 19c LIFT AND MOMENT IN A TWO-DIMENSIONAL SLIPSTREAM WITH LARGE SHEAR

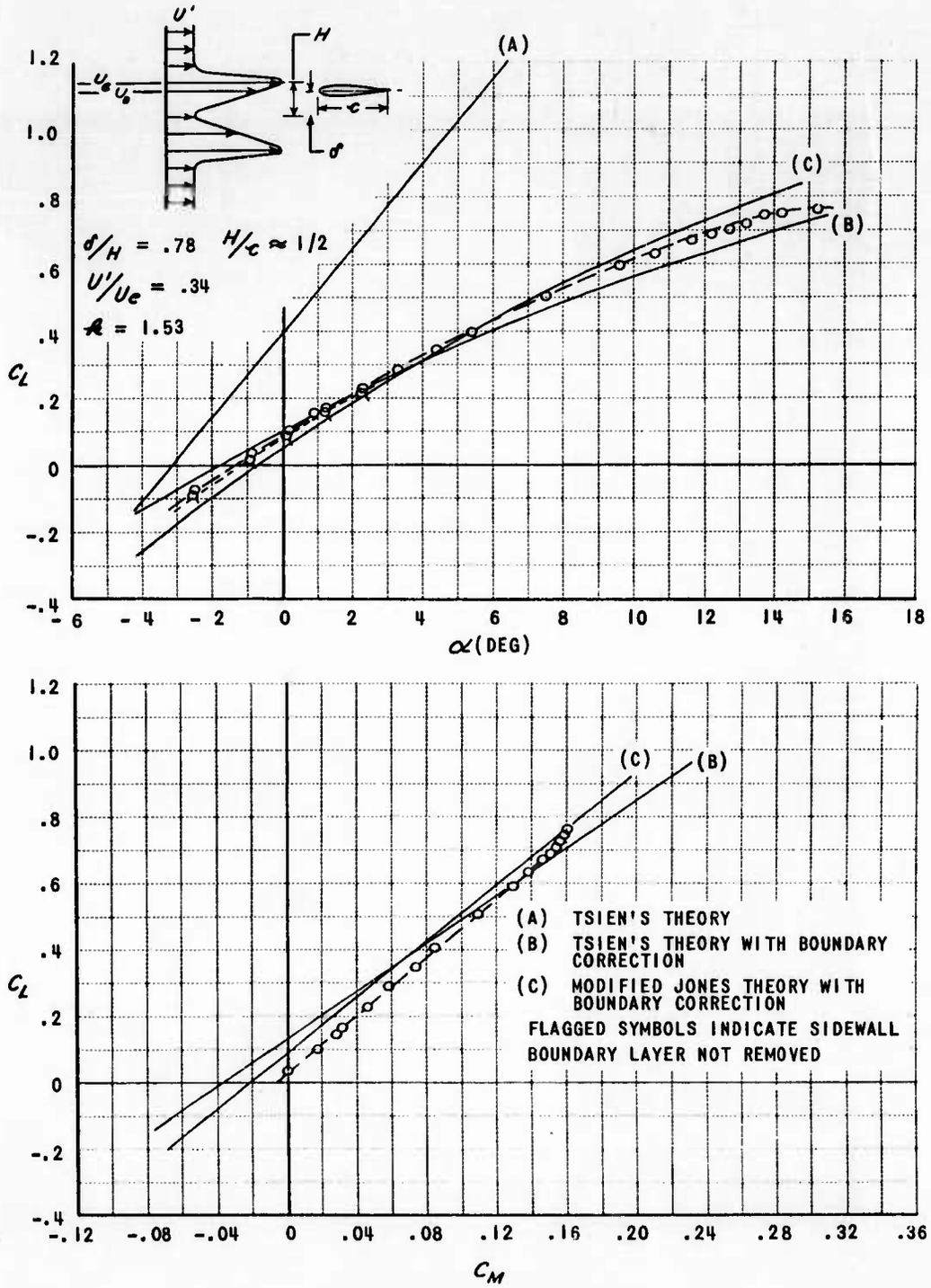

Figure 19d LIFT AND MOMENT IN A TWO-DIMENSIONAL SLIPSTREAM WITH LARGE SHEAR

This is substantiated by the moment data which shows there was no unusual motion of the center of pressure characteristic of a spreading region of boundary layer separation. This result is viewed with some reservations since it is recognized that unusual boundary layer separation patterns might be influencing the data. No boundary layer observations were made during this test; however, during the experiments in uniform shear flow, oil film techniques were employed to observe the separation patterns. A typical result is shown in Fig. 20. In this experiment the oil, colored with lamp black, was introduced from the trailing edge so that the oil was confined to the separated regions. One characteristic of the separation process was the formation of strong vortices standing normal to the surface; the dark regions in photograph. Under certain conditions a pair of these vortices would stand on either side of the instrumented section and energize the flow over the section to locally delay separation. It is not clear if this occurred with the data in Fig. 19a, so the extreme maximum lift coefficients must be substantiated with more detailed experiments.* It is noted, however, that a similar result was obtained by Brenckman[24] in experiments with a two-dimensional wing in a propeller slipstream. His results, obtained on the propeller centerline, showed a "destalling effect" both within the slipstream and exterior to the slipstream; that is, the maximum lift coefficent with a slipstream was about 20% more than in a comparable uniform stream.

The data obtained at $\delta/H = .23$ are compared with both uniform and non-

---

* Subsequent experiments with the airfoil near the slipstream plane of symmetry and employing boundary layer visualization techniques have confirmed the observed maximum lift and have shown that separation was acceptably two-dimensional. These results will be covered in a forthcoming report.

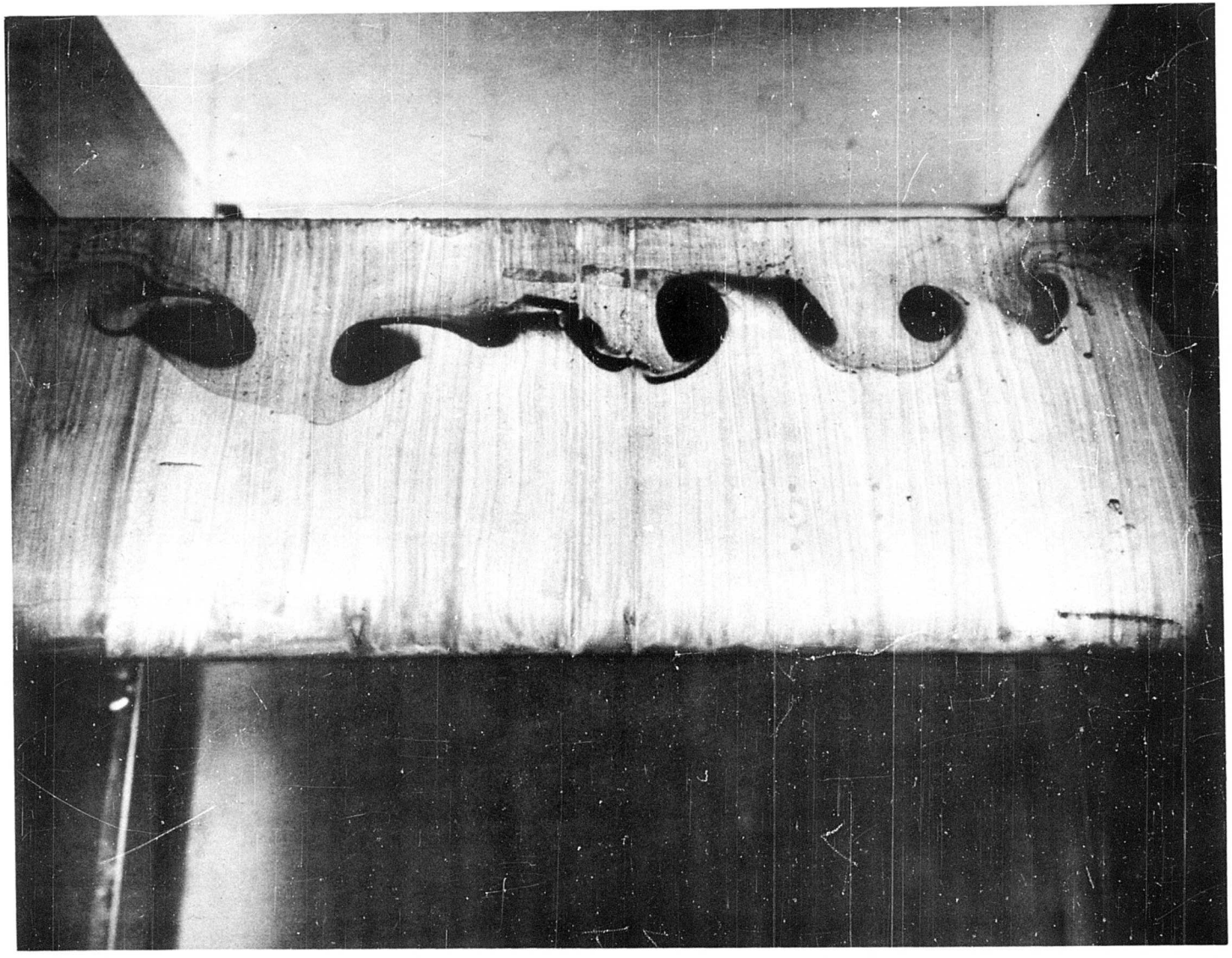

Figure 20 BOUNDARY LAYER SEPARATION IN UNIFORM SHEAR FLOW

uniform shear theory in Fig. 19b. The importance of two-dimensional slipstream boundary interference on airfoil lift can be seen by comparing Tsien's theory with and without the boundary correction. The boundary correction causes about a 30% loss in lift. Comparing the corrected Tsien's theory with the data, the theory underestimates both the lift curve slope and the angle of attack for zero lift. It appears that even though the shear is quite constant at this location, Tsien's uniform shear theory is inapplicable because of the close proximity of the region of non-uniform shear. The airfoil lower surface is within a quarter airfoil thickness of the slipstream center-plane and is influenced by the non-uniform shear. Jones' non-uniform shear theory would be applicable if the shear were smaller and if the theory included the effect associated with thickness and shear. On the basis of Tsien's exact theory for uniform shear and Jones' theory for an ellipse in non-uniform shear[8] one might anticipate that if this term were included in Jones thin airfoil theory, it would predict a lift increment given by $\Delta C_L = \frac{\pi}{2} k_\ell \tau$, and a moment increment given by $\Delta C_M = \frac{\pi}{64} k_\ell \tau$, where k_ℓ is the local shear. These increments have been added to Jones' thin airfoil theory and are compared with the data in Fig. 19b. It can be seen that this modified Jones theory is in fair agreement over a large angle of attack range, and yields better predictions than does uniform shear theory for both lift and moment.

The pitching moment data in Fig. 19b suggest that the airfoil is in the process of stalling since the center of pressure has begun to move. This is borne out by the lift data which has reached a near maximum value of $C_L \approx 1.4$. This behavior is contrasted with the data of Fig. 19a which shows twice the lift at the same angle of attack with no sign of impending stall.

The lift and moment data for the airfoil about midway out in the slipstream

(δ/H = .52) are compared with the uniform shear and the modified non-uniform shear theories in Fig. 19c. Comparing the uniform shear theory with and without the boundary correction, it is seen that the influence of the slipstream boundary is to cause a 50% loss in lift. Again the modified non-uniform shear theory with a boundary correction agrees well with the data, though it overestimates the lift curve slope. This same theory yields a good prediction of the airfoil center of pressure, as indicated by the slope of the moment curve, but overestimates the pitching moment at zero lift. At this position it is seen that the airfoil is approaching stall with a maximum lift coefficient of $C_L \approx 0.9$.

The two-dimensional airfoil characteristics at δ/H = .78, Fig. 19d, are quite similar to those at the other positions in the slipstream except that they are more pronounced. In this case the slipstream boundary proximity causes a 65% loss in lift and results in markedly non-linear effects. Both the uniform shear theory and the modified non-uniform shear theory predict the lift characteristics with about equal precision after the boundary correction is applied. The latter theory is more accurate for moment predictions, though it still overestimates the pitching moment at zero lift. Also in this instance the airfoil is perhaps beginning to stall at the highest test angles of attack, as suggested by the moment data.

To summarize, the experiments in a two-dimensional slipstream reveal that there is a profound effect of the boundary interference. In these experiments where the slipstream height was one chord length, the effect of the boundary interference is to cause a 30% - 65% loss in lift, depending on the airfoil location in the slipstream. This adverse effect is predicted by the slipstream boundary analysis in Section I.

The effects of slipstream shear on airfoil characteristics are to cause

an increase in lift and moment slope, and to cause a non-zero lift and moment at zero angle of attack. These are observed in the experiments, and it is found that because the experimental slipstream was a non-uniform shear flow, the airfoil characteristics are best predicted by a modified version of Jones' non-uniform shear theory. The modification consisted of adding the lift and moment increment due to shear predicted by uniform shear theory.

With the airfoil at the center of the two-dimensional slipstream, it is found that lift coefficients in excess of 3.0 are realized, with no apparent signs of stalling. This might be attributed to the peculiarities associated with the experiment, such as unusual three-dimensional boundary layer separation patterns causing locally high lift coefficients. Also it is recognized that the turbulence introduced by the shear screens cause alterations in the boundary layer so that very small viscous drags are observed. This might also influence the boundary layer separation. However, if this were the cause, the same high lift coefficients should be observed at other positions in the slipstream. On the contrary, rather clear indications of impending stall were observed. This leads to the conclusion that boundary layer separation is being influenced by the local flow, and suggests that the derivative of the shear exerts a beneficial influence on separation.

Uniform Slipstream

Experiments were made with the symmetrical Joukowsky airfoil in a uniform two-dimensional slipstream in order to have an experimental check on the influence of shear and to have a check on the accuracy of the image analysis for predicting the influence of boundary interference. The velocity calibration of this uniform slipstream is shown in Fig. 14. The data have been corrected for tunnel wall interference and are presented in Fig. 21. The coefficients are based on slip-

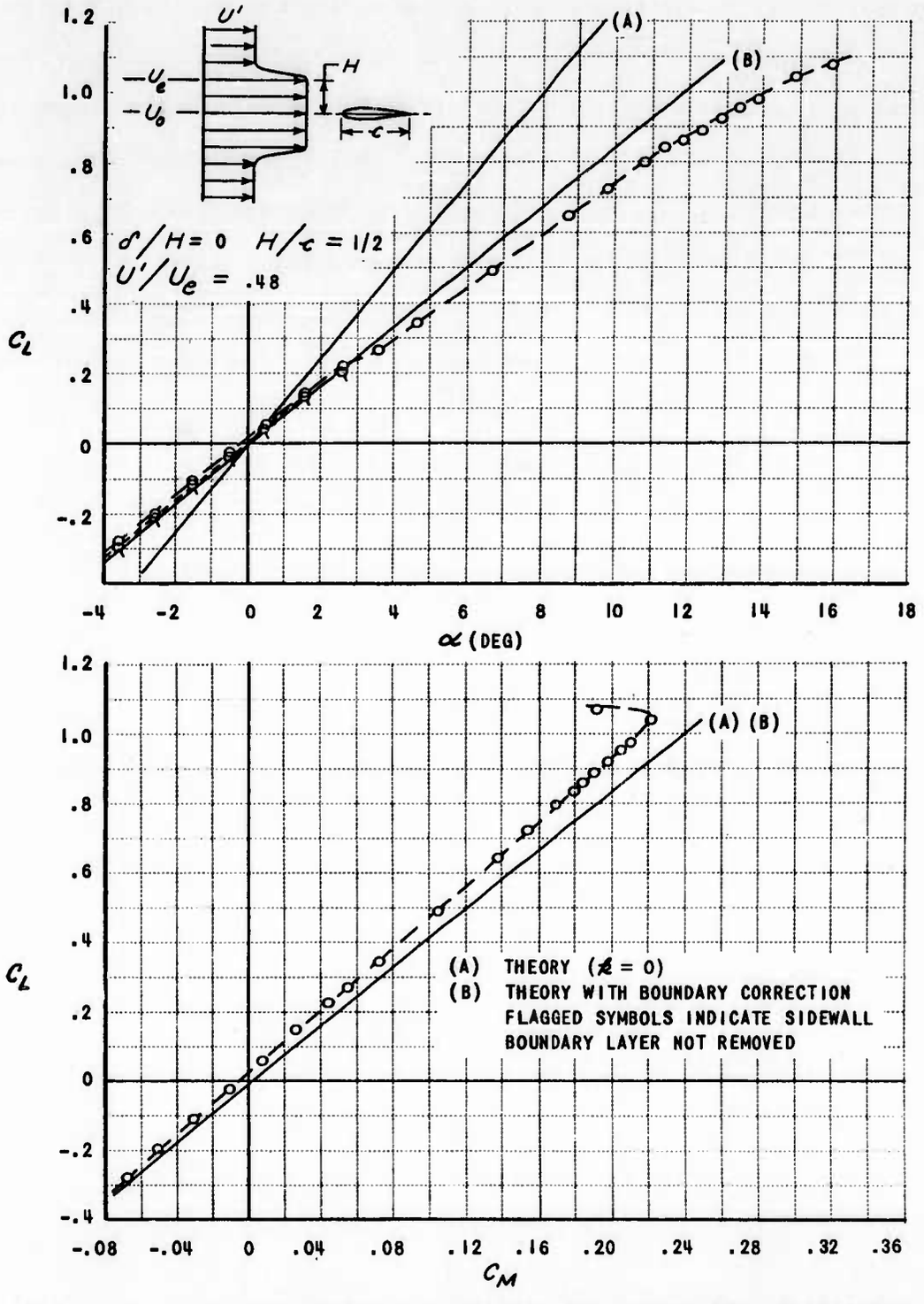

Figure 21a LIFT AND MOMENT IN A UNIFORM TWO-DIMENSIONAL SLIPSTREAM

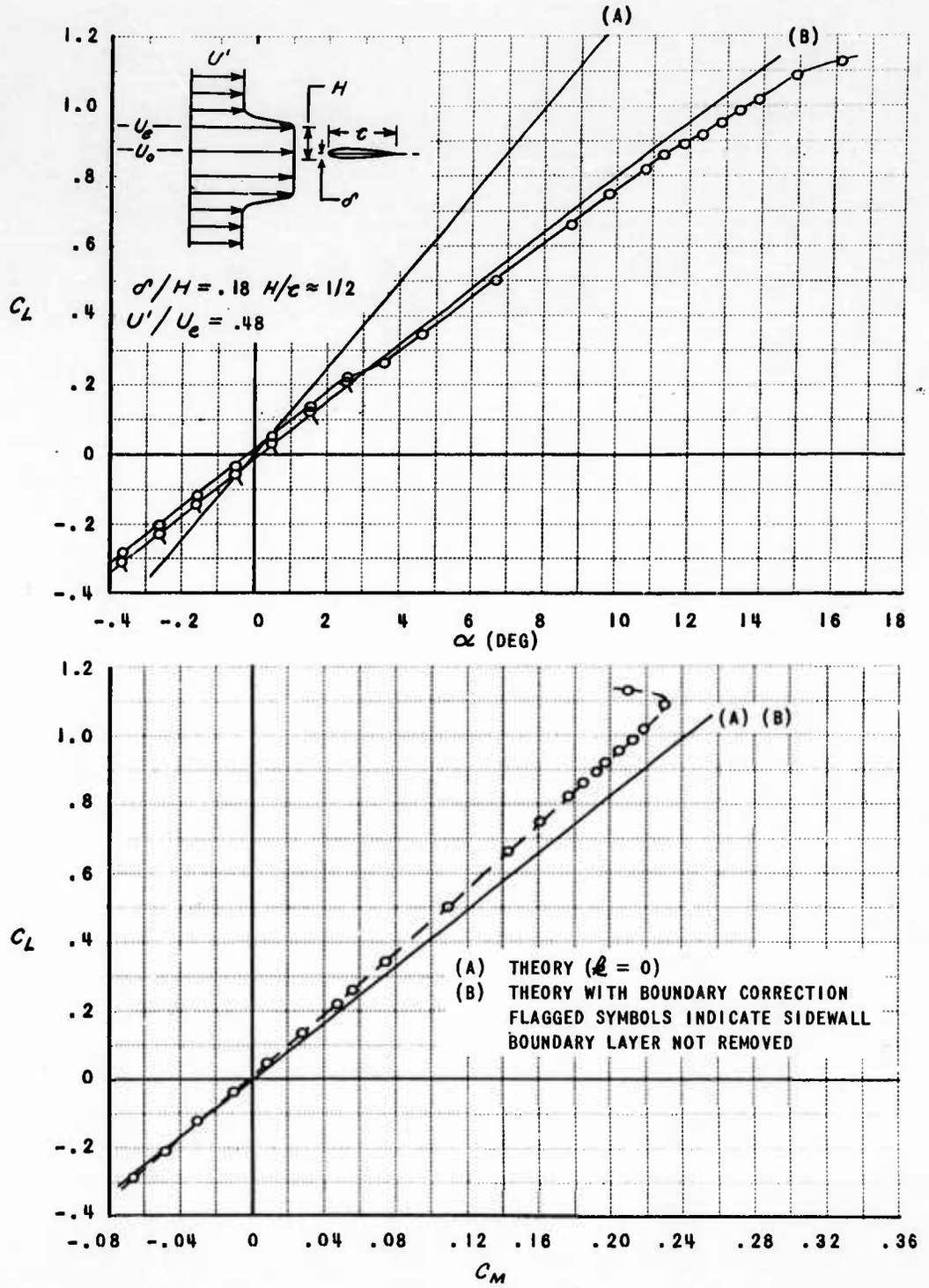

Figure 21b LIFT AND MOMENT IN A UNIFORM TWO-DIMENSIONAL SLIPSTREAM

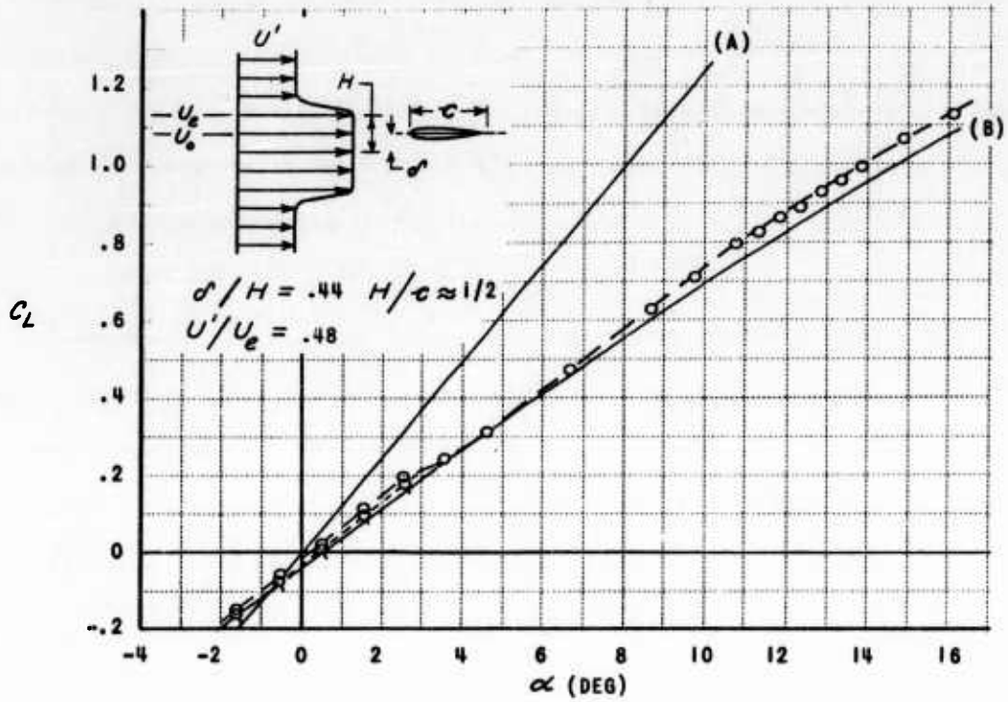

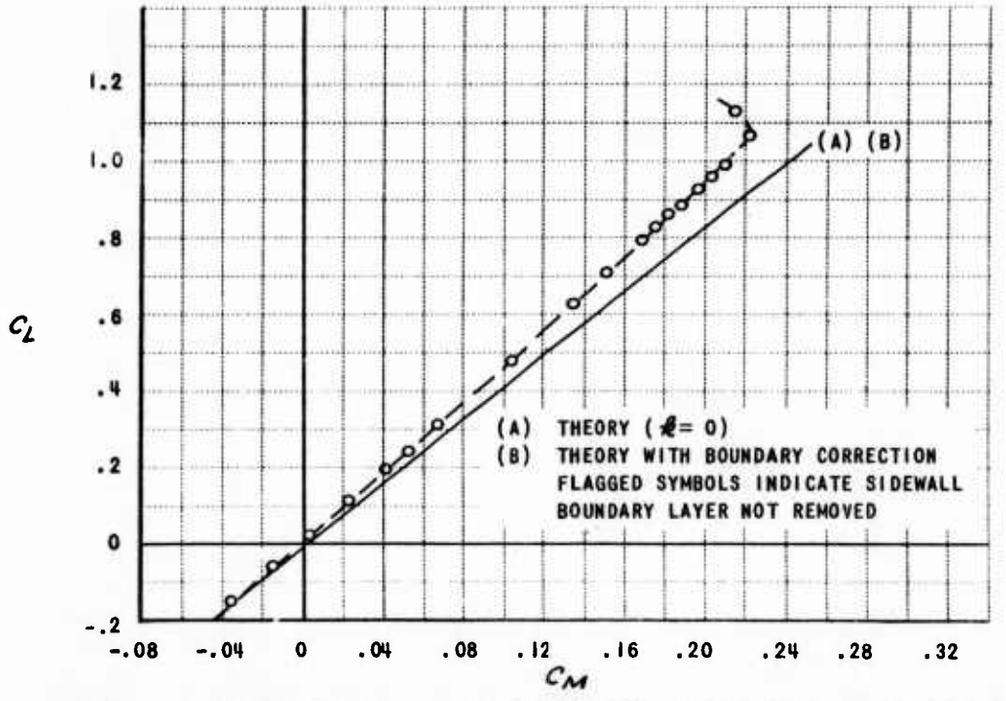

Figure 21c LIFT AND MOMENT IN A UNIFORM TWO-DIMENSIONAL SLIPSTREAM

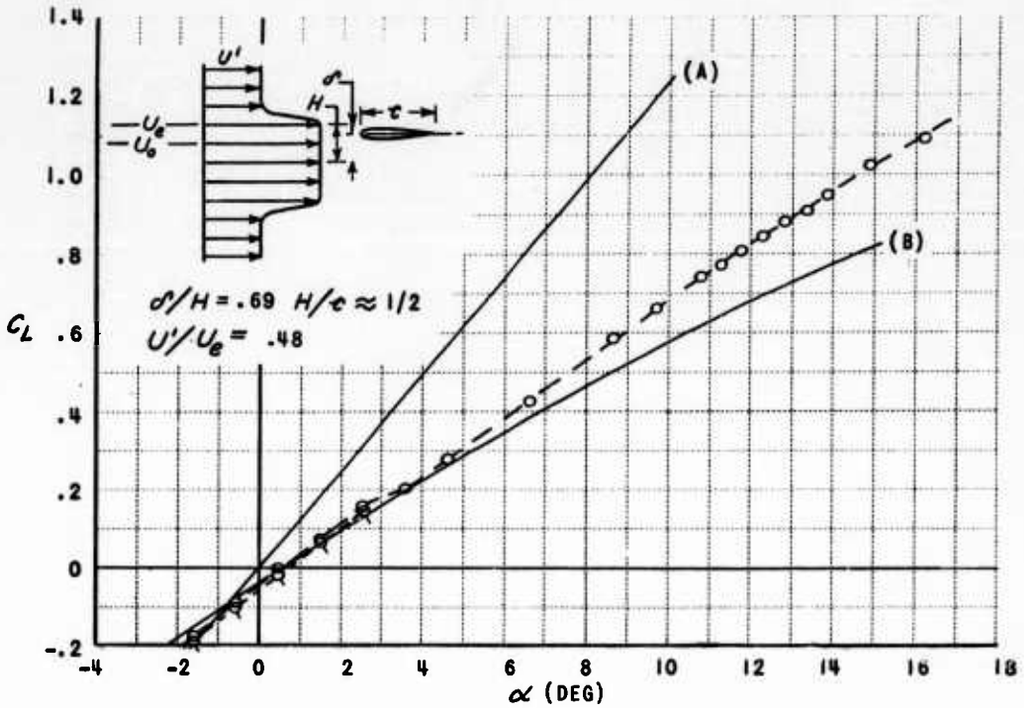

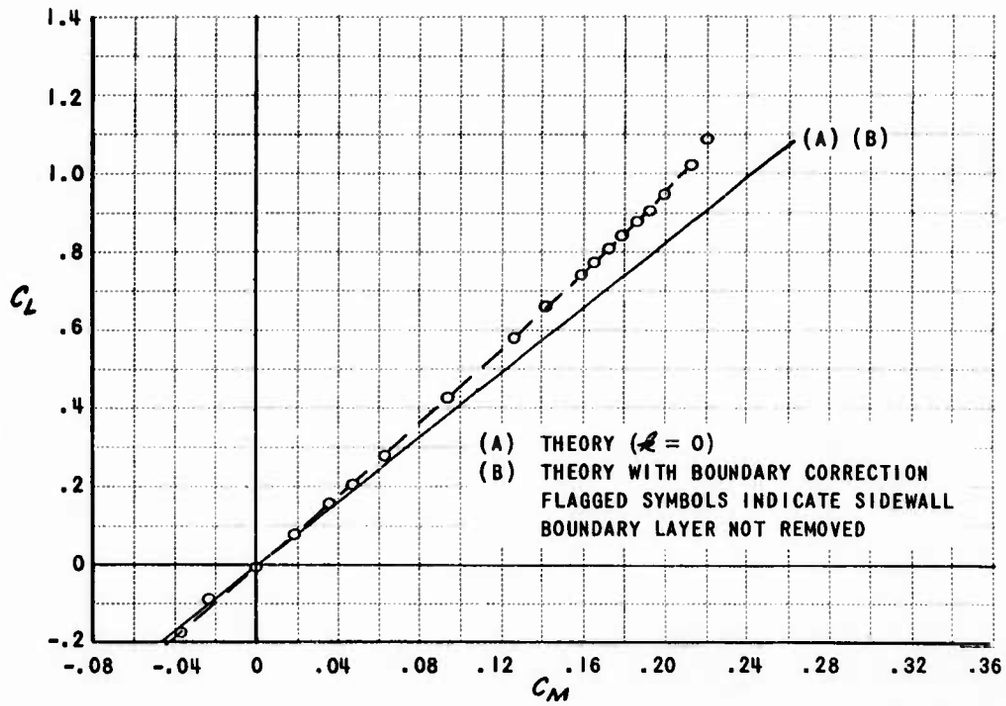

Figure 21d LIFT AND MOMENT IN A UNIFORM TWO-DIMENSIONAL SLIPSTREAM

stream velocity. It will be noted that all of the lift data in Fig. 21 show an abrupt loss in lift in the vicinity of $\alpha = 3°$, and the moment curves show a slight change in slope at this point. It appears that this stems from a change in the boundary layer, such as the sudden appearance of a leading edge separation bubble[25]. A separation bubble was observed on the airfoil at higher angles of attack.

The data shown by the flagged symbols are those obtained with the tunnel side wall boundary layer bleed inoperative. The difference between the two sets of data then indicates the magnitude of the error caused by the side wall suction; an increase of about .02. The theory shown is that of Ref. 4 for zero shear; that is classical two-dimensional Joukowsky airfoil theory.

The lift data obtained with no sidewall suction are seen to be, for small angles of attack, in excellent agreement with the theory when corrected for slipstream boundary interference. The lack of agreement at higher angles might be due to the boundary layer changes occurring at $\alpha \approx 3°$. However, one would expect the experimental lift curve slope to be less than the theoretical on the basis of the results obtained in uniform flow (Fig. 17). The good correlation at zero lift demonstrates the accuracy of calculating the slipstream boundary interference stemming from airfoil thickness by using source and sink images.

The moment data obtained with the tunnel boundary layer bleed inoperative are not shown. These data fall on the same curve with the presented data, and only demonstrate that the distribution of sidewall suction (Fig. 16) was correct. These data show that the center of pressure is further aft than predicted by theory. Or alternatively, the experimental slope of the moment curve plotted against angle of attack is smaller than predicted. This observation is in keeping with the data obtained in uniform flow.

It is significant to note in Fig. 21, that in all cases, the moment data indicate impending stall at the highest angle of attack. Moreover, the data suggest that in a uniform slipstream the maximum lift coefficient would be quite insensitive to airfoil position in the slipstream. This is in contrast to the data obtained in the non-uniform slipstream (Fig. 19) which show that the maximum lift coefficient is markedly influenced by position, shear, or the derivative of the shear.

Influence of Slipstream Velocity

The symmetrical airfoil was tested at one position in the slipstream with small shear and at the same position in the equivalent uniform slipstream (Fig. 13). The purpose of these experiments was to obtain a check with the theory for a case with a larger ratio of slipstream to free stream velocity. In the other case this ratio was about 2 whereas the ratio is about 4 for the slipstreams of Fig. 13. The lift and moment data obtained in these two slipstreams are compared with the appropriate theory in Fig. 22 and 23. The data in Fig. 22 are seen to agree well with uniform shear theory, corrected for slipstream boundary interference, over much of the angle of attack range. Judging from the moment data, the progressive lack of agreement at high angles of attack is due to the approaching stall.

The lift data obtained in the equivalent uniform slipstream, Fig. 23, are in fair agreement with the theory. The theory, corrected for slipstream boundary interference, predicts the angle of attack for zero lift of about $\alpha \approx$ ¾°, while the data shows an angle of about ¼°. It appears that in this instance either the data are in error or the effect of airfoil thickness on boundary interference is overestimated. The former seems more likely in view of the correlation obtained in Fig. 21.

One question that occurs when considering the influence of shear on airfoil characteristics is the determination of where in the slipstream the airfoil should

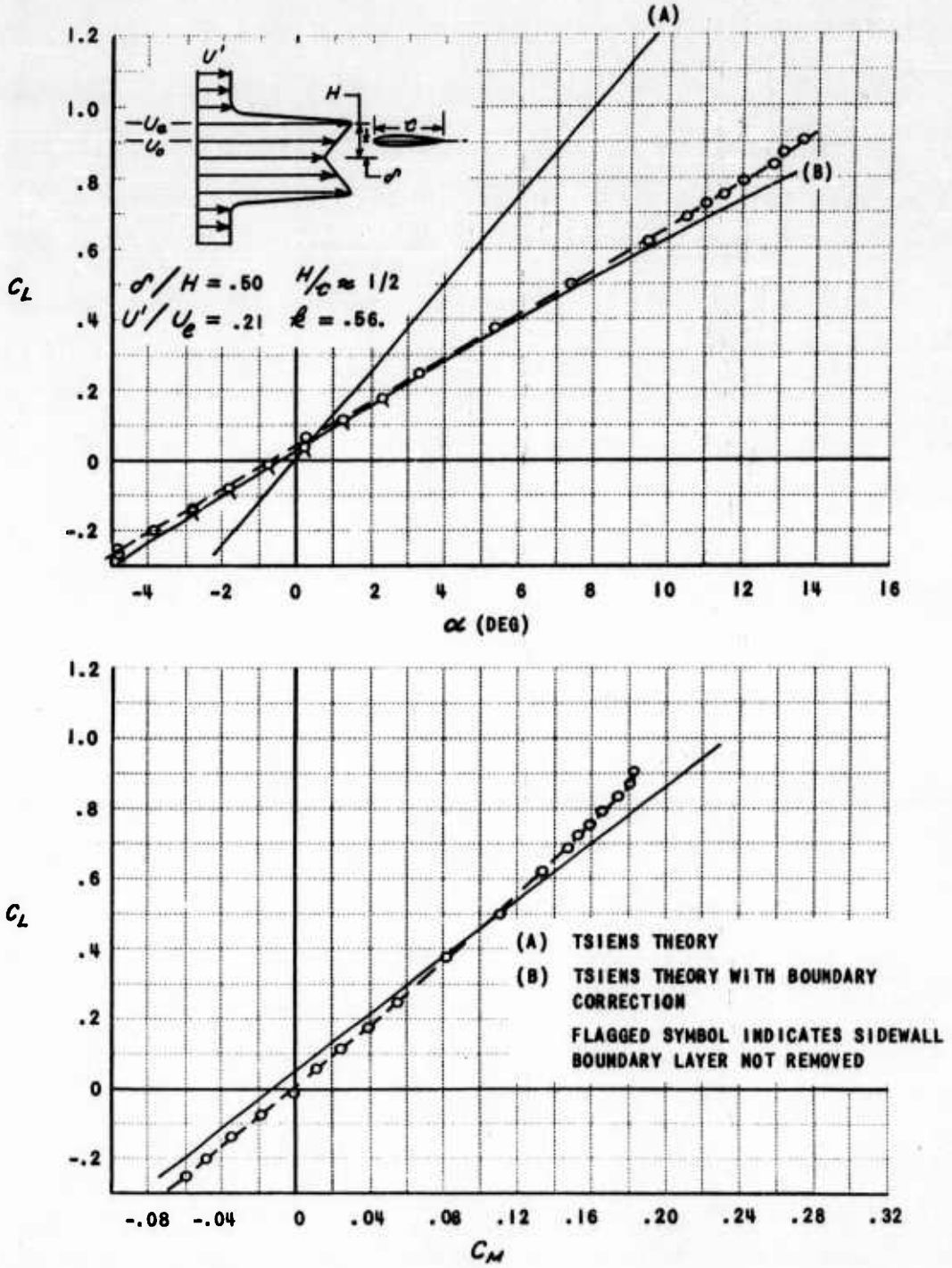

Figure 22 LIFT AND MOMENT IN A TWO-DIMENSIONAL SLIPSTREAM WITH SMALL SHEAR

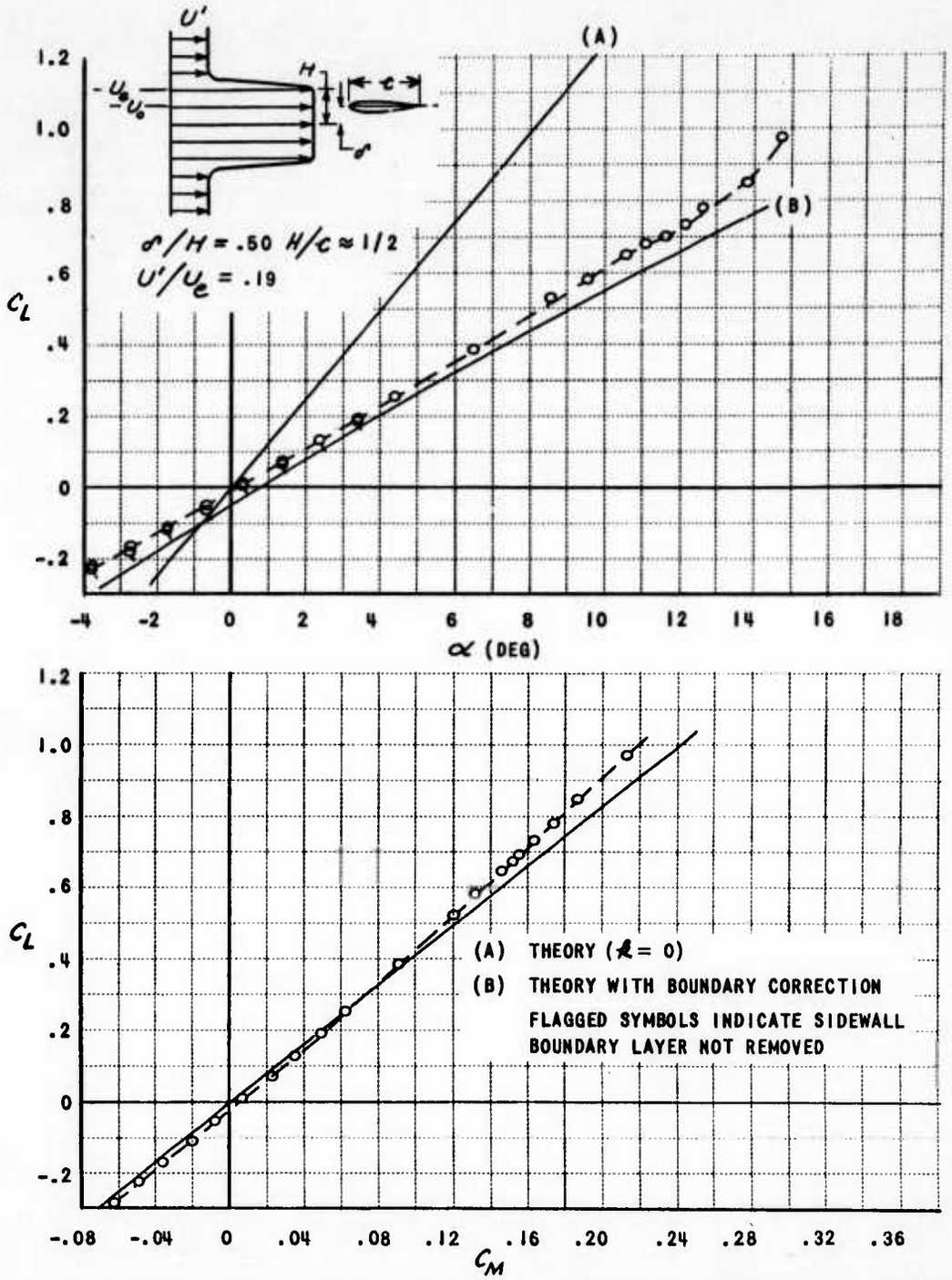

Figure 23 LIFT AND MOMENT IN A UNIFORM TWO-DIMENSIONAL SLIPSTREAM

be located to obtain the largest lift. The data in Fig. 19 do not yield any direct answer to this question since the coefficients are based on local velocity. These data have beer referred to the average slipstream velocity so that a comparison gives a direct indication of lift at the various positions in the slipstream. These data are presented in Fig. 24. This comparison shows that, for large angle of attack, the most desirable locations are either near the slipstream plane of symmetry. However, the airfoil showed no indications of stall at the latter position so that no firm conclusion can be reached.

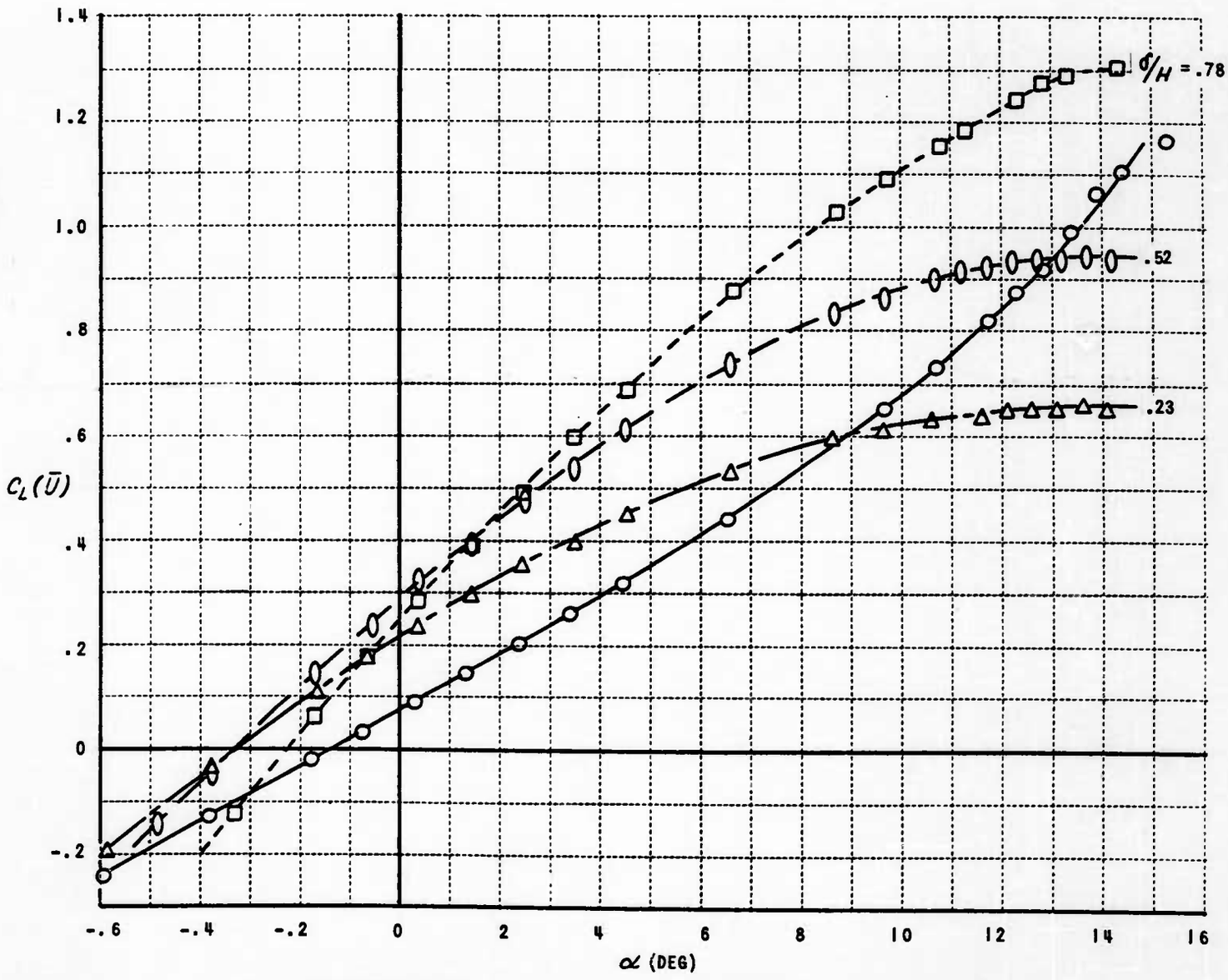

Figure 24 COMPARISON OF LIFT IN A TWO-DIMENSIONAL SLIPSTREAM

CONCLUSIONS

The available literature on the two-dimensional problem of airfoils in uniform shear[4,6] and non-uniform shear[7,8] show that there are two effects of shear on airfoil characteristics. The theories retaining terms involving both airfoil thickness and shear[4,6,8] show that there is an overall increase in lift and pitching moment in proportion to the local shear and the airfoil thickness and camber. For uniform shear the applicable theory also predicts a small increase in the slope of the lift and moment curves due to shear. Jones theory for thin airfoils in non-uniform shear[7] neglects products of the airfoil thickness and shear, and no overall increase in lift and moment is predicted. However, he does predict an increase in the slope of the lift and moment curves in proportion to the derivative of the shear.

The experiments made in simulated non-uniform propeller slipstreams quantitatively substantiate these theoretical results when the theories are corrected for slipstream boundary interference on the airfoil. It is found that the corrected uniform shear theory yields accurate predictions of the airfoil characteristics if the local slipstream shear is fairly uniform and if the airfoil is about 1/4 - 3/8 chord lengths from the slipstream plane of symmetry. The theory for thin airfoils in non-uniform shear flow is restricted to slipstreams with small changes in shear, while the experiments included large changes in shear. In spite of this, theory and experiment are in good agreement for those slipstream regions where the shear is small but the derivative of shear is large. When the shear too is large, it is found that by adding the lift and moment increment predicted by uniform shear theory to the non-uniform shear result, this modified theory yields good estimates of the airfoil characteristics. This

modified theory should be used with considerable caution, pending theoretical verification of its validity.

In the experiments in a simulated two-dimensional slipstream, lift coefficients in excess of 3.0 were realized with the symmetrical airfoil in the immediate vicinity of the slipstream plane of symmetry. This result is in qualitative agreement with Brenckman's result, and suggests that when the derivative of shear is large, boundary layer separation is delayed.*

---

* Subsequent experiments with the airfoil at various locations close to the slipstream plane of symmetry have confirmed this result and showed that no unusual boundary separation occurred. In these experiments, the maximum lift was obtained with the airfoil slightly below the plane of symmetry. These results will be published in a forthcoming report.

APPENDIX I

The Production of a Specified Two-Dimensional Shear Flow
by a Non-Uniform Screen

In order to determine the aerodynamic characteristics of airfoils in shear flow, it is necessary to produce a prescribed non-uniform flow in a wind tunnel with large rates of shear. As demonstrated by Owen and Zienkiewicz[15], this can be accomplished using screens or grids with the proper distribution of resistance mounted upstream of the test region. They present a method for designing screens to produce a known flow with a linear velocity gradient, subject to the restriction that the screen only slightly perturbs the flow. The present work is essentially an extension of the theory of Ref. 15 to allow for non-linear velocity gradients and to include large perturbations from the screen.

The model used is an initially uniform constant area channel flow (Station 0 in Fig. I-1) which subsequently passes through a non-uniform screen, Stations 1 and 2, and expands to its final configuration for a downstream at Station 3.

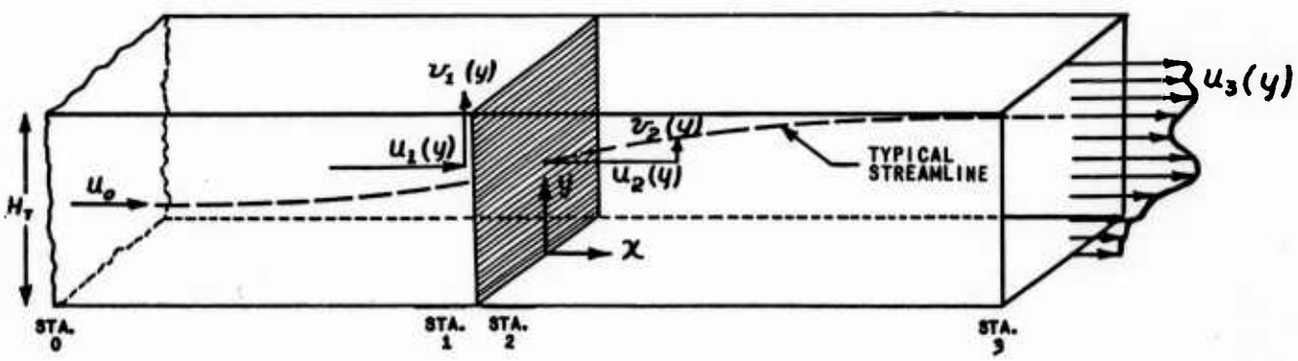

Figure I-1 CHANNEL FLOW THROUGH A SCREEN

Stations 1 and 2 refer to the upstream side and the downstream side of the screen, respectively. Using the nomenclature shown in Fig. I-1, the final velocity distribution at Station 3 can be considered to be the uniform stream velocity with a perturbation velocity added,

$$u_3(y) = u_o + w_x(y)$$

Introducing the stream function, the boundary conditions to be satisfied are:

(1) The transverse velocity component is zero at the channel wall

$$\left(\frac{\partial \psi}{\partial x}\right)_{y=0} = \left(\frac{\partial \psi}{\partial x}\right)_{y=H_T}$$

(2) The longitudinal velocity component is continuous through the screen

$$\left(\frac{\partial \psi}{\partial y}\right)_{x=-0} = \left(\frac{\partial \psi}{\partial y}\right)_{x=+0}$$

(3) The transverse velocity component changes by a factor, β in passing through the screen

$$\left(\frac{\partial \psi}{\partial x}\right)_{x=-0} = \frac{1}{\beta}\left(\frac{\partial \psi}{\partial x}\right)_{x=+0}$$

(4) On any streamline, the change in total pressure between Stations 0 and 3 is equal to the local resistance of the screen at the point where it is pierced by the streamline.

(5) At Station 3 the static pressure is constant across the channel.

It is assumed that the fluid is inviscid and incompressible, and that the desired velocity distribution can be represented by a Fourier series. Further, The local pressure drop through the screen is taken to be a function only of the local velocity ahead of the screen,

$$\frac{p_1 - p_2}{\rho/2\, u_o^2} = K\left(\frac{v_1^2 + u_1^2}{u_o^2}\right) \qquad \text{(I-1)}$$

and it is assumed that Taylor and Batchelor's refraction coefficient[26] for uniform screens applies for non-uniform screens

$$\beta = \frac{1.1}{\sqrt{1+K}} \tag{I-2}$$

where K is the local screen resistance.

The first boundary condition is satisfied by the following form for the stream function.

$$x \le 0 \qquad \psi(x,y) = u_0 y + u_0 H_T \sum_{n=1}^{\infty} A_n e^{n\pi \frac{x}{H_T}} \sin\left(n\pi \frac{y}{H_T}\right) \tag{I-3}$$

$$x \ge 0 \qquad \psi(x,y) = u_0 y + \int_0^y w_x(y)\,dy + u_0 H_T \sum_{n=1}^{\infty} B_n e^{-n\pi \frac{x}{H_T}} \sin\left(n\pi \frac{y}{H_T}\right) \tag{I-4}$$

where A_n and B_n are arbitrary coefficients to be determined by application of the boundary conditions. Defining

$$\int_0^y w_x(y)\,dy = u_0 H_T \sum_{n=1}^{\infty} C_n \sin\left(n\pi \frac{y}{H_T}\right) \tag{I-5}$$

and applying the second boundary condition to Eq. (I-3) - (I-5), the result is

$$\sum_{n=1}^{\infty} n A_n \cos\left(n\pi \frac{y}{H_T}\right) = \sum_{n=1}^{\infty} n C_n \cos\left(n\pi \frac{y}{H_T}\right) + \sum_{n=1}^{\infty} n B_n \cos\left(n\pi \frac{y}{H_T}\right)$$

$$A_n = B_n + C_n \tag{I-6}$$

Applying the third boundary condition to Eq. (I-3) - (I-4), another relation between the unknown coefficients is obtained.

$$\sum_{n=1}^{\infty} n A_n \sin\left(n\pi \frac{y}{H_T}\right) = -\frac{1}{\beta} \sum_{n=1}^{\infty} n B_n \sin\left(n\pi \frac{y}{H_T}\right) \tag{I-7}$$

$$A_n = -\frac{1}{\beta} B_n$$

Combining Eq. (I-6) and (I-7), we obtain the unknown Fourier coefficients in terms of the coefficients fixing the desired velocity distribution and the parameter

defining the local screen resistance.

$$A_n = \frac{C_n}{1+\beta} \tag{I-8}$$

$$B_n = -\frac{\beta}{1+\beta} C_n \tag{I-9}$$

Equations (I-8) and (I-9) provide the means for fixing the local screen resistance in terms of the parameters defining the final velocity distribution if it can be assumed that the streamlines are, for practical purposes, straight downstream of the screen. This might be a valid assumption for small values of $\frac{w_x(y)}{u_o}$. However, the present formulation is for large values of this parameter, and consideration must be given to the streamline curvature. A streamline is defined by $\psi(x,y)$ = Const., and the deflection of the streamline between the screen and downstream infinity (Station 3) is determined by the general relation,

$$\psi(0, y_2) = \psi(\infty, y_3)$$

where y_2 and y_3 respectively denote the vertical position of the streamline at the screen and at infinity. Applying this to Eq. (I-4), the equation for the streamline becomes

$$u_o y_2 + \int_o^{y_2} w_x(y)\,dy - u_o H_T \left(\frac{\beta}{1+\beta}\right) \sum_{n=1}^{\infty} C_n \sin\left(n\pi \frac{y_2}{H_T}\right) = u_o y_3 + \int_o^{y_3} w_x(y)\,dy \tag{I-10}$$

Substituting Eq. (I-5) in this result, the final equation for the streamline deflection is

$$y_2 + \frac{1}{1+\beta} \int_o^{y_2} \frac{w_x(y)}{u_o}\,dy = y_3 + \int_o^{y_3} \frac{w_x(y)}{u_o}\,dy \tag{I-11}$$

Along any streamline either upstream or downstream of the screen, the total pressure is conserved, and all losses occur at the screen. This requires that upstream of the grid

$$x_0 \le x \le x_1 : \quad p_0 + \frac{\rho}{2} u_0^2 = p_1 + \frac{\rho}{2} (u_1^2 + v_1^2) \qquad \text{(I-12)}$$

and downstream of the screen along the streamline defined by Eq. (I-11),

$$x_2 \le x \le x_3 \qquad p_3 + \frac{\rho}{2} \left[u_0 + w_x(y_3)\right]^2 = p_2(y_2) + \frac{\rho}{2} \left[u_2^2(y_2) + v_2^2(y_2)\right] \qquad \text{(I-13)}$$

Subtracting Eq. (I-13) from Eq. (I-12) and noting that $u_1 = u_2$, $v_1 = \frac{1}{\beta} v_2$, the loss in total pressure through the screen is given by

$$\frac{p_1 - p_2}{\rho/2\, u_0^2} = \frac{p_0 - p_3}{\rho/2\, u_0^2} + 1 - \left[1 + \frac{w_x(y_3)}{u_0}\right]^2 - \frac{1-\beta^2}{\beta^2} \left(\frac{v_2}{u_0}\right)^2 \qquad \text{(I-14)}$$

Now the static pressure at infinity upstream and downstream is uniform across the channel, and the difference in static pressure between these two stations is the average screen loss. Denoting this average loss and the local loss as $\bar{K}$ and K,

$$\bar{K} = \frac{p_0 - p_3}{\rho/2\, u_0^2} \qquad K = \frac{p_1 - p_2}{\rho/2\, (u_1^2 + v_1^2)}$$

the equation for the local screen losses follow from Eq. (I-14).

$$K\left[\frac{u_1^2}{u_0^2} + \frac{1}{\beta^2} \frac{v_2^2}{u_0^2}\right] = \bar{K} + 1 - \left[1 + \frac{w_x(y_3)}{u_0}\right]^2 - \left(\frac{1-\beta^2}{\beta^2}\right)\left(\frac{v_2}{u_0}\right)^2 \qquad \text{(I-15)}$$

At this point it is convenient to introduce the dimensionless variables,

$$\zeta_1 = \zeta_2 = y_2/H_T \qquad \zeta_3 = y_3/H_T$$

$$\gamma_2 = 1 + \frac{w_x(y_2)}{u_0} \qquad \gamma_3 = 1 + \frac{w_x(y_3)}{u_0}$$

$$F = \frac{1+\beta}{\beta} \frac{v_2}{u_0}$$

The longitudinal velocity at the screen is obtained from Eq. (I-3) and (I-5) as

$$\frac{u_1}{u_0} = 1 + \frac{1}{1+\beta}\,\frac{w_x(\gamma_2)}{u_0} = \frac{\beta+\gamma_2}{1+\beta} \tag{I-16}$$

After some manipulation Eq. (I-15) reduces to

$$K\left[\frac{(\beta+\gamma_2)^2+F^2}{(1+\beta)^2}\right] = \bar{K} + 1 - \gamma_3^2 - \frac{1-\beta}{1+\beta}F^2 \tag{I-17}$$

Finally introducing Eq. (I-2), the equation for the local screen resistance becomes

$$(-F^2+\gamma_3^2-\bar{K}-2)\beta^4 - 2(1+\bar{K}+\gamma_2-\gamma_3^2)\beta^3 + (0.21-\gamma_2^2+\gamma_3^2-\bar{K})\beta^2 + (2.42\,\gamma_2)\beta + 1.21(F^2+\gamma_2^2) = 0 \tag{I-18}$$

The function, $F(\zeta_2)$, may be computed by differentiating Eq. (I-4) and using Eq. (I-9) to obtain

$$F(\zeta_2) = -\pi \sum_{n=1}^{\infty} n\,C_n \sin(n\pi\zeta_2) \tag{I-19}$$

The coefficients, C_n, may be computed from the prescribed velocity distribution using Eq. (I-5). By the usual rules of Fourier analysis, the coefficients are

$$C_n = 2\int_0^1 d\zeta \int_0^{\zeta} [\gamma(t)-1] \sin n\pi\zeta\, dt \tag{I-20}$$

It is convenient also to express Eq. (I-11) in dimensionless form.

$$\zeta_2 + \frac{1}{1+\beta}\int_0^{\zeta_2}[\gamma(t)-1]\,dt = \zeta_3 + \int_0^{\zeta_3}[\gamma(t)-1]\,dt \tag{I-21}$$

Equation (I-17) - (I-21) are the basic equations for the design of a screen to produce any desired velocity distribution. The method of application used in the present research is to compute the coefficients, C_n , for the prescribed velocity distribution, γ_3 , using Eq. (I-20). Then for each value of the screen coordinate, η_2 , the corresponding value of the function, $F(\zeta_2)$, is calculated using Eq. (I-19). Now in the final flow, there will be a maximum value of the velocity distribution, γ_3 , at the flow coordinate, ζ_3 . The maximum allowable value of β ($\beta_{max} \approx 1.0$) is assigned at this point and corresponds to the minimum local screen resistance that can be tolerated. Using this value of $\beta_{max.}$ and ζ_3 in Eq. (I-21), the corresponding value of the screen coordinate, ζ_2 , is calculated. These values of β_{max}, ζ_3 , ζ_2 , γ_3 , γ_2, and $F(\zeta_2)$, are then used in Eq. (I-17) to solve for the average screen resistance, $\bar{K}$.

With the average screen resistance, $\bar{K}$, so determined by the minimum screen resistance, one can then proceed to calculate the local screen resistance as a function of the prescribed velocity distribution and the screen coordinate, ζ_2 . The method used is to start at any convenient value of the screen coordinate and to solve Eq. (I-17) and (I-21) simultaneously for the corresponding screen resistance parameter, β , and the flow coordinate, ζ_3 . The technique used for this simultaneous solution depends on the type of prescribed velocity distribution.

APPENDIX II

Two-Dimensional Wind Tunnel Wall Corrections for Non-Uniform Streams

One aspect of this experimental research was concerned with the proper application of corrections to the data to account for the influence of the wind tunnel walls. The usual boundary corrections, such as those given by H. Glauert[27], are obtained using the method of images. This calculation consists of determining the disturbance velocities from the model at the position of the wall, and then postulating an array of images which will just cancel these lateral disturbance velocities at the wall position. This image array then satisfies the necessary boundary conditions and can be used to calculate the disturbance velocities from the wall at the model position.

The equivalent calculation can be made for two-dimensional models in two-dimensional non-uniform flows using the techniques described in the Theory Section. In particular, it was shown for uniform shear, that to the first order in thickness and angle of attack, the flow non-uniformity does not enter the problem directly except through the boundary condition at the slipstream boundary. Hence the problem could be reduced to a uniform flow problem with different boundary conditions. An image analysis was made to predict the influence of the slipstream boundary on the airfoil characteristics, and consisted of satisfying flow and pressure continuously at the slipstream boundary.

Now the presence of the solid wind tunnel walls in the problem is to introduce an additional disturbance at the outer edge of the slipstream boundary (see Fig. 3b). Through the continuity requirements, this implies an additional disturbance velocity within the slipstream. This disturbance velocity can be calculated by changing the image array of Fig. 3 slightly. The γ-array (Fig. 3c)

remains unchanged since this array still satisfies the slipstream boundary conditions. However, the magnitude of the parameter, γ , will change. The equivalent airfoil duplicating the disturbance velocities exterior to the slipstream is replaced with an array of airfoils with a lift of $\gamma' L$, and this array is such that there is no flow through the wind tunnel walls. (Fig. II-1). The effect of the walls on the model is obtained by satisfying flow and pressure continuity at the slipstream boundary, thereby fixing the magnitude of the parameter, γ , in terms of the γ' image array.

It can be seen in Fig. II-1 that this array satisfies the condition that there be no flow through the wall, and can be used to calculate the wall disturbance velocities exterior to the slipstream. Referring also to Fig. 3, the boundary conditions to be satisfied at the slipstream boundary are

$$\frac{w_y}{U_e} = \frac{w_y'}{U'} \qquad w_x U_e = w_x' U' \qquad \text{(II-1)}$$

Neglecting the details of the development, it can be shown that if the airfoil thickness effects are negligible, these conditions are satisfied for

$$\gamma_{L_w} = \frac{1 - K_2 \left(\frac{U'}{U_e}\right)^2}{1 + K_1 K_2 \left(\frac{U'}{U_e}\right)^2} \qquad \text{(II-2)}$$

$$\gamma'_{L_w} = \frac{U_e}{U_o} \frac{1 - \gamma_{L_w}}{1 + C} \qquad \text{(II-3)}$$

where the subscript, w , refers to solid wall correction. K_1 is given by Eq. (27), and K_2 and C are given by

$$K_2 = \frac{1 + C}{1 - B} \qquad \text{(II-4)}$$

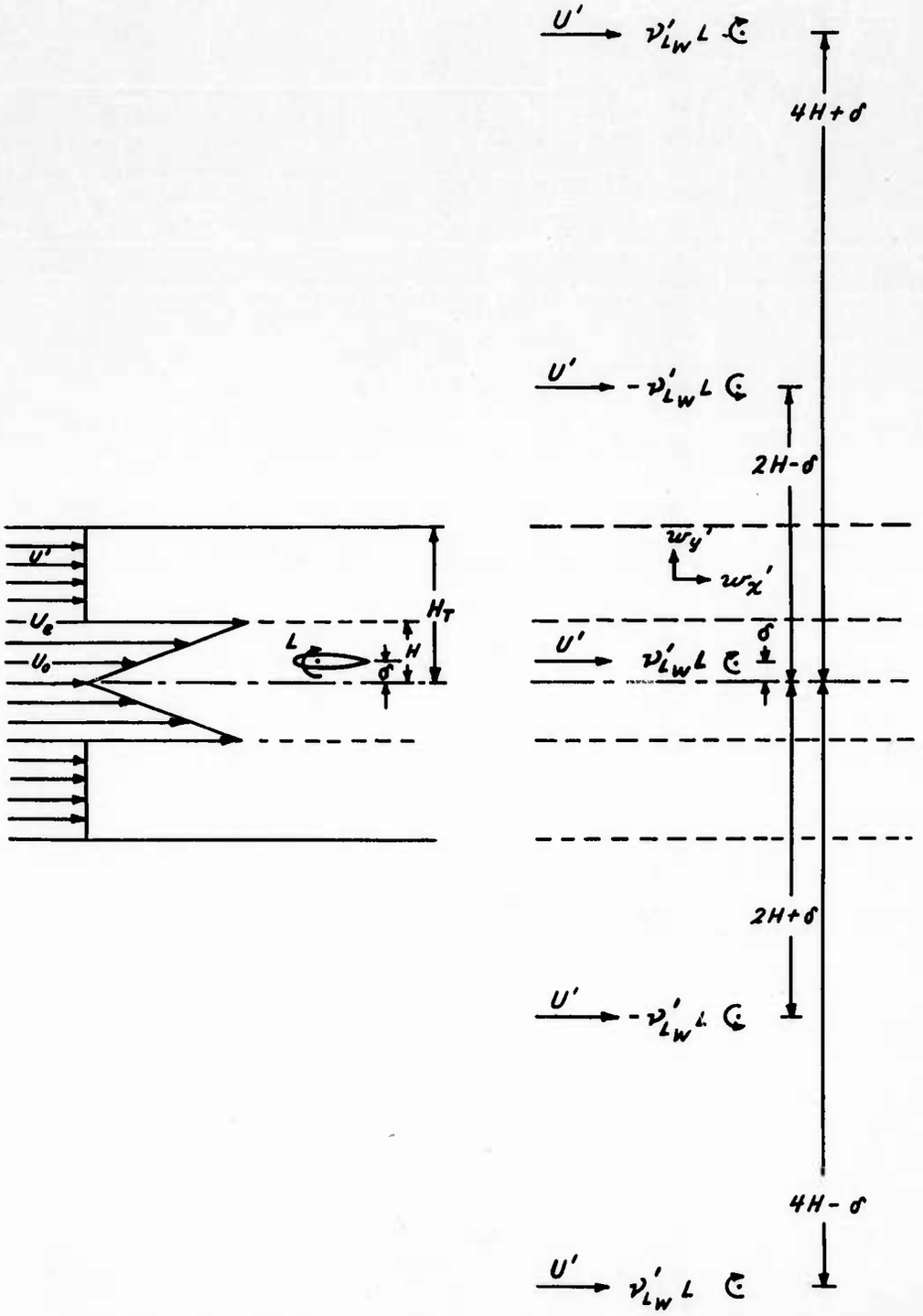

(a) TUNNEL FLOW SYSTEM

(b) TUNNEL IMAGE SYSTEM

Figure II-1 IMAGE SYSTEM FOR WIND TUNNEL WALL INTERFERENCE

$$B = -\left(\frac{\eta}{\omega}\right)^2 (1-\epsilon)^2 \left\{ \sum_{n=1}^{\infty} \frac{1}{\left[(4n-2) - \frac{\eta}{\omega}(1+\epsilon)\right]^2} + \sum_{n=1}^{\infty} \frac{1}{\left[(4n-2) + \frac{\eta}{\omega}(1+\epsilon)\right]^2} - \sum_{n=1}^{\infty} \frac{1}{\left[4n - \frac{\eta}{\omega}(1-\epsilon)\right]^2} - \sum_{n=1}^{\infty} \frac{1}{\left[4n + \frac{\eta}{\omega}(1-\epsilon)\right]^2} \right\} \qquad \text{(II-5)}$$

$$C = \frac{\eta}{\omega}(1-\epsilon) \sum_{n=1}^{\infty} \left\{ \frac{1}{(4n-2) - \frac{\eta}{\omega}(1+\epsilon)} - \frac{1}{(4n-2) + \frac{\eta}{\omega}(1+\epsilon)} - \frac{1}{4n - \frac{\eta}{\omega}(1-\epsilon)} + \frac{1}{4n + \frac{\eta}{\omega}(1-\epsilon)} \right\} \qquad \text{(II-6)}$$

where $\omega = H_T/c$. The series in Eqs. II-5 and II-6 have been evaluated on a high speed computing machine for representative values of η, ω and ϵ retaining the first 100 terms in the series. The calculated values of K_2 are plotted in Fig. II-2.

The disturbance velocities at the model can now be calculated using the image array of Fig. 3c, noting that the parameter, ν_{L_w} , fixes the image strength. The results are those given by Eq. (29) and (31). It can be seen then that the influence of the solid walls enters only through the parameter fixing the image strength and the wall corrections are

$$\Delta\alpha = -\frac{C_L}{8\pi}(\nu_{L_w} - \nu_L)\left\{ \sum_{n=1}^{\infty} \frac{1}{1/4 + 4\eta^2(2n-1-\epsilon)^2} + \sum_{n=1}^{\infty} \frac{1}{1/4 + 4\eta^2(2n-1+\epsilon)^2} + 2\sum_{n=1}^{\infty} \frac{1}{1/4 + 4\eta^2(2n)^2} \right\} \qquad \text{(II-7)}$$

$$\frac{w_\pi}{U_o} = -\frac{C_L}{8\pi\eta}(\nu_{L_w} - \nu_L) \sum_{n=1}^{\infty} \left\{ \frac{1}{2n-1-\epsilon} - \frac{1}{2n-1+\epsilon} \right\} \qquad \text{(II-8)}$$

These corrections can be obtained from Figs. 6 and 8 by substituting the quantity, $\nu_{L_w} - \nu_L$, for ν_L in the figures.

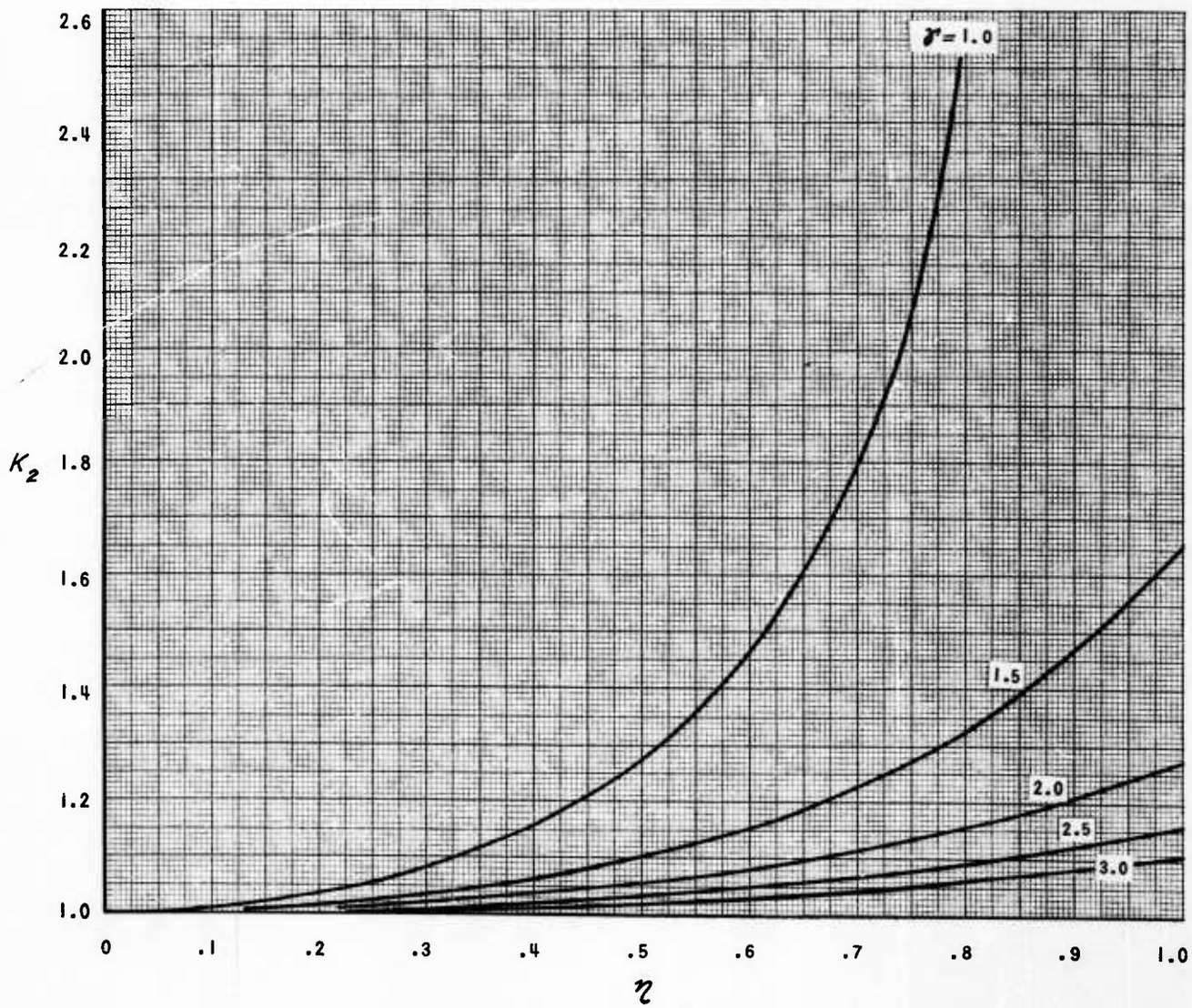

Figure II-2a IMAGE STRENGTH INCLUDING WALL INTERFERENCE $\epsilon = 0$

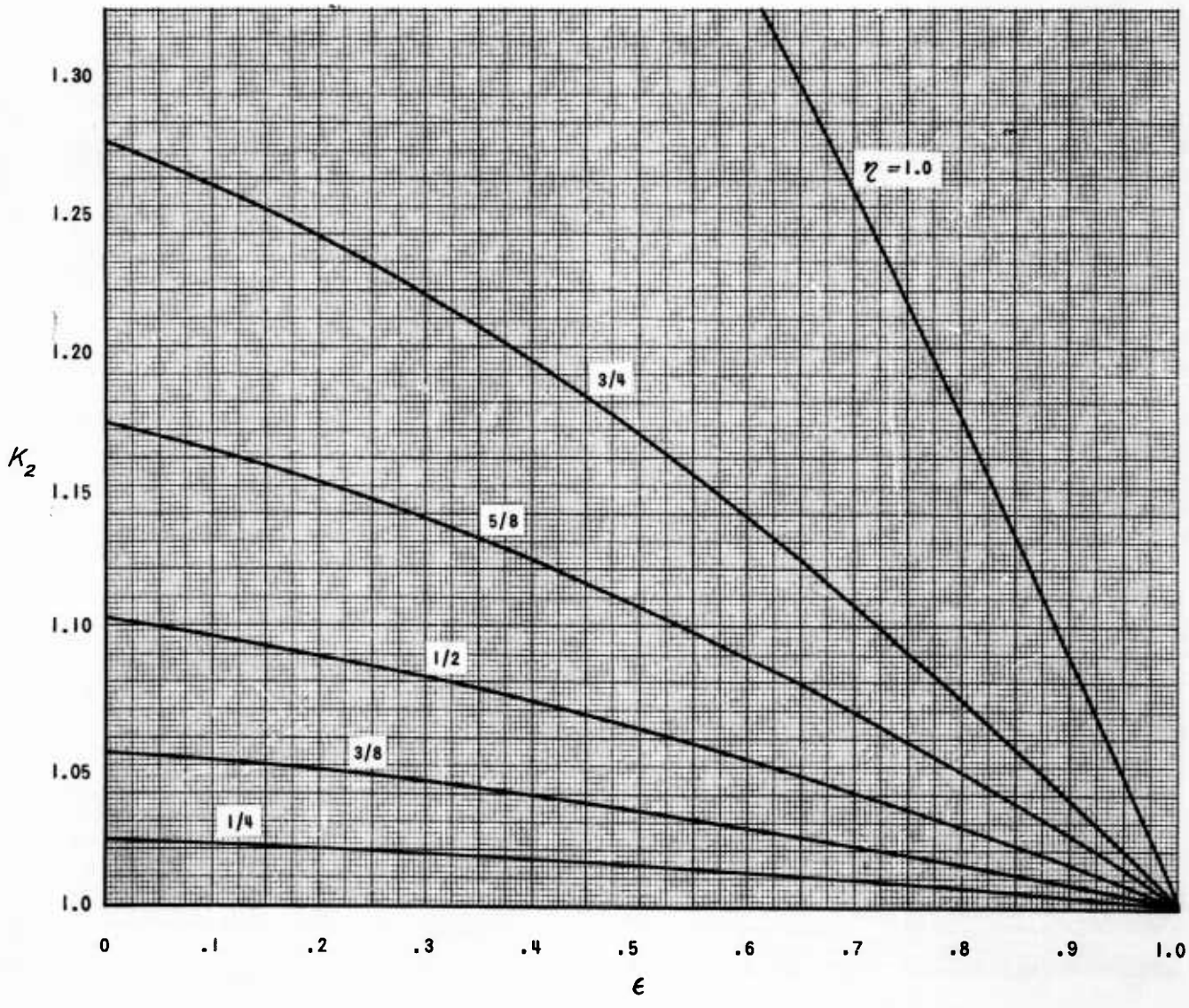

Figure II-2b IMAGE STRENGTH INCLUDING WALL INTERFERENCE $\gamma = 1.5$

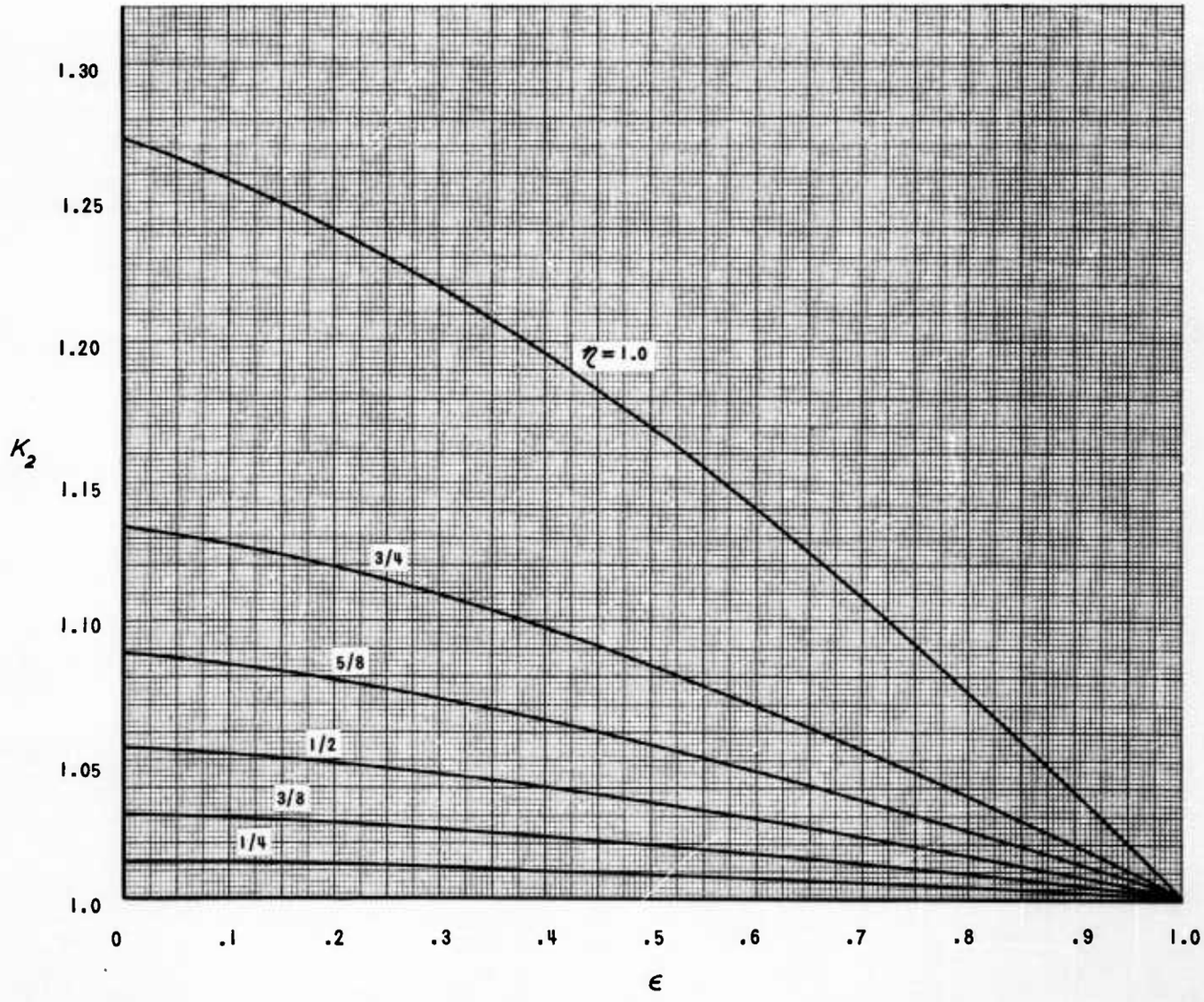

Figure II-2c IMAGE STRENGTH INCLUDING WALL INTERFERENCE $\gamma' = 2.0$

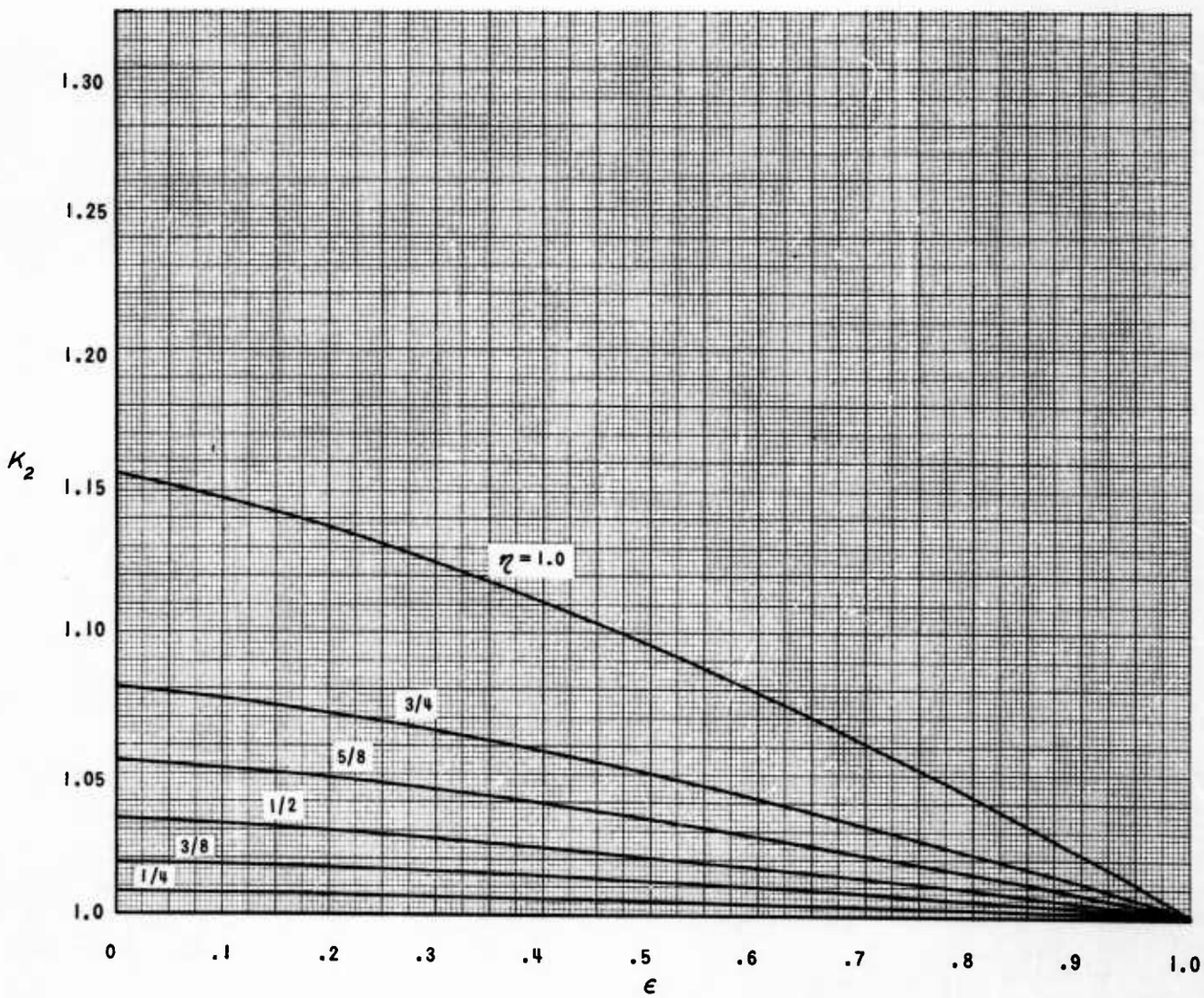

Figure II-2d IMAGE STRENGTH INCLUDING WALL INTERFERENCE $\mathscr{T} = 2.5$

REFERENCES

1. Koning, C. "Influence of the Propeller on Other Parts of the Airplane Structure", Aerodynamic Theory, (W. F. Durand, Editor), Vol. IV, Div. M., Pasadena, 1943.
2. Graham, E. W., Lagerstrom, P. A., Licher, R. M., and Beane, B. J. "A Preliminary Theoretical Investigation of the Effects of Propeller Slipstream on Wing Lift", Douglas Aircraft Company Report SM-14991, 1953.
3. Rethorst, S., "Aerodynamics of Non-Uniform Flows as Related to an Airfoil Extending Through a Circular Jet", Journal of the Aeronautical Sciences, Vol. 25, No. 1, Pg. 11-28, January 1958.
4. Tsien, H. S., "Symmetric Joukowsky Airfoils in Shear Flow", Quarterly of Applied Math., Vol. 1, pp. 130-148, 1943.
5. Von Karman, T. and Tsien, H. S., "Lifting Line Theory for a Wing in Non-Uniform Flow", Quarterly of Applied Math., Vol. III, No. 1, pp. 1-11, 1945.
6. Sowyrda, A., "Theory of Cambered Joukowsky Airfoils in Shear Flow", Cornell Aeronautical Laboratory Report, No. AI-1190-A-2, September 1958.
7. Jones, E. E., "The Forces on a Thin Airfoil in Slightly Parabolic Shear Flow", Z. Angew., Math. Mech., Vol. 37, pp. 362-370, 1957.
8. Jones, E. E., "The Elliptic Cylinder in a Shear Flow with Hyperbolic Velocity Profile", Quarterly Jour. Mech. App. Math., Vol. XII, Pt. 2, pp. 191-210, May 1959.
9. Murray, J. O. and Mitchell, A. R., "Flow with Variable Shear Past Circular Cylinders", Quarterly Jour. Mech. App. Math., Vol. X, Pt. 1, pp. 13-23, February 1957.

10. Von Karman, T. and Burgers, J. M., "Aerodynamic Theory - Perfect Fluids", Aerodynamic Theory, (W. F. Durand, Editor), Vol. II, Div. E., pp. 236-252, Pasadena, 1943.

11. Pistolesi, E., "Considerations Respecting the Mutual Influence of Systems Of Airfoils. Collected Lectures of the 1937 Principal Meeting of the Lilienthal Society, Berlin, 1937.

12. Weissinger, J., "The Lift Distribution of Swept-Back Wings", NACA TM 1120, March 1947.

13. Vidal, R. J., "Research on Rotating Stall in Axial Flow Compressors, Part III. Experiments on Laminar Separation From a Moving Wall", Cornell Aeronautical Laboratory Report No. AM-1076-A-3, (Also WADC TR 59-75, Part III) January 1959.

14. Wilder, J. G., Hindersinn, K., and Weatherston, R., "Design of an Air Supply System and Test Section For Research on Scavenging Systems for Propulsion Wind Tunnels", WADC TR 56-6, December 1955.

15. Owen, P. R., and Zienkiewicz, H. K., "The Production of Uniform Shear Flow in a Wind Tunnel", Jour. Fluid Mech., Vol. 2, Pt. 6, pp. 521-531, August 1957.

16. Hoerner, S. F., "Aerodynamic Drag", Dayton, Ohio, pp. 30-33, 1951.

17. Adler, A. A., "Variation With Mach Number of Static and Total Pressures Through Various Screens, NACA CB L5F28, February 1946.

18. von Bohl, J. G., "Das Verhalten paralleler Luftstrahlen" Ing.-Arch., Vol. 11, pp. 295-314, 1940.

19. Hall, I. M., "The Displacement Effect of a Sphere in a Two-Dimensional Shear Flow", Jour. Fluid Mech., Vol. 1, Pt. 2, pp. 129-141, July 1956.

20. Li, Ting-Yi, "Simple Shear Flow Past a Flat Plate in an Incompressible Fluid of Small Viscosity", Jour. Aero. Sci., Vol. 22, No. 9, pp. 651-652, September 1955.

21. Glauert, M. B., "The Boundary Layer in Simple Shear Flow Past a Flat Plate" Jour. Aero. Sci., Vol. 24, No. 11, pp. 848-849, November 1957.

22. Li, Ting Yi, "Authors Reply", Jour. Aero. Sci., Vol. 24, No. 11, pp. 849-850, November 1957.

23. Ting, L., "Boundary Layer Over a Flat Plate in Presence of Shear Flow", The Physics of Fluids, Vol. 3, No. 1, 1960.

24. Brenckman, M. E., "Experimental Investigation of the Aerodynamics of a Wing in a Slipstream", Jour. Aero. Sci., Vol. 25, No. 5, pp. 324-328, May 1958.

25. Gault, D. E., "A Correlation of Low-Speed, Airfoil-Section Stalling Characteristics with Reynolds Number and Airfoil Geometry", NACA TN 3963, March 1957.

26. Taylor, G. I., and Batchelor, G. K., "The Effect of Wire Gauze on Small Disturbances in a Uniform Stream", Quart. Jour. Mech. App. Math., Vol. II, Pt. 1, 1949, pp. 1-29.

27. Glauert, H., "Wind Tunnel Interference on Wings, Bodies and Airscrews", Aero. Res. Com. R. & M. No. 1566, September 1933.